Characterizing the Dimer Interface and Thermal Unfolding of Reduced, Zinc Bound Superoxide Dismutase-1

by

Harmeen K. Deol

A thesis
presented to the University of Waterloo
in fulfillment of the
thesis requirement for the degree of
Masters of Science
in
Chemistry

Waterloo, Ontario, Canada, 2018

Author's Declaration

I hereby declare that I am the sole author of this thesis. This is a true copy of the thesis, including any required final revisions, as accepted by my examiners.

I understand that my thesis may be made electronically available to the public.

Abstract

Superoxide dismutase 1 (SOD1) is a ubiquitously expressed metalloenzyme that reduces oxidative stress in cells by catalyzing the dismutation of superoxide radicals. Mutations in the gene encoding for SOD1 have been linked to the fatal neurodegenerative disease amyotrophic lateral sclerosis (ALS). The prevalent hypothesis for how mutant SOD1 causes disease is the formation of toxic intracellular protein aggregates. SOD1 undergoes posttranslational modifications *in vivo*, including metal binding, disulfide bond formation, and dimerization, to reach its final maturation form, a stable homodimer. Recent studies support the theory that more immature forms of SOD1 may play a key role in the disease pathology, and the monomeric species may be linked to toxicity. The zinc-bound form of SOD1 with a reduced disulfide bond (E,Zn-SOD1^{SH}) has been the center of debate with contradictory literature published regarding whether it exists as a monomer or dimer. Although this key form has been widely discussed, relatively little has been characterized compared to other forms of SOD1. Here we investigate E,Zn-pWT^{SH} SOD1 with certain fALS mutants using a combination of isothermal titration calorimetry (ITC) to measure dimer dissociation, and differential scanning calorimetry (DSC) to measure global unfolding of the protein, in order to dissect the contribution of dimer and monomer to protein stability. Results are compared to the effects of mutations in other forms of SOD1 to better understand protein maturation and different roles of SOD1 species in misfolding and disease.

Acknowledgements

I would like to express my deepest gratitude to my supervisor, Dr. Elizabeth Meiering, for approaching me with this opportunity and helping me not only grow as a scientist, but as a human.

I would also like to thank members of the Meiering lab, past and present, for their constant support. This would not be possible without all of them. I specifically like to thank Colleen Doyle for awakening my love of research through her dedication to teaching. I would also like to thank Volition La, Dalia Naser, and Duncan Mackenzie for their encouragement throughout this journey.

Lastly, to my family and friends, your patience and support mean more than I can express.

Dedication

To my grandma, I am forever grateful to you.

Table of Contents

Author's Declaration ii
Abstract iii
Acknowledgements iv
Dedication v
List of Figures viii
Chapter 1 ..... *viii*
Chapter 2 ..... *viii*
Chapter 3 ..... *viii*
Appendix ..... *viii*
List of Tables ix
Chapter 2 ..... *ix*
Chapter 3 ..... *ix*
Appendix ..... *ix*
List of Abbreviations x

Chapter 1 1
1.1 Protein folding, misfolding and aggregation 2
1.2 Amyotrophic Lateral Sclerosis 4
1.2.1 Cu, Zn Superoxide Dismutase-1 ..... *4*
1.2.2 Maturation of SOD1 ..... *6*
1.2.3 Energetics of SOD1 ..... *9*
1.3 Isothermal titration calorimetry (ITC) 13
1.4 Differential scanning calorimetry (DSC) 15
1.5 Research objectives 17

Chapter 2 19
2.1 Introduction 20
2.2 Materials and Methods 22
2.2.1 Recombinant expression and purification of holo human SOD1 ..... *22*
2.2.2 Demetallation and reduction of holo SOD1 ..... *22*
2.2.3 Titration of Various Zinc Stoichiometry *23*
2.2.4 Using isothermal titration calorimetry (ITC) to measure dimer dissociation *23*
2.2.5 Zinc titration using ITC *24*
2.2.6 Differential scanning calorimetry (DSC) *25*
2.3 Results and Discussion 26
2.3.1 The SOD1 dimer interface is less stable in E,Zn-pWT^{SH} than in E,E-pWT^{SS} *26*
2.3.2 DSC of E,Zn-pWT^{SH} global unfolding *33*
2.3.3 DSC at varying zinc concentrations uncovers the population of multiple species during thermal unfolding of E,Zn-pWT^{SH} *36*
3.0 Summary 39

Chapter 3 42
3.1 Introduction 43
3.2 Methods 44
3.3 Results and Discussion 44
3.3.1 Rationale for selected mutations *44*
3.3.2 fALS mutants E,Zn-SOD1^{SH} have varying effects on stability of the dimer interface relative to E,Zn-pWT^{SH} *45*
3.3.3 Zinc titration ITC reveals only H46R has large changes in zinc binding affinity *52*

3.3.4 A4V with bound zinc has thermal stability similar to that of Zn,Zn-pWT^{SH} dimer *55*
3.3.5 Zinc shuffling is not observed in H46R due to weakened metal affinity *60*
3.3.6 V148G serves as a monomer control for the zinc-bound form, whereas stabilizing mutant, V148I had a global endotherm similar to pWT *61*
3.4 SUMMARY 63

CHAPTER 4 65

References 67

Appendix 80
A1.0 Derivation of two state versus three state unfolding model *80*
A1.1 Thermodynamic analysis models for homodimeric protein folding *80*
A1.2 Three-state transition of dimer unfolding with monomer intermediate model *84*
A2.0 Par assay used to quanitate zinc and metal contamination *95*
A3.0 Iodoacetamide labeling SDS-PAGE *97*

List of Figures

Chapter 1

Figure 1.1 Energy landscape model for protein folding 3
Figure 1.2 Ribbon structure of holo superoxide dismutase 1 5
Figure 1.3 Mechanism of superoxide dismutation by SOD1 6
Figure 1.4 Maturation schematic of SOD1 7
Figure 1.5 Free energy diagram of 2-state unfolding for different maturation forms of SOD1 10
Figure 1.6 Free energy diagram for 3-state transition of SOD1 dimer with monomer intermediate.....11
Figure 1.7 Isotherm scan from isothermal titration calorimetry for subunit association.....14
Figure 1.8 Thermogram from differential scanning calorimetry of protein thermal unfolding 16

Chapter 2

Figure 2.1 ITC of dimer dissociation for pWT SOD1 28
Figure 2.2 Zinc titration ITC isotherm with varying concentration of E,E-pWT^{SH} 31
Figure 2.3 Zinc binding equilibrium to reduced SOD1 32
Figure 2.4 DSC of the disulfide reduced pWT as a function of added equivalents of Zn 35

Chapter 3

Figure 3.1 Dimer dissociation of fALS SOD1 mutants measured by ITC 49
Figure 3.2 Thermodynamics of E,Zn-SOD1^{SH} dimer dissociation.....50
Figure 3.3 ITC upon addition of zinc to E,E-SOD1^{SH} 53
Figure 3.4 Thermogram for fALS SOD1 mutants at varying protein concentrations 57

Appendix

Figure A1.1 3-state dimer unfolding with monomer intermediate model fits for fALS mutants.....88
Figure A1.2 2-state monomer unfolding model fits for fALS mutants.....90
Figure A1.3 2-state dimer unfolding model fits for fALS mutants.....91
Figure A1.4 3-state dimer unfolding with monomer intermediate model fits for fALS mutants.....93
Figure A1.5 2-state monomer unfolding model fits for fALS mutants.....94
Figure A1.6 2-state dimer unfolding model fits for fALS mutants.....95
Figure A2.1 Representative absorption spectra for PAR binding to Cu, Zn, and Zn from 2 samples.....97

List of Tables

Chapter 2

Table 2.1 ITC measurements of the dimer interface of E,Zn-pWT^{SH} at varying temperatures.....27

Chapter 3

Table 3.1 ITC measurements of the dimer interface of E,Zn-SOD1^{SH} mutants.....46
Table 3.2 Summary of ITC measurements of the dimer interface of E,Zn-SOD1^{SH} variants at various concentrations and temperatures 47-48
Table 3.3 Fraction of monomer at 25°C in DSC protein concentrations and their $t_{m,app}$.....58

Appendix

Table A1.1 3-dimer unfolding with monomer intermediate model fit values for different zinc equivalents and pWT.....87
Table A1.2 2-state dimer fit values for varying zinc equivalents and disulfide reduced pWT SOD1 89
Table A1.3 2-state monomer fit values for half and double zinc equivalent of pWT^{SH} 89
Table A1.4 2-state monomer fit values for varying concentrations for fALS mutants pWT^{SH} 92
Table A1.5 2-state dimer fit values for varying protein conc of E,Zn-SOD1^{SH} fALS mutants.....92

List of Abbreviations

A ..... intercept of the folded baseline in DSC thermogram
α ..... the extent of the unfolding reaction
ALS ..... amyotrophic lateral sclerosis
B ..... slope of the folded baseline in DSC thermogram
$\beta 1$ and $\beta 2$ ..... $\Delta H_{vH}/\Delta H_{cal}$ multiplied by the molecular weight of the cooperative unfolding unit
C ..... intercept of the monomer intermediate baseline in DSC thermogram
CEST ..... Chemical Exchange Saturation Energy Transfer
CCS ..... copper chaperone for superoxide dismutase
Cu or Cu^{2+} ..... copper
Cu,Zn-SOD1^{SS} ..... copper and zinc bound, disulfide oxidized, superoxide dismutase
ΔC_p ..... change in specific heat capacity
$\Delta C_{p,d}$ or $\Delta C_{p,N_2 \leftrightarrow 2M}$ ..... change in specific heat capacity of dimer dissociation
$\Delta C_{p,M \leftrightarrow U}$ ..... change in specific heat capacity of monomer unfolding
$\Delta C_{p,N_2 \leftrightarrow 2U}$ ..... change in specific heat capacity of total unfolding
D ..... slope of the monomer intermediate baseline in DSC thermogram
DLS ..... dynamic light scattering
DSC ..... differential scanning calorimetry
E ..... intercept of the unfolded baseline
EDTA ..... ethylenediaminetetraacetic acid
E,E-SOD1^{SH} ..... metal free, disulfide reduced, superoxide dismutase
E,E-SOD1^{SS} ..... metal free, disulfide oxidized, superoxide dismutase
E,Zn-SOD1^{SH} ..... zinc bound, disulfide reduced, superoxide dismutase
F ..... slope of the unfolded baseline
fALS ..... familial amyotrophic lateral sclerosis
f_m ..... fraction of monomer
f_U ..... fraction of unfolded monomer
ΔG ..... change in Gibbs free energy
$\Delta\Delta$G ..... ΔG of pWT minus ΔG of mutant
ΔG_d or $\Delta G_{N_2 \leftrightarrow 2M}$ ..... change in Gibbs free energy of dimer dissociation
GdmCl ..... guanidinium chloride
$\Delta G_{M \leftrightarrow U}$ ..... change in Gibbs free energy of monomer unfolding
$\Delta G_{N_2 \leftrightarrow 2U}$ ..... change in Gibbs free energy of total unfolding (folded dimer to unfolded monomer)
G_u ..... Gibbs free energy of the unfolded state
ΔG_{ref} ..... change in Gibbs free energy at reference temperature
HEPES ..... 4-(2-hydroxyethyl)-1-piperazineethanesulfonic acid
ΔH ..... change in enthalpy
Δh_{cal} ..... change in specific calorimetric enthalpy
ΔH_{cal} ..... change in calorimetric enthalpy
ΔH_{ref} ..... change in enthalpy at the reference temperature
ΔH_{vH} ..... van't Hoff enthalpy
$\Delta h_{0.5,M \leftrightarrow U}$ ..... change in specific enthalpy change of monomer unfolding
ΔH_d or $\Delta H_{N_2 \leftrightarrow 2M}$ ..... change in enthalpy of dimer dissociation

$\Delta H_{M\leftrightarrow U}$ ..... change in enthalpy of monomer unfolding
$\Delta H_{N_2\leftrightarrow 2U}$ ..... change in enthalpy of total unfolding (folded dimer to unfolded monomer)
ITC ..... isothermal titration calorimetry
k ..... Boltzmann constant
$K_{d,d}$ or $K_{d,N_2\leftrightarrow 2M}$ ..... equilibrium constant for dimer dissociation
$K_{d,Cu}$ ..... equilibrium constant for copper dissociation
$K_{d,Zn}$ ..... equilibrium constant for zinc dissociation
$K_{M\leftrightarrow U}$ ..... equilibrium constant for monomer unfolding
M ..... monomer intermediate state
$[M_i]$ ..... concentration of apo SOD1 monomer in the ITC cell after injection i
$[M_{i-1}]$ ..... concentration of apo SOD1 monomer in the ITC cell after injection i-1
$[M]_o$ ..... total concentration of apo SOD1 in units of mol monomer L^{-1}
n ..... molecularity
N ..... native state
N^* or M^* ..... native-like state
PAR ..... 4-(2-pyridylazo)rescorcinol
PDB ..... protein data bank
P_{dimer} ..... protein concentration in mol dimer L^{-1}
pWT ..... pseudo wild type superoxide dismutase
q ..... light scattering vector
q_i ..... heat associated with each injection in an ITC experiment
q_{dil} ..... the heat associated with sample dilution unrelated to dissociation in an ITC experiment
R ..... universal gas constant
sALS ..... sporadic amyotrophic lateral sclerosis
SEC ..... size exclusion chromatography
SDS-PAGE ..... sodium dodecyl sulfate polyacrylamide gel electrophoresis
SOD1 ..... superoxide dismutase 1
SOD2 ..... superoxide dismutase 2
SOD3 ..... superoxide dismutase 3
ΔS ..... change in entropy at the reference temperature
ΔS_{ref} ..... change in entropy at the reference temperature
ΔS_d or $\Delta S_{N_2\leftrightarrow 2M}$ ..... change in entropy of dimer dissociation
$\Delta S_{M\leftrightarrow U}$ ..... change in entropy of monomer unfolding
$\Delta S_{N_2\leftrightarrow 2U}$ ..... change in entropy of total unfolding (folded dimer to unfolded monomer)
T ..... temperature
t_{avg} ..... the average value of $t_{0.5}$ for all apo SOD1 variants
TCEP-HCl ..... tris(2-carboxyethyl)phosphine hydrochloride
T_{exp} ..... experimental temperature
T_{ref} ..... reference temperature
$T_{0.5}$ ..... the temperature in Kelvin at which half of the protein is unfolded
$t_{0.5}$ ..... the temperature in °C at which half of the protein is unfolded
$t_{m,app}$ ..... the temperature in °C at the maximum C_p
$t_{0.5,M\leftrightarrow U}$ ..... temperature midpoint for monomer unfolding
T_1 ..... the temperature at which the thermodynamics of dimer dissociation were measured by ITC

T_2 ..... the temperature at which the equilibrium constant $K_{M \leftrightarrow U}$ is equal to 1
U ..... unfolded state
v ..... volume of each injection in an ITC experiment
V ..... ITC reaction cell volume
WT ..... wild type superoxide dismutase
Zn or Zn^{2+} ..... zinc
Zn,Zn-SOD1^{SH} ..... zinc bound to both sites, disulfide reduced, superoxide dismutase

Chapter 1
Introduction

1.1 Protein folding, misfolding and aggregation

Proteins are one of the four main macromolecules that make up the living world. Initially, the protein's gene is transcribed and translated into its primary structure, which is comprised of an amino acid chain. This amino acid sequence is thought to be crucial to protein folding as it holds key information required for the primary sequence to fold into its native structure (1). There are multiple models proposed to explain exactly how a protein acquires its native structure from the amino acid sequence (1). Early in the folding process, the protein is thought to have multiple conformations available for sampling before reaching the native conformation (Figure 1.1). The nucleation mechanism involves the protein sampling various conformations to form a core with a native-like structure, followed by reorganization of the periphery (2-4). Under physiological conditions, a driving force of protein folding is the burial of hydrophobic residues, also known as hydrophobic collapse. However, another model for protein folding that encompasses both non-native and native folding models has been termed as the energy landscape model, often depicted by a protein folding funnel (Figure 1.1) (4). In this model, as the unfolded protein acquires a more native-like structure, there are fewer conformations available to sample. The multiple dips in the funnel (Figure 1.1) above the native structure represent the formation of intermediates that either form non-native structures that require a certain amount of energy to restructure, or an 'on-pathway' intermediate that occupies a metastable state (5). Although this funnel may appear inefficient, folding under physiological conditions is an efficient process; some initial unfolded structures appear to have a certain degree of nascent

structure allowing for a 'head-start' when folding initiates. Thus, a certain number of conformations are unavailable for the denatured protein to sample, and even more sampling limitations come from the side-chains that will interact and the fluctuating secondary structure.

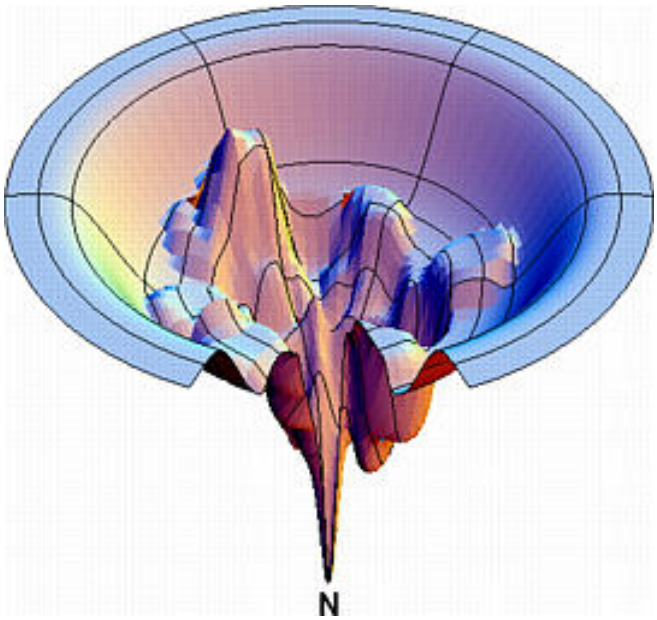

Figure 1.1- Energy landscape model for protein folding. The funnel shape represents the decrease in available conformations the protein can sample as it folds. The dips before native state (N) folding are due to metastable non-native or native intermediates that require a certain amount of energy to change conformation to continue on the folding pathway. Adapted from Toal and Schweitzer-Stenner, 2014 (5, 6).

Partially folded or misfolded intermediates may potentially interact with each other due to their exposed hydrophobic groups, which are normally buried in the native conformation, and can lead to aggregation (7). The drive to bury hydrophobic regions from the hydrophilic environment, such as in protein folding, also drives aggregation. Aggregates structures can range from well-structured fibrillar amyloid to an amorphous structure. Misfolded proteins and aggregates tend to be toxic to cells by interrupting regular cellular function and removing essential proteins due to aggregation of their folding intermediates. Aggregation is linked to

numerous diseases, including various neurodegenerative diseases such as Alzheimer's, Parkinson's, Huntington's, and of interest for this project, Amyotrophic Lateral Sclerosis (ALS) (8).

1.2 Amyotrophic Lateral Sclerosis

ALS is a fatal motor neuron disease typically with adult onset that specifically targets neurons of the spinal cord, brainstem and cortex (9). Motor neurons are responsible for relaying signals to voluntary muscles; however upon death of motor neurons, they become incapable of carrying signals and cause muscle atrophy (9, 10). This leads to the eventual loss of vital muscle control in the individual, commonly followed by respiratory failure (10). ALS is postulated as a protein misfolding disease and can be either sporadic or familial, occurring due to unknown causes or genetically inherited, respectively. There are many genes where mutations linked to ALS have been identified in patients, one well studied is the *sod1* gene, which encodes Cu, Zn-superoxide dismutase 1 (SOD1). For *sod1*-linked ALS, the familial ALS (fALS) is autosomal dominant and is associated with the chromosome 21q (11). The *sod1* gene encodes an enzyme called copper, zinc-superoxide dismutase-1, and mutations in SOD1 account for 20% of familial ALS with over 180 mutations identified to date (see ALSoD http://alsod.iop.kcl.ac.uk) (12-14)

1.2.1 Cu, Zn Superoxide Dismutase-1

Mature superoxide dismutase is a homodimeric metalloenzyme found mainly in the cytoplasm with minimal amounts found in the mitochondrial inner membrane space (9, 12, 15). SOD1 has 153 amino acid residues per subunit, with a molecular

weight of 32 kDa as a dimer (10). Each monomer forms an intrasubunit disulfide bond between Cys57 and Cys146 (Figure 1.2) (16) and also binds a structural zinc ion, which binds at residues His63, His71, His80 and Asp83, and a catalytic copper ion binding to His46, His48, His63 and His160 (17). Two functional loops are the electrostatic loop, responsible for guiding the superoxide to the active site, and the zinc-binding loop (18).

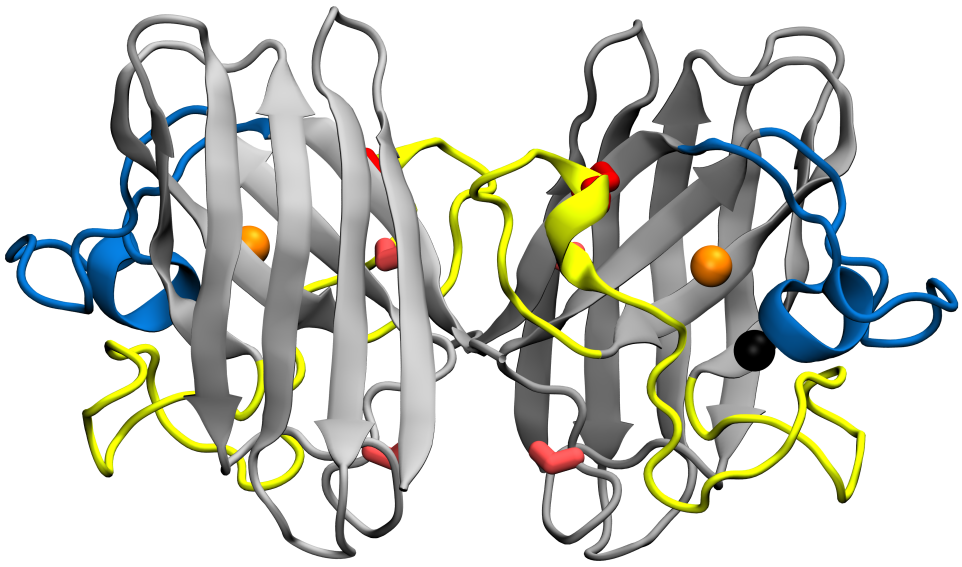

Figure 1.2- Ribbon structure of holo superoxide dismutase 1. Holo SOD1 consists of two 8-stranded Greek key beta-barrel monomers, with one zinc ion (black sphere) and one copper ion (orange sphere) per monomer. The red represents the Cys57-Cys146 disulfide bond and two free cysteines at positions 6 and 111, and loop IV (yellow) contributes to the dimer interface and zinc binding and loop VII (blue) is the electrostatic loop. Adapted from Broom et al., 2014 (19).

SOD1 acts as an antioxidant defense against toxic superoxide (O_2^-) radicals (9). Superoxide is formed naturally as a byproduct of many cellular processes (e.g. respiration), and is a product of immune cells such as neutrophils. SOD1 works by converting toxic superoxide radicals into hydrogen peroxide and molecular oxygen through opposite two-step reaction (Figure 1.3) (9, 20). In the first step, the enzyme oxidizes a superoxide anion by reducing the Cu^{2+} in the SOD1 to Cu^{1+}, and produces

molecular oxygen (9). The reduced copper reduces a second superoxide, which with two hydrogen ions form hydrogen peroxide and the copper returns to Cu^{2+} (9).

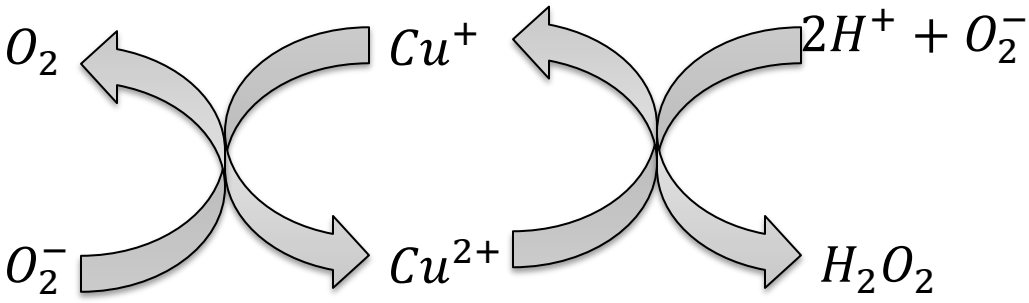

Figure 1.3- Mechanism of superoxide dismutation by SOD1. Superoxide species in cell are very destructive and with redox reactions, SOD1 is able to convert superoxide to molecular oxygen and hydrogen peroxide. The Cu^{2+} oxidizes the first superoxide molecule, and the now reduced Cu^{2+} reduces the second superoxide radical to form hydrogen peroxide. Adapted and modified from Rakhit and Chakrabartty, 2006 (20).

With over 180 different SOD1 mutations identified associated with fALS, there are multiple hypotheses for the cause of lethal effects in ALS (21). SOD1 knock out experiments in mice suggest that the pathogenicity of SOD1 is not due to the loss of the normal function but a gain of toxic function (22, 23). Transgenic mice had a gain of toxic function when they were exposed to exogenous human SOD1 mutants associated with ALS (such as G93A). The mice expressed the ALS phenotype for loss of motor neuron function, regardless of the endogenous mouse SOD1 expression (23-25). Based on this hypothesis, further experiments involve determining which maturation form, if specifically one, is responsible for the toxic misfolding of SOD1.

1.2.2 Maturation of SOD1

SOD1 undergoes several posttranslational modifications to reach the mature, functional homodimeric enzyme. The most immature form of SOD1, known as the reduced apo SOD1 (from here on referred to as E,E-$SOD1^{SH}$), has no metals bound

and with a reduced disulfide bond. E,E-SOD1^{SH} must undergo acetylation of the N-terminus, bind zinc and copper, form a disulfide bond, and undergo dimerization to reach its mature form (Figure 1.4) (26). E,E-SOD1^{SH} has marginally low stability compared to other globular proteins but exceptionally low compared to the holo form of SOD1 (27). After the modifications, SOD1 is an extremely stable homodimeric protein, referred to as oxidized holo SOD1 (Cu, Zn-SOD1^{SS}), with a high melting temperature (t_m) of approximately 92°C (28). It is currently unknown how the zinc is obtained by SOD1, but it is important not only for normal function and protein stabilization but for interacting with the copper chaperone for superoxide dismutase 1 (CCS), which has been shown to play an important role in copper delivery (29, 30).

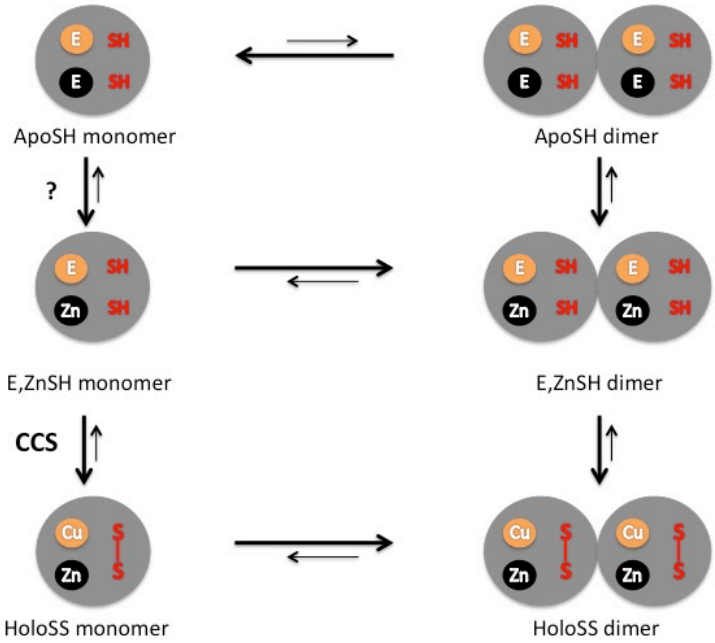

Figure 1.4- Maturation schematic of SOD1. The most immature form, reduced apo (E,E-SOD1^{SH}) is the starting form for maturation. The mechanism by which the zinc ion is obtained is unknown, but it is thought to be the initial maturation step. The copper chaperone for SOD1 (CCS) binds to E,Zn-SOD1^{SH} to deliver the copper and oxidize the conserved disulfide bond between Cys57 and Cys146. Modified picture from Banci et al., 2012 (26).

CCS is comprised of three domains; domains 1 and 3 have a functional role whereas domain 2 serves as a structural function. Domain 1 binds Cu(I), which transfers to the SOD1 monomer once domain 2, which is homologous to SOD1 monomer, forms a heterodimer with SOD1 via its normal homodimer interface (16, 26, 31). Domain 3 of CCS is involved in the formation of the disulfide bond between Cys-57 and Cys-146, via disulfide transfer from Cys-244 and Cys-246 in the CCS (16, 26, 32). Formation of the disulfide bond can occur before any metals are bound resulting in oxidized apo SOD1 (E,E-SOD1^{SS}). The exact order of these post-translational modifications is not completely clear, however certain processes have been confirmed to occur sequentially. For instance, Banci *et al.,* found that when oxidized, zinc bound SOD1 (E,Zn-SOD1^{SS}), which is predominately dimeric, forms before the CCS has the ability to add a copper, it will not reach the fully metallated form as efficiently as reduced, zinc bound SOD1 (E,Zn-SOD1^{SH}) (26). The disulfide bond greatly increases the affinity of the homodimerization of SOD1 that CCS likely acts on the disulfide reduced SOD1, via formation of a CCS-SOD1 heterodimer. Thus, metallation has been proposed to occur before disulfide bond formation, and perhaps the CCS, which prefers forming a heterodimer with a zinc bound state, catalyzes the formation of the disulfide bond.

The binding affinity of zinc and copper ions to SOD1 is extremely high ($K_{d,d}$ of $\sim 10^{-14}$ M and $10^{-18,}$ respectively) (33) and difficult to measure accurately. Variations in conditions that affect protein folding, such as denaturant concentration and temperature, can be used to characterize different transitions of SOD1 that may be difficult to access (19, 34, 35). Crow *et al*. used a method that involves destabilizing

the wild-type (WT) SOD1 with chemical denaturant (3 M urea) and then adding metal chelators to assess the metal dissociation constants ($K_{d,Zn}$ and $K_{d,Cu}$), which were found to be $2.3x10^{-14}$ M and $6.0x10^{-18}$ M for zinc and copper, respectively (33). The SOD1 dimer dissociation was also measured by chemical denaturation, for a $K_{d,d}$ of $\sim 1.0x10^{-10}$ M at pH 7.8 for Cu, Zn-WT^{SS} (wild-type) (36), and $<10^{-8}$ M at pH 7.8 for E,E-WT^{SS} (37), indicating tight association and stable dimer. The changes in $K_{d,d}$ and K_d from apoSS to holoSS illustrates how maturation pathway alters the energetics of the dimer interface and the metal binding affinities.

1.2.3 Energetics of SOD1

A working hypothesis for the cause of ALS is toxic protein misfolding, likely originating from early maturation forms of SOD1 (19). In cells, SOD1 is found mainly in the oxidized holo form, however, mutations may alter the populations of other forms due to changes in the relative stabilities and rates of formation of different maturation species (19). Thermodynamic stability evaluates the population of different states at equilibrium and kinetic data describes the conversion rates between the states; this may involve two-state or three-state (un)folding transitions, for example (Figure 1.5 and Figure 1.6) (38). The various maturation forms of SOD1 have varying energetics associated with them. The E,E-SOD1^{SH} form is the least stable form of SOD1, and undergoes two-state unfolding (folded monomer, M, to unfolded monomer, U) according to thermal and chemical denaturation studies (39-41). However, the oxidation of the sulfhydryl groups to produce the E,E-SOD1^{SS} form slightly stabilizes the folded monomer and strongly stabilizes the dimer interface

(37, 39, 40, 42). E,E-WT^{SS} can populate a folded dynamic monomeric structure at physiological conditions (27, 40, 43), and kinetic studies indicate that disulfide bond reduction increases the rate of unfolding (40, 44). In the mature form of SOD1 (Cu, Zn-SOD1^{SS}), the bound metals greatly stabilize the protein relative to E,E-WT^{SS} (28, 45).

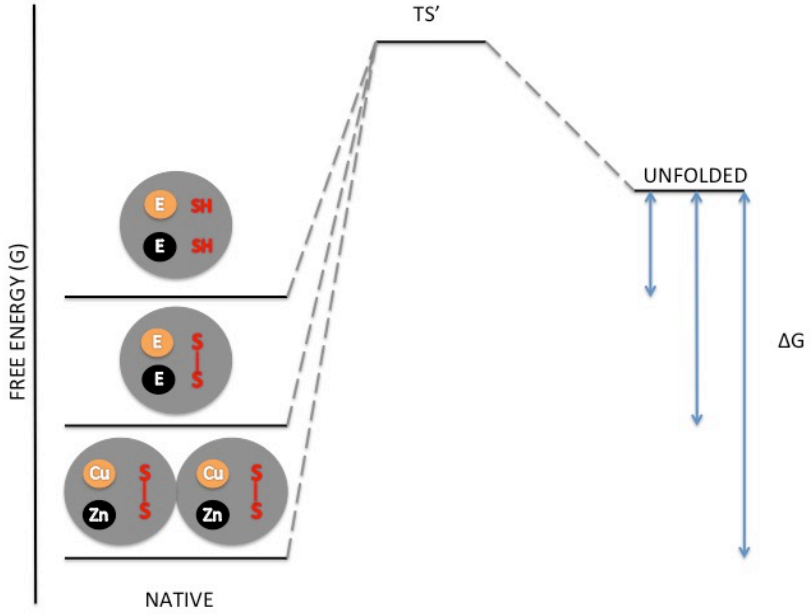

Figure 1.5- Free energy diagram of 2-state unfolding for different maturation forms of SOD1. The Cu,Zn-SOD1^{SS} form is the most stable, mature form of SOD1, followed in decreasing stability by the apoSS form and apoSH as the least stable. This energy diagram depicts a 2-state transition, and the energy difference for unfolding the native form to the unfolded monomeric species, indicated by ΔG. The transition state (TS') represents the energy barrier for folding, and the conversion from the un/folded to the transition state represents the kinetic rates. The transition state is depicted at the same free energy for the 3 forms due to unknown free energies of their respective transition states. Proteins with higher kinetic stability will access the transition state less and remain in the native form longer.

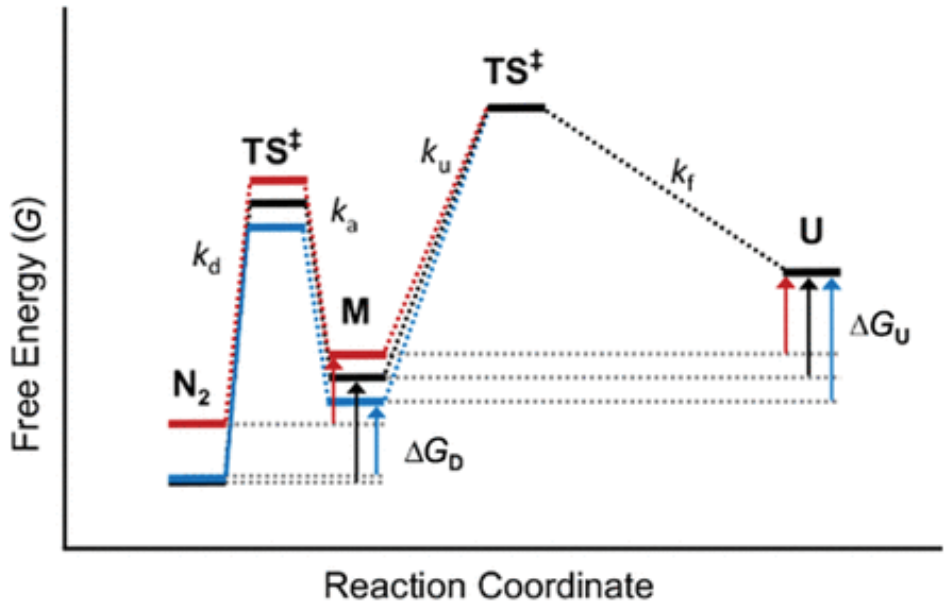

Figure 1.6- Free energy diagram for 3-state transition of SOD1 dimer with monomer intermediate. Native dimer (N_2) is the most stable state for all 3 SOD1 variants, black, red and blue indicate WT, A4V and H46R (ALS-associated mutants), respectively. In the 3-state model, there is the formation of a folded monomeric intermediate that denatures further into the unfolded monomer (U). ΔG_D and ΔG_U are the change in free energy for dimer dissociation and monomer unfolding, respectively. The transition states are depicted by TS, and the rates of conversion are depicted by k_d, k_a, k_u, and k_f, for dimer dissociation, monomer association, monomer unfolding and monomer folding, respectively. Figure adapted from Broom et al., 2014 (19, 45).

The energetics associated with disulfide bond formation and copper binding has been a focus of various studies of SOD1, however, there are relatively little quantitative data on the effects of zinc binding. Zinc binding to SOD1 has been found to favor CCS binding, and thus promotes copper binding and disulfide bond formation (26). In recent studies, Kayatekin *et al*. found that zinc bound readily to a monomeric variant of E,E-SOD1^{SS} of ALS mutants and significantly stabilized the folded state, however zinc bound with a 750-fold lower affinity to the E,E-SOD1^{SH} form, corresponding to a $K_{d,Zn}$ of 75 ± 33 nM (46, 47). If zinc binding is truly the initial maturation step, decreased zinc binding affinity may allow for the reduced

apo form to aggregate readily, due to the decreased protein stability of the most immature form, since the dynamics between zinc bound and unbound increases.

ALS may manifest from not only the E,E-SOD1^{SH} form but also other maturation forms. It has been proposed that mutations may cause increased fluctuations in the metal binding regions leading to metal loss and that mutations may also interfere with the dimer interface affecting its stability (42, 45, 48, 49). fALS mutations tend to have the greatest destabilizing effects on E,E-SOD1^{SH}, however certain mutations, such as ones involved in metal binding, showed either minimal destabilizing or even stabilizing effects (10, 40, 44). Using hydrogen-deuterium (H/D) exchange, which indicates any structural openings, metal-binding mutants showed similar structural fluctuations as E,E-pWT^{SH} (pseudo-wildtype) (50, 51). This may be due to the fact that the stabilizing metal binding mutants such as H46R tend to add a positively charged group close to where the zinc ion normally binds. However, the effects of mutations vary for each of the maturation forms as supported by Broom *et al*., who studied a range of fALS mutants. Although each mutation weakened the dimer interface relative to the control (52), they did so to varying extents, and varied in their monomer stability from being slightly more stabilizing to significantly destabilizing relative to the pWT control. Studying the stabilizing effects of fALS variants on other SOD1 forms, such as E,Zn-SOD1^{SH} will provide further insight on SOD1 maturation and its role in ALS.

1.3 Isothermal titration calorimetry (ITC)

The stability effect of fALS mutations on other forms such as E,Zn-SOD1^{SH} can be studied with the use of isothermal titration calorimetry (ITC). ITC is a valuable technique for direct measurement of thermodynamic parameters, for example, involved in protein subunit dissociation (52), such as change in Gibbs free energy (ΔG), enthalpy (ΔH), entropy (ΔS), and change in heat capacity at constant pressure (ΔC_p) (53). ITC involves injections of one solution into the calorimetric cell containing another solution, causing an exothermic or endothermic reaction. The heat associated with the reaction is measured for a thermodynamic analysis of the relationship between the associated heat and concentration of sample in the reaction cell (Figure 1.7). Traditionally ITC has been used for measuring binding equilibrium such as ligand binding energetics, enzyme-substrate interactions or reactions of multimolecular complexes (54).

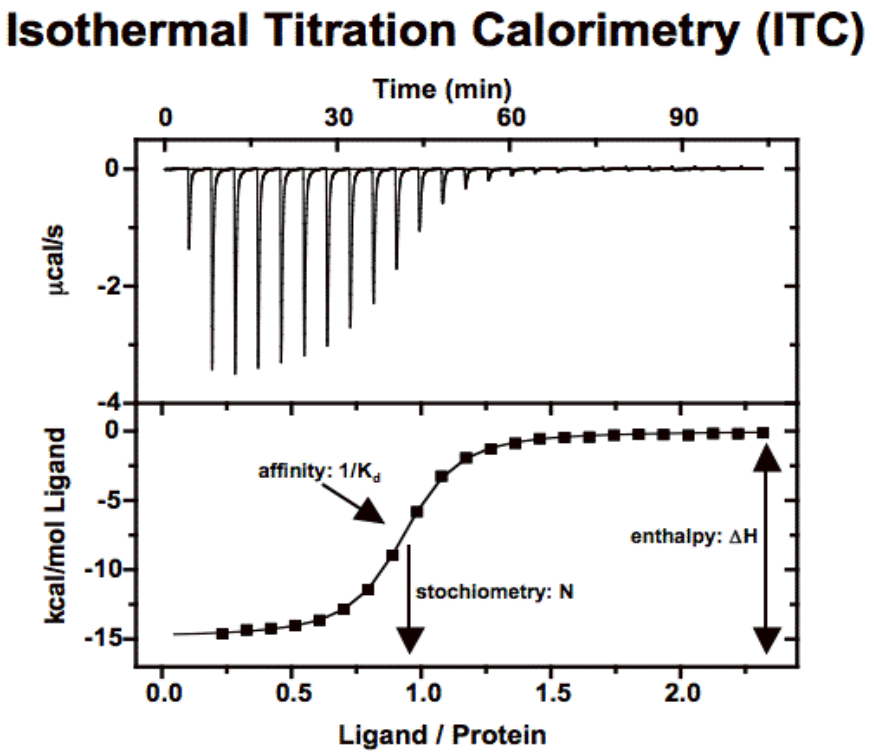

Figure 1.7- Isotherm scan from isothermal titration calorimetry for subunit association. Through a series of injections of reactant 1 into reactant 2 in the reaction cell, there is a decreasing heat associated with each injection. Eventually the reaction cell is saturated with reactant 1 where there is no substrate left to react with or the concentrations between the injection and reaction cell are too similar. Integrating the isotherm is able to give data on the dissociation constant, binding sites (stoichiometry) and the change in enthalpy for the reaction. Adapted from McMahon (53, 55).

Recently, a useful method for measuring oligomer dissociation, specifically applied to dimer dissociation, was described for SOD1 (52, 56). ITC experiments are conducted at a defined temperature, which can allow for the isolation of dimer dissociation thermodynamics from those of monomer unfolding, provided the two events occur at different temperatures. Broom *et al*. found via ITC that the dimer interface in E,E-SOD1^{SS} is less stable as temperature increases, favoring dissociation (52, 56). As temperature increases, the dissociation occurs more readily and results in an increase in the heat of dissociation. All of the fALS mutants studied by Broom

et al., which were chemically diverse and distributed throughout the protein structure, weaken the dimer interface to varying extents. Thus, the mutations generally increase the population of monomer, supporting the idea that the monomer is a species that contributes to ALS. Upon subunit dissociation, there is large structure disruption involving an increase in exposure of hydrophobic residues leading to a highly dynamic monomer structure (57, 58). We used ITC here to investigate the effects of ALS mutations on the dimer interface of E,E-SOD1^{SH} as described further below in Chapters 2 and 3.

1.4 Differential scanning calorimetry (DSC)

A complementary tool to ITC is the differential scanning calorimetry (DSC), which has been extensively used to study global stability of proteins, including different forms of SOD1 (28, 37, 40, 43, 50). DSC involves two identical cells, a reference and sample cell, which are maintained at the same temperature (59, 60). However, different substances in the cells result in a difference in power required to maintain the cells at the same temperature. These experiments measure the thermal transition midpoint (t_m), change in heat capacity for unfolding (ΔC_p) and the change in enthalpy of unfolding (ΔH) (Figure 1.8). DSC is commonly used to assess global stability of protein samples by increasing the temperature and allowing the protein to thermally unfold; a higher t_m is indicative of a more thermally stable protein (59-63). DSC also determines the stability effects that certain sample conditions (e.g. buffers) have on the protein- if it were stabilizing, the protein would unfold at a higher temperature, whereas the opposite would be true if it were destabilizing.

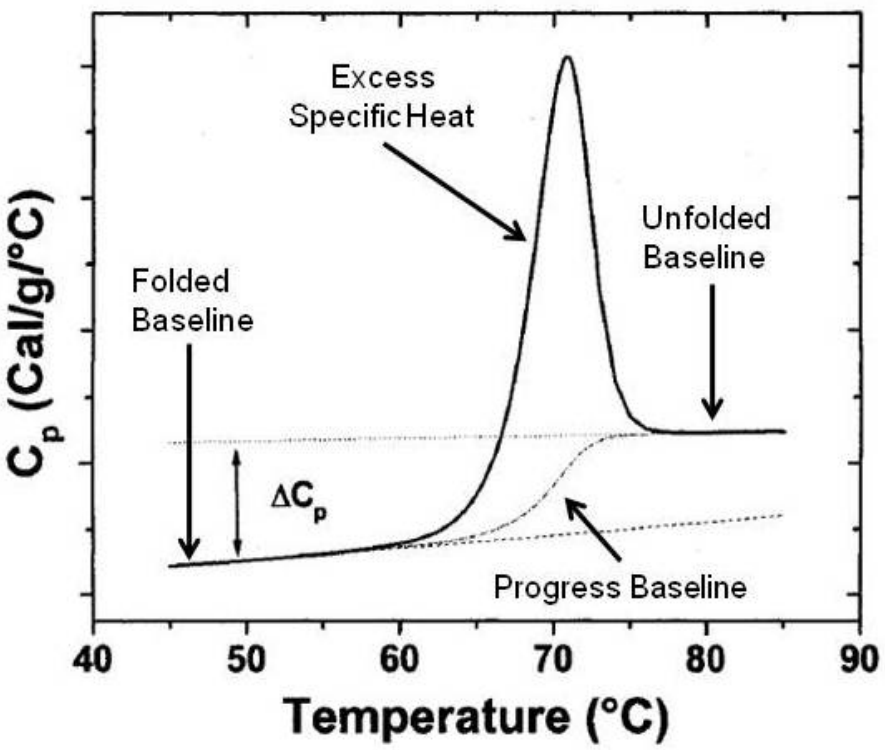

Figure 1.8- Thermogram from differential scanning calorimetry of Protein Thermal Unfolding. DSC scans provide valuable thermodynamic information especially when fit to specific models such as the 2-state or 3-state models, e.g. as developed by the Meiering group for SOD1 (56). The ΔC_p is derived from the difference in slopes of the folded and unfolded baselines. The shape and the area under the peak represent the van't Hoff and the calorimetric enthalpies, respectively. Excess specific heat is the heat released from SOD1 during thermal denaturation. Adapted and modified from Bruyants et al., 2005 (4, 60, 64-66).

Broom *et al*. explored the total stability of E,E-SOD1^{SS} dimers using DSC (56). Many fALS mutations decrease the global stability but some (i.e. H46R and V148I) increase the stability relative to pWT (56). Each variant DSC scan was fit to a 2-state (monomer to unfolded monomer, M↔U) and 3-state (dimer dissociation to a folded monomer intermediate to an unfolded monomer, N_2↔2M↔2U) unfolding model. The fits provided the Gibbs free energy of global unfolding (ΔG), and fALS mutants that showed a molecularity (*n,* number of subunits involved in unfolding) of 2, exhibited similar values for Gibbs free energy for both models. A molecularity of 2 is representative of the unfolding reaction is truly 2-state, and the monomer

intermediates are not significantly populated. The fit values for the dimer two-state and three-state models differ considerably when the monomer intermediate formation is favored. The monomer intermediate becomes populated and observable at lower protein concentration because of mass action (67). Mutants have varying effects on the stability of the monomer intermediate but all mutants decrease the stability of the dimer interface. Accordingly monomer formation is favored when the mutations either considerably destabilize the dimer interface (i.e. V148G), or increase monomer stability (i.e. H46R or V148I) (56). In addition, the monomer unfolding was characterized by calculating the difference in global stability (obtained from DSC) and the dimer dissociation (obtained from ITC) (52, 56).

1.5 Research objectives

Here we investigate the energetics and structural aspects of the E,Zn-SOD1^{SH} form of SOD1 for pseudo-wildtype (pWT) and several fALS mutants in the pWT background (e.g. with Cys 6 and Cys 111 mutated to Ala and Ser, respectively) using calorimetry techniques. In E,Zn-SOD1^{SH}, the disulfide bond is reduced (SH) and only zinc is bound in the zinc-binding site of each monomer while the copper site is empty (E); SOD1 will be replaced with the respective mutant under observation. ITC was applied to study pWT and various mutants at a range of temperatures to determine the dimer dissociation energetics. In addition, DSC was used to study the same variants to obtain information on global stability. Each DSC thermogram was fit to a 2-state transition (native dimer to the unfolded monomer; or folded to

unfolded monomer) and a three-state transition (native dimer to folded monomer intermediate to unfolded monomer), at varying protein concentrations. The protein concentration-dependences of the apparent melting transitions were determined which helped define when the monomer intermediate is populated. The three-state fitting used parameters obtained by ITC to fix variables relating to dissociation to allow for the fitting of the energetics for monomer unfolding. All of these results were compared to a similar study done previously with E,E-SOD1^{SS} variants (56, 68). Understanding the energetics and structural details of the E,Zn-SOD1^{SH} form will provide insights into normal SOD1 maturation as well as impacts of fALS mutants and potentially their role in ALS.

Chapter 2
Combining ITC and DSC to thermodynamically characterize E,Zn-pWT^{SH}

Author Contributions

Some of the calorimetry results in this chapter (Figure 2.1) have been published previously (69). Section 2.1 was modified from Culik *et al.,* (69). These calorimetry data were obtained by Harmeen Deol.

2.1 Introduction

Amyotrophic lateral sclerosis (ALS) is a neurodegenerative disorder that results in paralysis and ultimately death. About 20% of the familial ALS cases are linked to mutations in Cu, Zn-superoxide dismutase (SOD1); a 32 kDa homodimeric protein responsible for catalyzing superoxide radicals into either oxygen or hydrogen peroxide (70). The mutations are not localized to a certain region in the protein; rather they are spread throughout the entire protein structure and almost all result in a gain of toxic function (71). ALS has a characteristic phenotype shared with other neurodegenerative diseases involving protein misfolding and aggregation that are implicated in toxicity (19, 72). Although the mechanisms of protein misfolding and aggregation remain unclear, it is widely accepted that immature forms of SOD1 contribute to aggregate formation (36, 73-75).

A destabilized protein, such as an intermediate along a maturation pathway or a mutation, is a likely candidate for misfolding, leading to aggregation (19). The SOD1 monomer undergoes a series of maturation steps involving zinc and copper binding, and formation of a disulfide bond. The fully mature monomer undergoes dimerization through various hydrogen bonding, hydrophobic and water-mediated interactions (74), and introducing mutations may hinder the maturation process leading to misfolding and disease related aggregation (76-80). Previous studies have shown the effects of metal binding on the thermal stability of SOD1 (41, 47, 81) and acquisition of the copper ion has been studied extensively, particularly for the wild-type protein (16, 26, 32). However the mechanisms of zinc binding and interactions of mutant SOD1 with the human copper chaperone (CCS) remain elusive. Zinc

binding is known to stabilize the protein (47, 50, 82) and the reduced zinc bound form of SOD1 (E,Zn-SOD1^{SH}) is the preferred form for interacting with CCS (26, 32, 83). E,Zn-SOD1^{SH} is poorly characterized and there is controversy around it existing as a monomer or dimer, but recent research supports that zinc binding orients the zinc binding loop to promote dimerization (84-87). Prior studies have shown two key findings: inclusion bodies contain metal-deficient and disulfide reduced SOD1 (81, 88, 89), and there is a pool of E,Zn-SOD1^{SH} *in vivo* (90-92). Collectively, these studies hint at zinc binding, or the lack of maturation post zinc binding, being responsible for misfolding and thus far the dimer interface of E,Zn-SOD1^{SH} was poorly described thermodynamically.

In this chapter, we characterize the dimer interface and monomer stability of E,Zn-pWT^{SH} using isothermal titration calorimetry (ITC) and differential scanning calorimetry (DSC). ITC is used to define the equilibrium dissociation constant ($K_{d,d}$), enthalpy of dissociation (ΔH_d), and other thermodynamic parameters, such as the entropy and Gibbs free energy of dissociation (ΔS_d and ΔG_d, respectively). Also, the specific heat capacity of dissociation ($\Delta C_{p,d}$) is determined by measuring the temperature dependence of ΔH_d. We used ITC to characterize the E,Zn-pWT^{SH} dimer and found it to have a significantly weakened dimer interface compared to the E,EpWT^{SS} dimer and Cu,Zn-pWT^{SS} dimer. ITC was used to characterize the dimer interface, and in hopes to dissect the thermodynamics of the monomer, DSC was used to define the global unfolding of E,Zn-pWT^{SH}. In this chapter, we describe the difficulty of capturing a homogenous form of SOD1 involving a metal ion with an

affinity for both the zinc and copper site. Based on the analysis of $t_{m,app}$ values, the E,Zn-pWT^{SH} form is thermally less stable than both the E,E-pWT^{SS}, and Cu, Zn-pWT^{SS}.

2.2 Materials and Methods

2.2.1 Recombinant expression and purification of holo human SOD1

Expressed human pWT SOD1 (varies from wild-type by substituting Cys 6 and 111 with Ala and Ser, respectively)(40, 93) was expressed in *Escherichia coli* (strain QC799) cells with a pHSOD1ASlacI1 vector as described previously (28, 40, 41). Protein was purified using osmotic shock to release SOD1 from the periplasm and hydrophobic interaction chromatography to separate hSOD1 from other proteins present. Purity was determined using a sodium dodecyl sulfate polyacrylamide gel electrophoresis (SDS-PAGE).

2.2.2 Demetallation and reduction of holo SOD1

All chemicals are from BioShop Canada, unless otherwise stated. Holo SOD1 was demetallated through pH-induced unfolding and metal chelation using ethylenediaminetetraacetic acid (EDTA) as described previously (28, 70). Complete removal of metals was confirmed by differential scanning calorimetry, providing a characteristic t_m. The disulfide bonds formed by Cys 57 and 146 was reduced using chemical unfolding with 2 M guanidine hydrochloride followed by reduction with TCEP-HCl (40). Protein concentration was measured by the absorbance and the molar extinction coefficient of 5,400 M^{-1} cm^{-1} for SOD1 monomer at 280nm (94).

Reduction of the sample was confirmed by iodoacetamide modification of the free thiols and subsequently run on a SDS-PAGE (44).

2.2.3 Titration of Various Zinc Stoichiometry

A range of stoichiometric equivalents (0.5-2) of zinc sulfate (Fisher Scientific) was added to a reduced apo pWT sample, followed by an anaerobic incubation at ambient temperature. Correct metal status was verified using a chelator, 4-(2-pyridylazo)rescorcinol (PAR, Sigma-Aldrich). The assay was adopted from Crow *et al.* (33) and Mulligan *et al.* (95) as modified by the Meiering lab (96) (further explained in S2.0).

2.2.4 Using isothermal titration calorimetry (ITC) to measure dimer dissociation

ITC experiments were performed to characterize the dimer interface by measuring the heats of dissociation as described previously (97, 98) using a Microcal Isothermal Titration 200 instrument (Microcal Inc., Northhampton, MA). A concentrated sample of E,Zn-SOD1^{SH} (0.934-1.14 mM dimer in 20 mM HEPES and 1 mM TCEP (pH 7.4)) was prepared using ultrafiltration concentration. Small volumes (0.2-0.5 uL) of the sample were injected into the reaction cell containing an identical buffer, to measure the heat associated with dissociating the dimer. The dissociation was measured at a range of temperatures (10-37°C). Integrating the power versus time trace quantified the heats for each injection. The heat plots were fit using Microcal Origin 7.0 (Microcal Inc, Northhampton, MA, USA) to a dimer dissociation model (97, 98) using (Eq. 2.1):

$$q_i = V\Delta H_d\left(\left[M_i\right]-\left[M_{i-1}\right]\left(1-\frac{v}{V}\right)-f_m\left[M_o\right]\frac{v}{V}\right)+q_{dil} \qquad \text{(Eq. 2.1)}$$

where q_i is the heat of dissociation normalized per mol of total monomer injected, i is the injection number, V is the reaction cell volume, ΔH_d is the enthalpy of dimer dissociation (per mole of total protein as monomer), v is injection volume, $\left[M_o\right]$ is the total monomer concentration in the syringe, $\left[M_{i-1}\right]$ and $\left[M_i\right]$ is the total protein concentration in the cell before and after injection respectively, and q_{dil} is the heat of titrant dilution not related to dissociation. The fraction of monomer, f_m, present in the syringe is described by (Eq. 2.2):

$$f_m = \frac{1}{4\left[M_o\right]}\left(-K_d+\sqrt{K_d^2+8K_d\left[M_o\right]}\right) \qquad \text{(Eq. 2.2)}$$

where K_d is the dissociation constant from driving reduced E,Zn-pWT dimer $\left(N_2\right)$ to folded monomers $\left(M\right)$, $N_2 \rightleftharpoons 2M$. When fitting, ΔH_d, q_{dil} and K_d were set as floating parameter and were used to calculate $\Delta G_d(T_{\exp})$ using (Eq. 2.3):

$$\Delta G_d(T_{\exp}) = -RT_{\exp}\ln K_d(T_{\exp}) \qquad \text{(Eq. 2.3)}$$

where R is the universal gas constant.

2.2.5 Zinc titration using ITC

Zinc titrations were performed using ITC (Microcal Isothermal Titration 200 instrument (Microcal Inc., Northhampton, MA)) in a more commonly used manner to assess zinc affinity for both metal-binding sites in E,E-SOD1^{SH}. Both protein sample and titrant were degassed thoroughly prior to experiments, and the

reference cell was filled with MilliQ water. Volumes of 0.35 uL of $ZnSO_4$ (0.193 mM and 0.394 mM, Fischer Scientific) were injected into samples of pWT (0.0042 mM and 0.0079 mM, respectively) in 20 mM Hepes, 1mM TCEP at pH 7.4. Data were fit to a 2-site sequential binding model built into Microcal Origin 7.0.

2.2.6 Differential scanning calorimetry (DSC)

DSC experiments were performed as described previously (28), using an LLP cap DSC (MicroCal Inc., Malvern Instruments Ltd.). Varying concentrations of samples (0.68-4.143 mg mL^{-1}) in 20 mM Hepes, 1 mM TCEP at pH 7.4 were scanned at a rate of 1 °C $minute^{-1}$. Prior to data fitting, each protein scan has the reference scan, buffer versus buffer, subtracted from it and normalized to the protein concentration. Each scan was fit to both 2-state and 3-state with monomer intermediate models using Microcal Origin 7.0 (Microcal Inc., Northampton, MA, USA), represented by (Eq. 2.4) and (Eq. 2.5) respectively (28, 37, 99):

$$C_p = (A + Bt)(1-a) + (E + Ft)a + \left(\frac{b\Delta h_{cal}^2(t)}{RT^2}\right)\left(\frac{a(1-a)}{2-a}\right) \qquad \text{(Eq. 2.4)}$$

$$\begin{aligned} C_p = {} & (1-a_1)(A+Bt) + a_1(1-a_2)(C+Dt) + a_1a_2(E+Ft) + \\ & \left[\frac{b_1\Delta h_{cal,N_2\leftrightarrow 2M}(t) + a_2b_2\Delta h_{cal,M\leftrightarrow U}(t)}{RT^2}\right]\Delta h_{cal,N_2\leftrightarrow 2M}(t)\frac{a_1(1-a_1)}{2-a_1} + \\ & \left[\left[\frac{b_1\Delta h_{cal,N_2\leftrightarrow 2M}(t) + a_2b_2\Delta h_{cal,M\leftrightarrow U}(t)}{RT^2}\right]\frac{a_1a_2(1-a_1)}{2-a_1} + \left[\frac{b_2\Delta h_{cal,M\leftrightarrow U}(t)}{RT^2}\right]a_1a_2(1-a_2)\right] \\ & \Delta h_{cal,M\leftrightarrow U}(t) \end{aligned} \qquad \text{(Eq. 2.5)}$$

where C_p is the total specific heat absorption at temperature, t (in Celcius); A (E) represents the intercepts of the folded (unfolded) baseline; B (F) is the slope of the folded (unfolded) baseline; α is the extent of protein unfolding; β is the molecular

weight of the dimer multiplied by the ratio of van't Hoff to calorimetric enthalpy; Δh_{cal} is the specific calorimetric enthalpy of unfolding at unfolding; *R* is the universal gas constant; *T* is the temperature in Kelvin. The subscripts *1* and *2* are notation for dimer dissociation ($N_2 \leftrightarrow 2M$) and monomer unfolding ($M \leftrightarrow U$), respectively, and derivations are defined in A1.0.

2.3 Results and Discussion

2.3.1 The SOD1 dimer interface is less stable in E,Zn-pWT^{SH} than in E,E-pWT^{SS}

Through the unconventional use of ITC, the dimer interface was thermodynamically characterized (Table 2.1) by driving the dimer to dissociate in the calorimeter cell. When the predominately dimer sample (83-90% dimer in the syringe) dissociates in the ITC cell, small endothermic heats are observed that when integrated, result in small enthalpies of dissociation (Figure 2.1A, B). Fitting the integrated heats to a dimer dissociation model showed the interface for E,Zn-pWT^{SH} has a $K_{d,d}$ of 51μM and ΔH_d of 4.0 kcal (mol monomer)$^{-1}$ at pH 7.4 at 25°C. These values suggest a weak dimer interface relative to E,E-pWT^{SS} (52). To further characterize the E,Zn-pWT^{SH} dimer, the temperature-dependence of the dissociation enthalpy was measured over a range of 15-37°C. It was found that with increasing temperature, the dissociation heats increase and the interface weakens as expected for endothermic dissociation (Figure 2.1C). From the linear temperature dependence of ΔH_d, the change in heat capacity upon dimer dissociation, $\Delta C_{p,d}$, was measured as 0.22 ± 0.01 kcal (mol monomer)$^{-1}$ (Table 2.1, Figure 2.1). This value was determined using data for a temperature range of 15-32°C, and measurements

taken at the physiological temperature of 37°C were omitted due to the ΔH_d value being larger than predicted from the linear trend (Table 2.1, Figure 2.1). This deviation may be accounted for by additional heats from processes such as partial monomer unfolding upon dissociation at higher temperatures (see section 2.2).

Table 2.1. ITC measurements of the dimer interface of E,Zn-pWT^{SH} at varying temperatures.

SOD1 mutant	Temperature (°C)	$K_{d,d}$[1] (μM)	ΔH_d[1] (kcal (mol dimer)$^{-1}$)	ΔS_d[4] (kcal (mol dimer)$^{-1}$)	ΔG_d[5] (kcal (mol dimer)$^{-1}$)	$\Delta\Delta G_d$[6] (kcal (mol dimer)$^{-1}$)
pWT	15	71 ± 62	1.79 ± 0.62	-0.0128 ± 0.0002	5.47 ± 0.05	-0.39
	20	25 ± 5	3.11 ± 0.46	-0.0104 ± 0.0005	6.18 ± 0.06	0.31
	25	51 ± 41	4.01 ± 0.92	-0.0062 ± 0.0004	5.86 ± 0.04	na
	30	42 ± 21	5.16 ± 1.57	-0.0030 ± 0.0006	6.08 ± 0.04	0.21
	32	45 ± 8	5.6 ± 0.28	-0.0016 ± 0.0005	6.08 ± 0.03	0.21
	37	66 ± 8[2,3]	7.13 ± 0.14[2,3]	0.0039 ± 0.0003	5.93 ± 0.01	0.07

na, not applicable.

[1]Values are from fitting the integrated heats from ITC to a dimer dissociation model (Eq. 2.1).

[2]The first data point included heats from processes other than dissociation.

[3]Experiments were not repeated; therefore error is from the fit, not multiple experiments.

[4]Values were calculated using $\triangle S_d = -\frac{(\triangle G_d)(\triangle H_d)}{T}$

[5]Values were obtained from $K_{d,d}$ using Eq. 2.3.

[6]Difference of free energy mutant relative to pWT, $\triangle\triangle G_d = \triangle G_{mutant} - \triangle G_{pWT}$. Positive values represent destabilizing free energy.

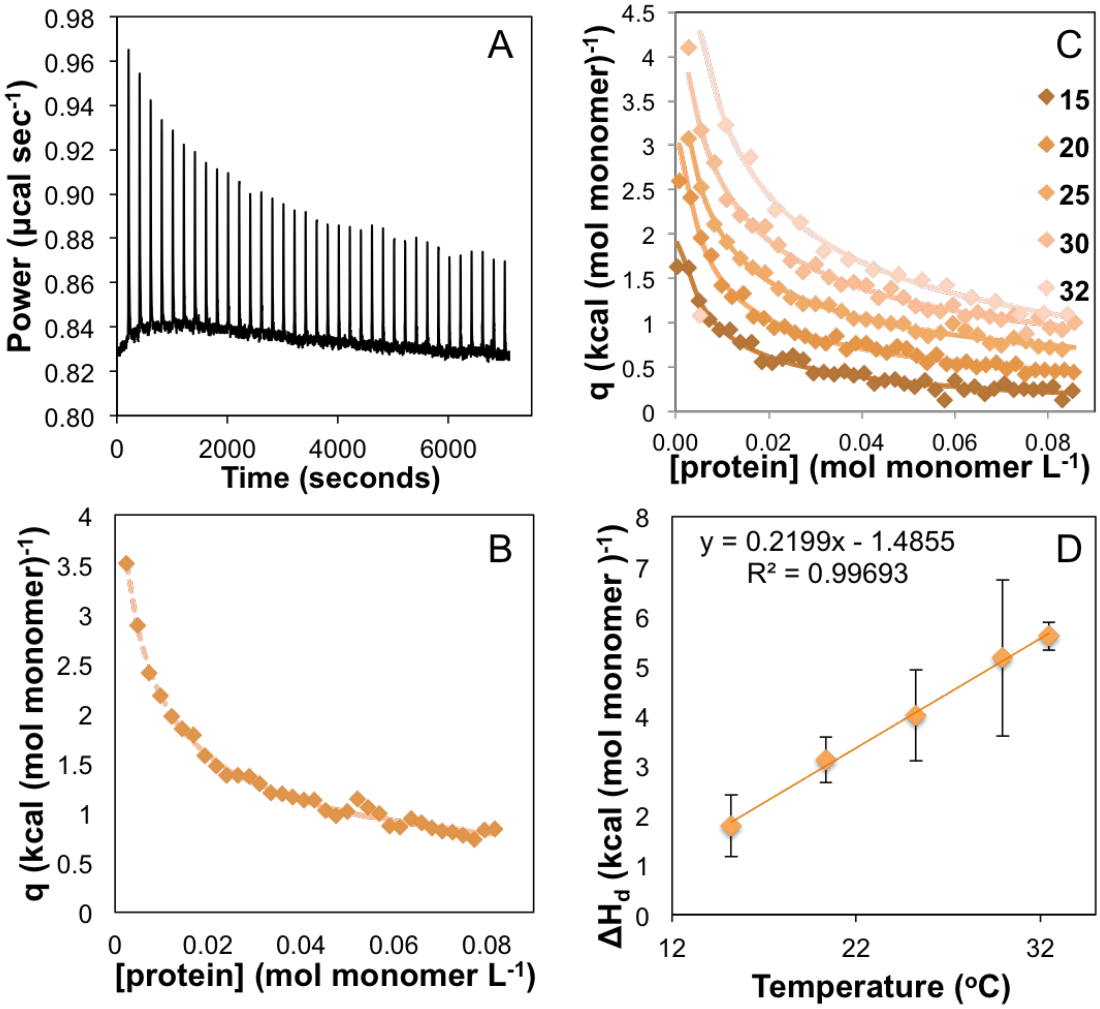

Figure 2.1. ITC of dimer dissociation for E,Zn-pWT^{SH} SOD1. A) Representative raw ITC isotherm of E,Zn-pWT^{SH} at 25°C. Each endothermic peak corresponds to the injection of concentrated (0.55-2.20 mM) E,Zn-pWT^{SH} into an identical buffer of 20 mM HEPES and 1 mM TCEP, pH 7.4. The heat measured for each peak results from the dimer dissociating in the reaction cell, which decreases with each successive injection due to the increase in protein concentration in the cell. (B) Integrated heats, q, from the raw data are plotted against protein concentration of the monomer (diamonds) which is fit to a dimer dissociation model (dashed line). (C) Integrated heats, q, for various temperatures overlaid with their respective fits to the dimer dissociation model (solid line), which show a weakened interface at higher temperatures. Data are offset for clarity. (D) Kirchoff plot of ΔH_d dependance on temperature. The ΔC_p, determined from the slope, is 0.22 ± 0.01 kcal (mol monomer)$^{-1}$°C^{-1}. Error bars were obtained from the fit values.

Traditionally, ITC is used to assess the interaction between two different binding partners, such as the binding affinity of a ligand to its cognate protein. Zinc has an extremely high affinity for the zinc site of E,E-pWT^{SH} (75 nM) (100), but also has the ability to bind to the copper site of E,E-pWT^{SH} with a relatively lower affinity (100 uM) (69). Although zinc has a high affinity for the zinc site, the affinity may be weakened for the monomer relative to the dimer, such that the initial ITC injection into the calorimeter cell might drive zinc release upon dimer dissociation. Zinc titrations into E,E-pWT^{SH} were monitored by ITC to ensure the dimer dissociation ITC experiments are measuring only heats from dimer dissociation and do not include zinc release upon monomerization. For the zinc titrations, protein concentrations were chosen to be low to ensure minimal protein dimerization upon zinc binding (>80% monomer), as well as to be representative of the protein concentration in the calorimeter cell after the initial injection in the ITC dimer dissociation experiment. The initial injection commonly results in the highest observed heat in the experiments (i.e. relative to subsequent injections) because the percent of protein that dissociates upon injection is highest due to mass action (Figure 2.1A). However, as we show here for pWT and for mutants in Section 3.3.2, such zinc dissociation is likely minimal.

Measuring quantitatively the binding of zinc to E,E-pWT^{SH} is at the limit of ITC capability (<10^{-6} M (101)), yet ITC can nevertheless be used qualitatively to assess zinc binding to both metal sites in SOD1. Figure 2.2 represents the zinc titration performed on E,E-pWT^{SH} at two protein concentrations, 4.2 μM and 7.9 μM total monomer, while Figure 2.3 gives a schematic of metal binding and SOD1

subunit association processes that may occur during the ITC experiment. The zinc ITC results for E,E-pWT^{SH} agree with previous findings of the zinc binding to the zinc site being very tight (75 nM) (69, 100); the observed heats up to ~1 equivalent of added zinc is referred to as Phase 1 (green dashed line in Figure 2.2, process 1 in Figure 2.3). Zinc binding to the copper site has a significantly lower affinity to E,Zn-pWT^{SH} (~80 uM, (69)), and the combined calorimetry data obtained here (ITC (Figure 2.2) and DSC (section 2.3.2)) indicate there is an additional process producing heat during the second zinc binding, referred to as Phase 2 (blue dashed line in Figure 2.2, processes 2 and 3 in Figure 2.3). The protein concentrations of 4.2 and 7.9 μM used for the E,E-pWT^{SH} zinc titration are well below the dimer dissociation $K_{d,d}$ for E,Zn-pWT^{SH} of ~51 μM (Figure 2.2, Table 2.1), ensuring that when zinc binds during Phase 1 there is limited dimerization (Figure 2.3). However, this appears not to be the case for the second zinc binding during Phase 2. In Phase 2 of the ITC experiment adding additional zinc results in smaller heats relative to Phase 1. We interpret these heats as arising from a combination of zinc binding and protein dimerization for the following reasons. First, experiments performed at higher protein concentration for predominantly dimeric E,Zn-V148I^{SH} (Section 3.3.2) exhibit smaller heats in Phase 2 (process 5 in Figure 2.3), relative to Phase 2 in E,E-pWT^{SH} (process 2 and 3 in Figure 2.3), that presumably reflect relatively small heats for weakened Zn binding to the copper site. These heats in Phase 2 for E,E-pWT^{SH} included the second Zn binding and dimerization, whereas due to the high concentration of V148I, it is already a dimer upon Phase 2, and thus heats are only from second Zn binding. Second, DSC of reduced pWT with various Zn

equivalents (see Section 2.3.2) show a significant $t_{m,app}$ dependence on SOD1 concentration that is consistent with a high affinity dimer interface in Zn,Zn-pWT^{SH} (35). Additional zinc equivalents can drive the Zn to bind to the copper site of a dimer, or to a monomer and simultaneously causes the now Zn,Zn-pWT^{SH} to dimerize, hence the heats are from zinc binding and dimerization. If the Zn,Zn-pWT^{SH} form is indeed dimerizing, it has a significantly tighter interface than the E,Zn-pWT^{SH} dimer, because the observation of dimerization at such a low protein concentration means the K_a is increased.

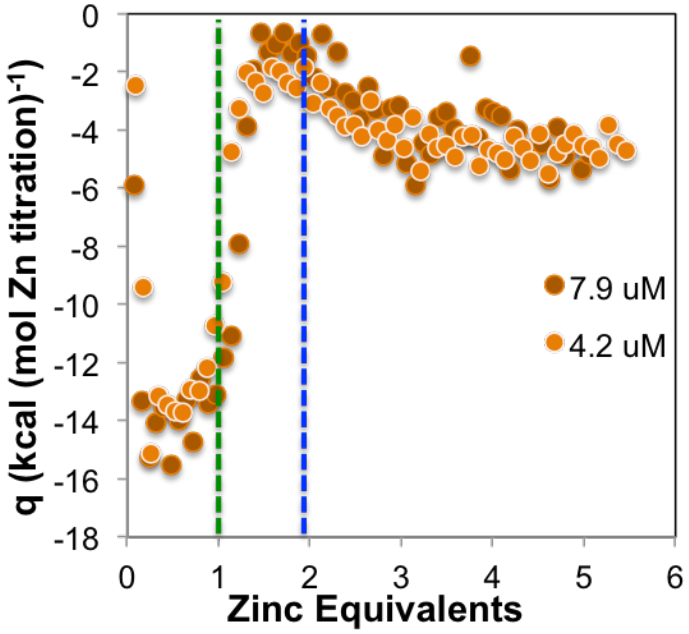

Figure 2.2. Zinc titration ITC isotherm with varying concentration of E,E-pWT^{SH}. E,E-pWT^{SH} (at two different concentrations, 4.2 µM and 7.9 µM) binding zinc in the first site (Phase 1, green dotted line) results in very large exothermic peaks. The smaller exothermic peaks for the zinc binding to the copper site (Phase 2, blue dashed line) are due to its decreased binding affinity and potential dimerization.

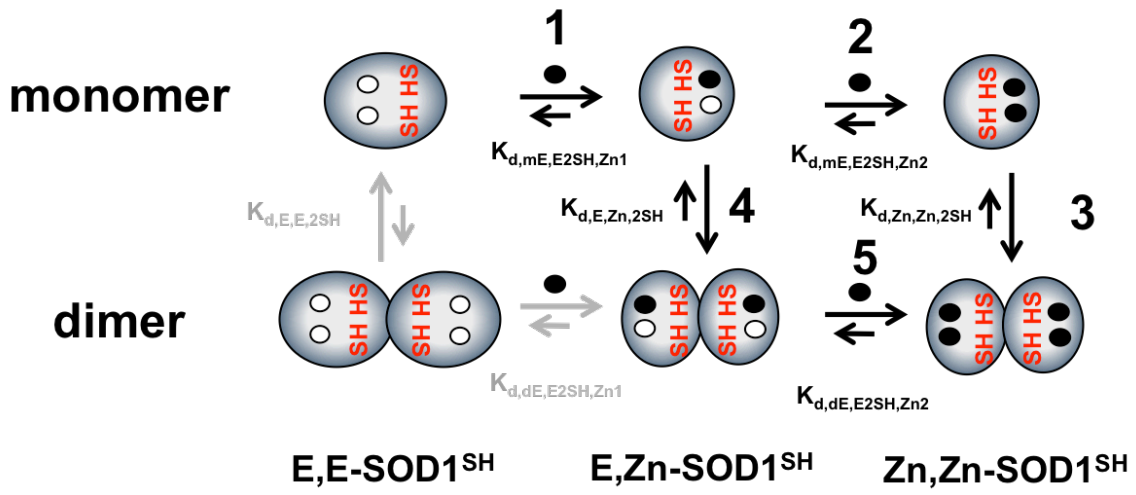

Figure 2.3. Zinc binding equilibrium to reduced SOD1. At low protein concentrations (0.0042-0.0079 mM) (Section 2.3.1 and 3.3.2), zinc titrating heats in Phase 1 are from process 1, and in Phase 2 it is from processes 2 and 3. At high protein concentrations (Section 3.3.2), Phase 1 has heats from processes 1 and 4 being coupled, followed by Phase 2 heats from process 5.

It is of interest to compare the characteristics of the dimer interface in E,Zn-pWT^{SH} with other forms of SOD1 to better understand maturation. Comparing effects of oxidation of the disulfide bond relative to zinc binding on the dimer interface revealed the $K_{d,d}$ for E,E-pWT^{SS} dimer is 67 nM (56), thus the dimer interface in this form of SOD1 is 1000-fold tighter than the E,Zn-pWT^{SH} dimer (51 μM) . Other studies support our results using different methodologies showing the equilibrium for the E,E-pWT^{SS} form favors dimer more than the E,Zn-pWT^{SH} form (84), which is consistent with the results presented here. The $\Delta C_{p,d}$ for E,E-pWT^{SS} was determined previously to be 0.85 ± 0.1 kcal (mol monomer)$^{-1}$ (52) indicating a relatively large structural change in the protein upon dissociation. The values of $\Delta C_{p,d}$ and ΔC_p of monomer unfolding relative to each other determine whether the dimer or monomer form predominately contribute to structure formation. The ΔC_p of unfolding for the E,E-pWT^{SS} monomer is considerably smaller than expected for a

well folded monomer of this size, suggesting formation of the dimer significantly contributes to structural formation (56). In contrast, the small ΔH_d and $\Delta C_{p,d}$ for E,Zn-pWT^{SH} suggest relatively little structural change upon dissociation, indicating that structure formation arises predominately from the monomer, rather than from the formation of the dimer. This hypothesis is supported by DSC results for E,Zn-pWT^{SH} which suggest the zinc-bound monomer has a relatively high $T_{m,app}$ of 55.8°C (Section 3.3.4).

This weakened interface of E,Zn-pWT^{SH} based on the ITC results above agree with previous studies that have shown at least a fraction of this form existing as a monomer (26, 44, 84, 102, 103), although no prior studies have precisely quantitated the strength of the interface thus far. E,Zn-pWT^{SH} is proposed to bind transiently to the CCS and continue along the maturation pathway (26), suggesting having a strong dimer interface would not be advantageous. Despite the requirement that a monomer bind to the CCS, transient homodimerization of E,Zn-SOD1^{SH} may nevertheless provide protection against aberrant interactions due to exposed dimer interfaces.

2.3.2 DSC of E,Zn-pWT^{SH} global unfolding

DSC was used to investigate the global protein unfolding of E,Zn-pWT^{SH}. It is of note that the pWT background is thermodynamically similar to the wild-type, but less prone to aggregation arising from the formation of aberrant disulfide bonds; thus this background is amenable to thermodynamic analysis, as has been conducted previously for other forms of SOD1 (28, 37, 41, 104). Instead of giving a

characteristic single peak as observed for prior studied forms of SOD1 (28, 37, 56), the unfolding endotherm for E,Zn-pWT^{SH} is a broad peak with multiple transitions (Figure 2.4A). The DSC scans were performed at 0.68-2.30 mg/mL, corresponding to concentrations of 34-53% monomer, respectively at 25°C based on the measured $K_{d,d}$ from ITC (Table 2.1). In principle, during thermal unfolding one might expect only two processes: dimer dissociation and monomer unfolding, however, a third process involving unfolding of a more thermally stable species is also observed ($t_{m,app}$ at 62°C, purple dashed line in Figure 2.4A). Prior DSC data on apo forms, E,E-pWT^{SH} (40)and E,E-pWT^{SS} (56), results in a single peak for global unfolding, however, adding Zn significantly complicated the endotherm with additional forms becoming populated. The $t_{m,app}$ (temperature at which the maximum of the thermogram occurs upon visual inspection), at ~57°C (green dashed line in Figure 2.4A), corresponding to the initial region of the unfolding thermogram, remained constant and independent of protein concentration, which is indicative of a monomeric form. However the second transition (purple dashed line in Figure 2.4A) shifts to higher $t_{m,app}$ with increasing protein concentration, which is characteristic of a dimer form. In attempts to dissect the different forms contributing to the E,Zn-pWT^{SH} thermogram, varying zinc stoichiometry and protein concentration were studied.

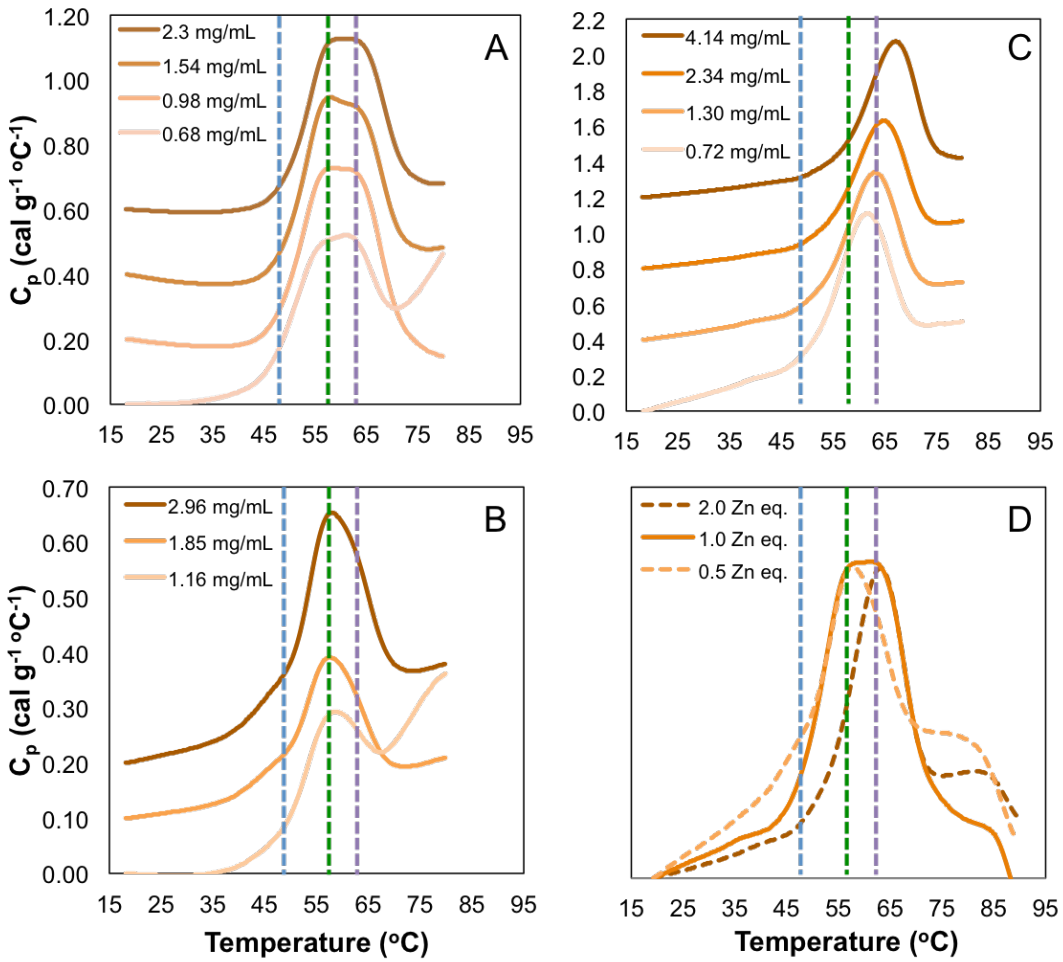

Figure 2.4. DSC of the disulfide reduced pWT as a function of varying equivalents of Zn. Each scan was offset for clarity, with the lowest concentration being the lower of the three scans and the highest concentration being at the top of each plot. The different dashed lines represent the t_m of different forms, E,E-pWT^{SH} monomer (blue line, obtained from Vassall *et al.,* 2011), E,Zn-pWT^{SH} monomer (green line, maximum of the thermogram for 0.5 Zn equivalents), and Zn,Zn-pWT^{SH} dimer (purple line, maximum of the thermogram for 2 Zn equivalents at 1.30 mg/mL), respectively. A) Endotherm of 1 Zn equivalence at varying protein concentrations in 20 mM Hepes, 1 mM TCEP, pH 7.4. 1 Zn equivalence concentrations were 0.68 mg/mL, 0.98 mg/mL, 1.54 mg/mL and 2.30 mg/mL. B) Thermal unfolding of disulfide reduced pWT with half a zinc equivalents at increasing protein concentrations. Half a Zn equivalents concentrations were 1.16 mg/mL, 1.85 mg/mL, and 2.96 mg/mL. C) Consecutive thermograms of Zn,Zn-pWT^{SH} are shown. 2 Zn equivalents concentrations included 0.72 mg/mL, 1.30 mg/mL, 2.34 mg/mL and 4.14 mg/mL. (D) Overlay of disulfide reduced pWT (1.16 mg/mL, 0.98 mg/mL and 1.30 mg/mL) at varying zinc equivalents (0.5, 1, and 2, respectively) to understand which forms are unfolding in E,Zn-pWT^{SH}. Data is normalized to overlay with the endotherm of E,Zn-pWT^{SH}.

2.3.3 DSC at varying zinc concentrations uncovers the population of multiple species during thermal unfolding of E,Zn-pWT^{SH}

Measuring the total protein unfolding at various zinc equivalents relative to SOD1 concentration explained the broadness of E,Zn-pWT^{SH} DSC endotherm. At half zinc equivalent, there was significant peak broadening due to the increased forms present (Figure 2.4B). In principle, multiple Zn-bound species may be populated due to the following: affinity of different SOD1 species for Zn, protein concentration, and Zn concentration. Therefore protein sample can include monomer with 0-2 Zn bound, and dimer with 1-4 Zn bound. Prior to thermal unfolding, there is at least half E,E-pWT^{SH} present, which unfolds at 48°C (blue dashed line in Figure 2.3B). The $t_{m,app}$ at 57°C (green dashed line, Figure 2.4B) remains constant regardless of increasing protein concentration, which is representative of monomer unfolding, as observed in section 2.3.2. Due to the consistent $t_{m,app}$ for both half Zn equivalents and 1 Zn equivalence, this $t_{m,app}$ is indicative of E,Zn-pWT^{SH} monomer (Figure 2.3A,B). This implies the dimer dissociation occurs at a lower temperature, and the larger heats at the initial endothermic transition of E,Zn-pWT^{SH} result from monomer unfolding. In comparison to E,E-pWT^{SS} monomer, which unfolds at 59.5°C, metal binding is less thermally stabilizing than disulfide formation (56). However as protein concentration increases an additional peak is observed ~62°C (purple dashed line, Figure 2.4B), which increases with increasing protein concentration indicative of dimer-like behavior; this was also observed with 1 zinc equivalent (purple line in Figure 2.4A, Section 2.3.2). This more thermally stable species

occurring at ~62°C (purple dashed line in Figure 2.4A-C) was defined by the thermogram for Zn,Zn-pWT^{SH} form (Figure 2.4C). Zn,Zn-pWT^{SH} endotherm has a very characteristic increase in $t_{m,app}$ with increasing protein concentration, which is consistent with this form existing as a dimer. This further reinforces that Zn,Zn-pWT^{SH} dimer has a strong interface because its dimer unfolding occurs at high temperatures, similar to the conclusions made with the zinc titration using ITC (Section 2.1). In addition, Zn,Zn-pWT^{SH} dimer is more thermally stable than E,Zn-pWT^{SH} dimer, which is intuitive since zinc binding in the copper site may have similar to the stabilizing effects on the interface from copper binding in fully mature Cu,Zn-SOD1^{SS}. Although zinc binding to the copper site has a lower affinity, dimerization of Zn,Zn-pWT^{SH} prevents the release of the zinc on the copper site, allowing for a single transition to be observed. As may be expected, Zn,Zn-pWT^{SH} is less stable than Cu,Zn-pWT^{SS}, due to the inability of the second zinc to completely imitate copper, and the lack of the disulfide bond.

Similarly, previous studies have reported difficulties with observing a single transition endotherm for a metal-binding protein, like SOD1 (47, 105, 106), where the endotherm shows multiple transitions. The thermogram for E,Zn-pWT^{SH} was dissected into the initial peak at ~57°C corresponding to E,Zn-pWT^{SH} monomer and the second transition at ~62°C belonging to Zn,Zn-pWT^{SH} dimer. In Figure 2.4D, the overlay of the half zinc equivalent and double zinc equivalent overlap with the one zinc equivalent endotherm and cumulatively describe the 2 zinc per dimer endotherm well. Initially the E,Zn-pWT^{SH} dimer dissociates at low temperatures due

to its weakened interface and then the resulting monomers begin to unfold (green dashed line in Figure 2.4A) which release their zinc. This free zinc can then bind to remaining folded E,Zn-pWT^{SH} monomer to form Zn,Zn-pWT^{SH}, which then dimerizes and unfolds in a 2-state manner at ~62°C (purple dashed line in Figure 2.4A). The ability for the zinc to shuffle and bind to the copper site creates difficulty in capturing solely E,Zn-pWT^{SH}, but also incorporates additional heats from processes such as zinc dissociation and association, as well as dimerization. DSC data was fit to various models: 2-state monomer, 2-state dimer and 3-state dimer with monomer intermediate unfolding, and the fits poorly described the endotherm (Figure A1.1-3, Table A1.1-3).

A prior study disregards the ability of the zinc to disassociate and bind to the copper site during thermal unfolding, and oversimplifies their thermograms for other forms of SOD1 (47). For instance, the multiple forms present in the thermogram of half zinc equivalent with a reduced disulfide bond (Figure 2.4B) is contrary to previous research done with the disulfide bond intact that claimed to have a homogenous species of E,E-pWT^{SS}-E,Zn-pWT^{SS} heterodimer (47). Instead of a broad asymmetric peak observed for half zinc equivalent in the reduced form (Figure 2.4B), the half zinc equivalent with the disulfide bond gave distinct peaks with minimal overlap. They concluded the initial peak belonged to dimer dissociation of the E,E-pWT^{SS}-E,Zn-pWT^{SS} heterodimer and the E,E-pWT^{SS} unfolding, followed by the now E,Zn-pWT^{SS} monomer forming a E,Zn-pWT^{SS} homodimer which then unfold at the later peak. However, there appears to be zinc shuffling occurring considering the thermogram with Zn,Zn-pWT^{SS} unfolded at roughly the same $t_{m,app}$

as their claimed E,Zn-pWT^{SS}-E,Zn-pWT^{SS} homodimer $t_{m,app}$. The slight variation in $t_{m,app}$ between the two thermograms can be accounted for by various populations existing with the E,E-pWT^{SS}-E,Zn-pWT^{SS} heterodimer. Less of the protein fraction exists as Zn,Zn-pWT^{SS} homodimer, compared to one homogenous population in the Zn,Zn-pWT^{SS} homodimer, hence the increased dimer shifts to higher $t_{m,app}$. Oversimplifying the DSC thermogram can lead to mischaracterization of thermal stability of metal-binding proteins and their various forms.

3.0 Summary

Through ITC, it was confirmed that E,Zn-pWT^{SH} is able to dimerize, although not as strongly as other maturation forms of SOD1. Recent studies used NMR to structurally characterize E,Zn-pWT^{SH}, and found binding of zinc structures the electrostatic loop and favours dimerization of E,Zn-pWT^{SH} (69). When comparing zinc binding to disulfide formation, it is abundantly clear that zinc bound forms exist as a weaker dimer and a less thermally stable monomer. The weakened dimer interface may allow for the CCS interaction to be transient, however, the ability to form weak homodimers may help protect against aggregation and proteolysis (107). Upon monomer formation, there is an increase in exposed hydrophobic residues that may aberrantly interact with itself and other proteins. Considering there is more SOD1 than CCS in the cell, it would mean that multiple SOD1 are catalyzed by one CCS, resulting in a potential backlog of SOD1 waiting to mature. These awaiting immature monomeric forms of SOD1 have an increased chance to non-natively interact to form aberrant stable structures (108, 109).

Previous studies have also found that metal bound forms of SOD1 have a decreased susceptibility to proteolysis compared to their metal-free counterparts form (107), which is likely due to the restructuring that occurs upon zinc binding (95). The thermal stability of the E,Zn-pWT^{SH} form results from the structure of the monomer and not the act of dimerization proven by characterizing the interface through ITC, and thermal unfolding through DSC. Studies have found structurally, the E,E-pWT^{SH} monomer has taken on a more open β-barrel structure with increased fluctuations in the loops, however with Zn addition, the protein structurally resembles that of the Cu, Zn-pWT^{SS} (69, 110). Both loops have high conformational freedom without the zinc or disulfide bond being present, which reduces affinity for dimerization (85), but binding the zinc ion leads to the zinc binding loop and electrostatic loop becoming more structurally restricted (69). This significant structural change agrees with the large change in heat capacity seen upon zinc binding (47).

Thermal unfolding of the E,Zn-pWT^{SH} form revealed multiple transitions occurring, which were attributed to zinc shuffling (47, 106). Using various zinc equivalents, the thermogram was dissected into the initial transition corresponding to E,Zn-pWT^{SH} monomer unfolding and the later half of the transition representing Zn,Zn-pWT^{SH} dimer unfolding. With the ITC data for the zinc titration of E,E-pWT^{SH}, the binding of the second zinc to the copper site leads to the formation of a strong dimer interface, which agrees with the DSC thermogram of Zn,Zn-pWT^{SH} (Figure 2.2). However, both the ITC and DSC concluded the dimer interface of E,Zn-pWT^{SH} is significantly weaker than other mature forms. This may be why it is the preferred

binding partner for CCS considering other forms with tighter interfaces, have been found to bind irreversibly.

Chapter 3
Thermodynamic characterization of E,Zn-SOD1^{SH} fALS mutants

3.1 Introduction

SOD1 undergoes multiple post-translational modifications to reach its highly stable homodimer native form (72). Previous studies indicate that maturation starts with the E,E-SOD1^{SH} monomer binding zinc through a currently unknown process to form E,Zn-SOD1^{SH} (26, 87). The copper chaperone (CCS) dimerizes with a E,Zn-SOD1^{SH} monomer and catalyzes both the copper binding and disulfide formation to produce Cu,Zn-SOD1^{SS} (29). Mutations may affect the various post-translational modifications, which may hinder proper maturation of the protein and promote misfolding and aggregation. To understand where the process may deviate from the norm, one needs to understand all the maturation steps including one of the least characterized forms of SOD1, E,Zn-SOD1^{SH}. Various studies have reported that some fALS mutants have a decreased affinity for binding zinc, and suggest that the E,E-SOD1^{SH} may be a key toxic species (33, 78, 94, 111, 112). As well, relative to the dimer dissociation of E,E-WT^{SS}, with a $K_{d,d}$ value of 67 nM (56), and the dimer interface of E,Zn-pWT^{SH} form is ~1000-fold weaker than that of E,E-pWT^{SS}, it indicates that the formation of the disulfide bond is more stabilizing for the dimer interface than zinc binding (43, 69, 85, 100). Decreased zinc affinity in fALS mutants, combined with a weakened dimer interface may explain why the interaction between mutant SOD1 and CCS may be disrupted (69, 113). This is further supported by studies that found some fALS mutants have zinc free populations, which is implicated in impairing the functionality of CCS (26, 32, 83). Recent research has shown that overexpression of CCS and copper can restore maturation of unstructured mutant SOD1 species that are unable to bind zinc (112).

In this chapter, we used ITC and DSC in a similar way as described in chapter 2 to define the dimer interface and monomer thermodynamic parameters for fALS mutants (A4V, H46R, V148G, and V148I) in the E,Zn-SOD1^{SH} form. Using both calorimetry approaches allows dissecting the two-step process of monomer folding and dimerization into its individual components, and discerning their relative contributions to stability. We found that aside from V148I, the mutants have significantly weakened dimer interfaces compared to pWT. For mutants with weakened dimer interfaces, we found that the DSC reported mainly on monomer stability. However for the stabilized V148I mutant, the thermal unfolding resembled that of the pWT, with multiple processes observed. Thus the mutants have a range of impacts on both the dimer and monomer E,Zn-SOD1^{SH} stability.

3.2 Methods

Methods for the preparation of mutant E,Zn-SOD1^{SH} and their analysis by ITC and DSC were as described in Section 2.2. for E,Zn-pWT^{SH} SOD1.

3.3 Results and Discussion

3.3.1 Rationale for selected mutations

In this chapter, four fALS mutants are characterized: A4V, H46R, V148G and V148I, all in a pWT background. These mutants were chosen because they have been previously well characterized thermodynamically and structurally for other forms of SOD1 previously, but not yet for the E,Zn-SOD1^{SH} form. A4V is a dimer interface mutant with one of the shortest average disease durations (~1 year); in contrast H46R is a metal binding mutant in the copper-binding site and has one of the longest average disease durations (~18 years). V148G and V148I are dimer

interface mutants that differ greatly in their thermodynamic stability (28, 40, 56) and aggregation propensities (34, 114), but are both associated with short disease durations (~2 years). Thus, these mutations represent both diverse structural and disease impacts.

3.3.2 fALS mutants E,Zn-SOD1^{SH} have varying effects on stability of the dimer interface relative to E,Zn-pWT^{SH}

Similar to E,Zn-pWT^{SH} in Chapter 2, ITC was used to characterize the thermodynamics of dimer dissociation for fALS mutants. The dissociation data fit well to a 2-state dimer dissociation model ($N_2 \leftrightarrow 2M$, Eq. 2.1) (summarized in Tables 3.1 and 3.2). Figure 3.1 illustrates that the integrated heats for pWT and the mutants all have noticeably small heats of dissociation, and small positive $\Delta C_{p,d}$ values (Figure 3.1B) relative to E,E-SOD1^{SS} (56). All fALS mutant E,Zn-SOD1^{SH} interfaces are significantly weaker than their E,E-SOD1^{SS} counterparts (Table 3.1), supporting that the formation of the disulfide contributes to a stronger interface than zinc binding (56, 65). However, unlike the E,E-SOD^{SS} form, not all mutations have destabilizing effects on the dimer interface relative to E,Zn-pWT^{SH} (Table 3.1). The interface for E,Zn-V148I^{SH} ($K_{d,d}$ of 39 μM at 25°C) is the only mutant seen to be slightly more stable than that of E,Zn-pWT^{SH} ($K_{d,d}$ of 51 μM at 25°C) (Figure 3.2A, Table 3.1). However, it is not possible to conclude that the interface stabilities differ significantly since the $K_{d,d}$ values have considerable variation among experiments and these values are deemed within error. It is interesting that E,Zn-V148I^{SH} dimer is similar in strength as in E,Zn-pWT^{SH}, but the interface is weaker for E,E-V148I^{SS}

relative to E,E-pWT^{SS}. This suggests that increased structuring of the dimer interface upon disulfide bond formation results in the effect of the mutation becoming more pronounced. The other three fALS mutants, H46R, A4V and V148G, significantly decrease the dimer strength, matching the trend for E,E-SOD1^{SS}, where H46R is less destabilizing and V148G has the weakest interface (65).

Table 3.1 ITC measurements of the dimer interface of E,Zn-SOD1^{SH} mutants.

SOD1 mutant	$K_{d,d}$[1] (μM) 25 °C	ΔH_d[1] (kcal (mol dimer)$^{-1}$) 25°C	ΔS_d[2] (kcal (mol dimer)$^{-1}$) 25 °C	ΔG_d[3] (kcal (mol dimer)$^{-1}$) 25 °C	$\Delta\Delta G_d$[4] (kcal (mol dimer)$^{-1}$) 25 °C	ΔG_d[5] (kcal (mol dimer)$^{-1}$) 15 °C
pWT	51 ± 41	4.01 ± 0.92	-0.0062 ± 0.0004	5.86 ± 0.03	na	5.47 ± 0.05
A4V	1056 ± 224[6]	2.07 ± 0.06	-0.007 ± 0.005	4.07 ± 0.96	1.79	4.41 ± 0.27
H46R	331± 507	3.40 ± 1.07	-0.005 ± 0.008	4.77 ± 0.79	1.09	4.09 ± 0.75
V148G	126044± 218200[7]	11.3 ± 9.66[7]	0.034 ± 0.124[6]	1.23 ± 3.14[6]	4.63[6]	3.49 ± 4.68[6]
V148I	39 ± 5[6]	4.12 ± 0.11[6]	-0.0064 ± 0.0002	6.02 ± 0.02	-0.16	5.80 ± 0.08
pWT^{SS}[8]	0.067 ± 0.050	30.8 ± 8.8	0.066 ± 0.019	10.30 ± 0.50	na	nd
A4V^{SS}[8]	34.2 ± 13.3	37.2 ± 3.8	0.099 ± 0.008	6.40 ± 0.30	3.8	nd
H46R^{SS}[8]	1.4 ± 1.1	16.2 ± 4.4	0.025 ± 0.009	8.4 ± 0.4	1.9	nd
V148G^{SS}[8]	76.8 ± 34	50.6 ± 1.4	0.144 ± 0.003	5.9 ± 0.3	4.3	nd
V148I^{SS}[8]	0.5 ± 0.2	11.4 ± 2.2	0.008 ± 0.005	8.9 ± 0.2	1.3	nd

na, not applicable.
nd, not determined.
[1]Values are from fitting the integrated heats from ITC to a dimer dissociation model (Eq. 2.1). Values are the average and standard deviation of 2-4 experiments.
[2]Values were calculated using $\Delta S_d = -\frac{(\Delta G_d)(\Delta H_d)}{T}$
[3]Values were calculated from $K_{d,d}$ using Eq. 2.3.
[4] Difference of free energy mutant relative to pWT, $\Delta\Delta G_d = \Delta G_{mutant} - \Delta G_{pWT}$. Positive values represent destabilizing interface for the mutant relative to pWT.
[5]Values were obtained from $K_{d,d}$ using Eq. 2.3, at 15°C since heats only from dimer dissociation were observed.
[6]Experiments were not repeated, therefore error is from the fit, not multiple experiments
[7]The first data point included processes other than dissociation.
[8]Data for dimer dissociation is for E,E-SOD1^{SS}, at 37°C. Values are average and standard deviation of 3-10 experiments. Data were obtained and analyzed by Helen R. Broom.

Table 3.2 Summary of ITC measurements of the dimer interface of E,Zn-SOD1^{SH} variants at various concentrations and temperatures.

SOD1 mutant	[SOD1] mM	t_{cell} (°C)	K_d[1] (μM)	ΔH_d[1] (kcal (mol dimer)$^{-1}$)
pWT	0.93	15.45	27.2 ± 5.7	2.23 ± 0.10
	1.10	14.98	115.0 ± 56.7	1.35 ± 0.09
	0.93	19.96	21.4 ± 3.2	3.44 ± 0.13
	1.14	20.76	29.0 ± 2.2	2.79 ± 0.26
	0.934	25.79	22.6 ± 2.3	5.04 ± 0.12
	1.14	24.98	32.2 ± 5.9	3.72 ± 0.16
	2.2	24.98	97.5 ± 10.4	3.27 ± 0.07
	0.55	24.98	8.03 ± 6.5	7.24 ± 1.95
	0.934	29.96	18.1 ± 2.3	6.96 ± 0.22
	1.14	29.96	63.2 ± 9.7	4.07 ± 0.10
	1.14	29.96	43.3 ± 7.0	4.45 ± 0.15
	2.2	32.45	50.8 ±6.8	5.80 ± 0.21
	0.75	32.46	39.6 ± 5.5	5.40 ± 0.13
	1.14[2]	36.96[2]	66.3 ± 8.3[2]	7.13 ± 0.14[2]
pWT avg (25°C)	**na**	**25.25**	**51 ± 41**	**4.01 ± 0.92**
A4V	1.34	10.09	177 ± 384	0.41 ± 0.14
	1.01	10.05	461 ± 686	0.51 ± 0.33
	1.01	14.98	403 ± 465	0.79 ± 0.37
	1.34	15.01	506 ± 273	1.25 ± 0.26
	1.34	20.89	497 ± 209	1.77 ± 0.29
	1.01	20.94	67 ± 79	0.71 ± 0.12
	1.27	25.38	798 ± 296	1.87 ± 0.36
	0.75	25.83	1190 ± 2440	2.13 ± 3.20
	1.99	25.69	1180 ± 327	2.21 ± 0.31
A4V avg (25°C)	**na**	**25.63**	**1056 ± 224[2]**	**2.07 ± 0.06**
H46R	1.3	10.06	180 ± 270	0.34 ± 0.09
	1.78	10.08	693 ± 364	1.12 ± 0.24
	1.3	14.98	1540 ± 1930	2.20 ± 1.86
	1.78	14.9	49 ± 27	0.86 ± 0.12
	1.3	19.87	5200 ± 8000	7.55 ± 10.00
	1.78	19.96	101 ± 46	0.95 ± 0.07
	1.3	25.22	907 ± 691	2.69 ± 1.13
	0.75	24.97	3 ± 6	4.63 ± 4.20
	1.75	25.71	57 ± 14	2.88 ± 0.17
H46R avg (25°C)	**na**	**25.30**	**331 ± 507**	**3.40 ± 1.07**
V148G	1.47	10.12	60 ± 79	0.37 ± 0.10
	1.55	10.17	412 ± 584	0.59 ± 0.26
	1.44	16.31	410 ± 304	0.75 ± 0.18
	1.55	15.24	4200 ± 32000	1.15 ± 7.21
	1.44[2]	19.92[2]	3 ± 54[2]	2.65 ± 19.20[2]
	1.47[2]	25.05[2]	0.63 ± 4.54[2]	15.70 ± 55.40[2]
	1.55[2]	25.75[2]	378000 ± 549000[2]	18.00 ± 16.00[2]
	1.55[2]	26.02[2]	133 ± 1070[2]	0.24 ± 0.41[2]
V148G avg (25°C)	**na**	**25.61**	**126044± 218200[3]**	**11.3 ± 9.66[3]**

V148I	1.1	10.54	42.3 ± 27.6	1.30 ± 0.18
	1.1	14.97	48.9 ± 17.3	2.21 ± 0.15
	1.42	15.37	31.1 ± 17.5	1.30 ± 0.18
	1.42	20.26	40.6 ± 14.3	1.87 ± 0.15
	1.42	19.98	27.2 ± 23.1	2.41 ± 0.62
	1.5	19.97	20.7 ± 16.0	2.13 ± 0.50
	1.5	19.97	5.4 ± 2.9	4.54 ± 0.96
	1.1	25.5	39.0 ± 4.6	4.12 ± 0.11
V148I avg (25°C)	**na**	**25.5**[3]	**39 ± 5**[3]	**4.12 ± 0.11**[3]

na, not applicable.
nd, not determined.
[1]Values are from fitting the integrated heats from ITC to a dimer dissociation model (Eq. 2.1).
[2]The first data point included processes other than dissociation.
[3]Experiments were not repeated, therefore uncertainty estimates are from the fit, not multiple experiments

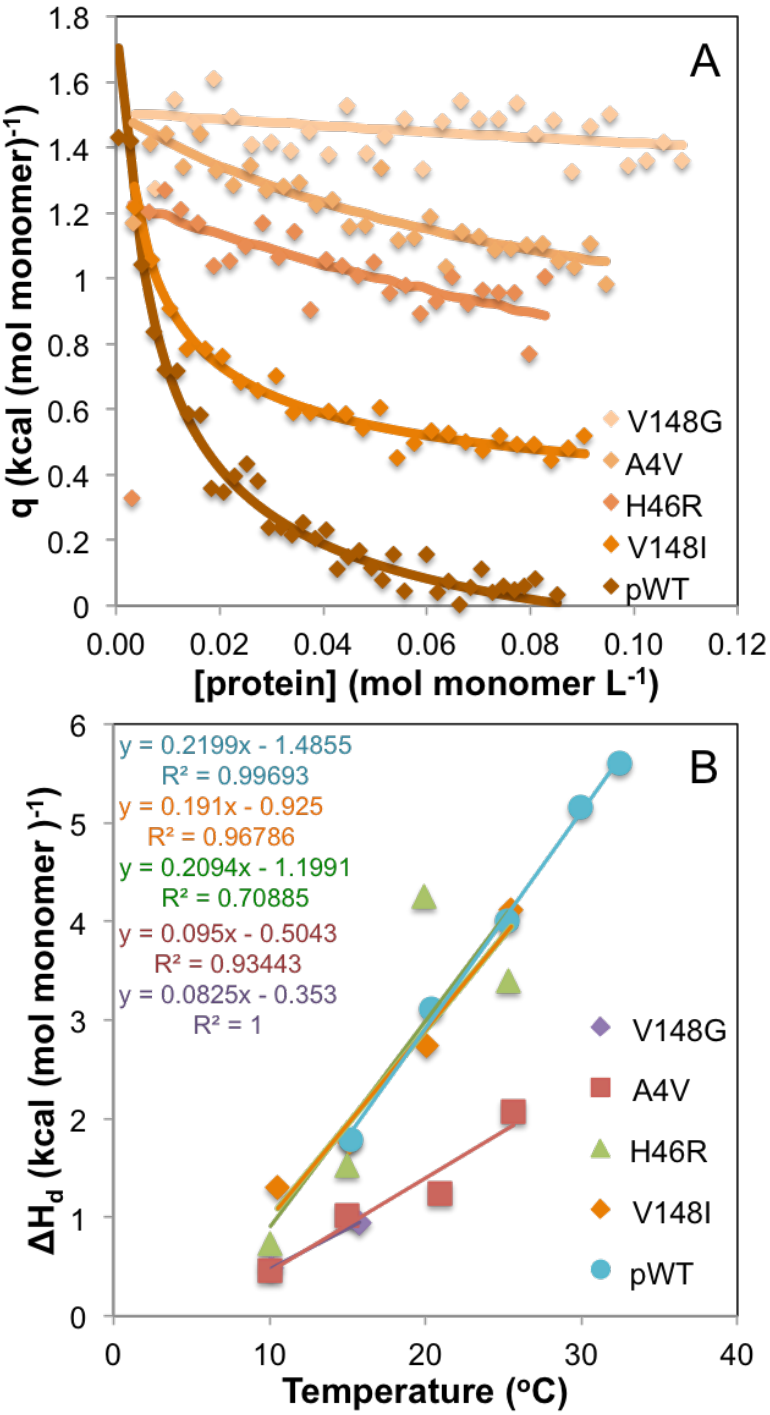

Figure 3.1. Dimer dissociation of fALS SOD1 mutants measured by ITC. A) Integrated heats, q, from the raw data of each mutant and pWT at 15°C are plotted (diamonds) against SOD1 monomer (diamonds) which is fit to a dimer dissociation model (solid line) Data are offset for clarity in order of increasing values of $K_{d,d}$. (B) Kirchoff plot of ΔH_d dependence on temperature. The ΔC_p, determined from the slope of the data (solid line), is 0.08 ± 0.00, 0.09 ± 0.02, 0.21 ± 0.09, 0.19 ± 0.02 kcal (mol monomer)$^{-1}$°C^{-1} for V148G, A4V, H46R, and V148I, respectively.

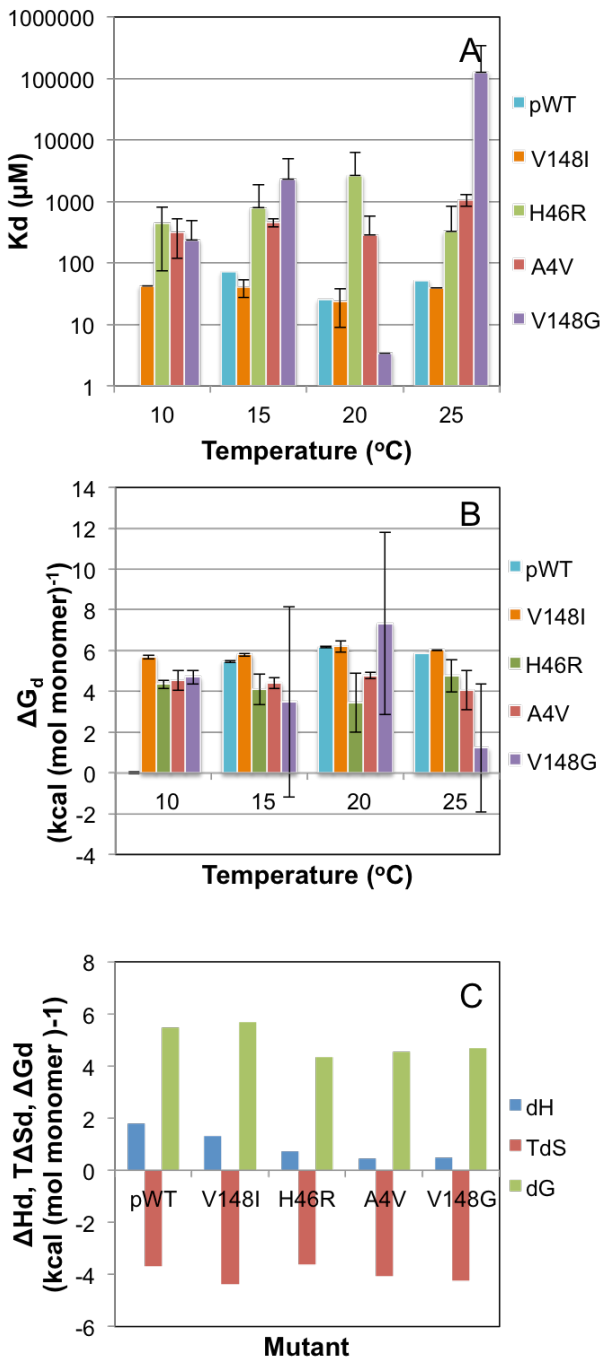

Figure 3.2. Thermodynamics of E,Zn-SOD1^{SH} dimer dissociation. (A) For H46R, A4V and V148G, the $K_{d,d}$ values typically increased with increasing temperature. V148I and pWT remain relatively constant throughout the temperature range. V148G at 20°C and 25°C had additional heats from monomer unfolding which contributed to skewed fit values. pWT was not measured at 10°C. (B) ΔG_d determined from ITC fit values using eq. 2.3. (C) ΔH_d, ΔS_d, and ΔG_d were determined by fitting heats of dissociation at 15°C. The values are summarized in Table 3.1.

The temperature dependence of the dissociation enthalpy for V148I and H46R is very similar to pWT (0.22 ± 0.01 kcal (mol monomer)$^{-1}$), with $\Delta C_{p,d}$ values of 0.19 ± 0.09 kcal (mol monomer)$^{-1}$ and 0.21 ± 0.02 kcal (mol monomer)$^{-1}$, respectively (Figure 3.1B). ΔH_d, ΔS_d, and ΔG_d values are shown in Figure 3.2. V148I and H46R also have similar enthalpies of dissociation as pWT at the varying temperatures (10-25°C), suggesting upon dimer dissociation there are similar increases in exposed hydrophobic residues or structural rearrangement (116). However, for A4V and V148G the enthalpy and heat capacity of dissociation are smaller than for the other variants, which is likely attributed to the weak interface that forms for the population that does dimerize. The ΔH_d at each temperature and $\Delta C_{p,d}$ values for A4V are roughly half of those for pWT, H46R and V148I, consistent with less structural change upon dissociation. Interestingly, for V148G at the higher end of the temperature range explored (particularly 20°C, Table 3.2), heats of dimer dissociation behave similarly to pWT at 37°C (section 2.3.1, Table 2.1), where the heats from the initial injection are very large and do not follow a linear dependence. As a result, the $K_{d,d}$ and ΔH_d values for V148G at higher temperatures (Table 3.2) are overestimated like the pWT values at 37°C, which suggests other processes were occurring aside from dimer dissociation, such as partial monomer unfolding and potential zinc dissociation. For V148G at 20°C and 25°C, the large initial heat influenced the fit values to give an unreasonably high enthalpy and unrealistically low $K_{d,d}$, hence the data from 20°C and 25°C were not used for $\Delta C_{p,d}$ analysis. Although taking $\Delta C_{p,d}$ from just two temperature points has a high uncertainty

associated with it, the value of 0.08 kcal (mol monomer)$^{-1}$ does not appear to be unreasonable, due to its similarities in value to that of A4V. Considering the propensity to dimerize is quite low for V148G, it yields smaller heats from dissociation, but also the small $\Delta C_{p,d}$ value indicates a smaller temperature dependence of dissociation enthalpy and less hydrophobic residue exposure upon dissociation.

In comparison to the E,E-SOD1^{SS} counterpart, all E,Zn-SOD1^{SH} mutants have a smaller temperature dependence of dissociation enthalpy consistent with less structural rearrangement upon dimer dissociation. In the E,E-SOD1^{SS}, the global protein stability is strongly dependent on dimerization, and the $\Delta C_{p,d}$ is large relative to the smaller $\Delta C_{p,M\leftrightarrow U}$ (56). However, the higher $t_{m,app}$ value (Section 2.3.2) for the E,Zn-SOD1^{SH} monomer relative to the small $\Delta C_{p,d}$ dimer interface indicates that the structural stability for this form is predominately from the monomer. Antibody studies corroborate the weakened dimer interface for this form, since conformation specific antibodies were able to bind to exposed dimer interfaces in aggregates from ALS patients (115, 116).

3.3.3 Zinc titration ITC reveals only H46R has large changes in zinc binding affinity

To ensure the ITC dimer dilution experiments are not measuring heats of zinc dissociating upon monomerization, mutants were titrated with zinc as described for pWT in Chapter 2. Figure 3.3A,B shows the isotherms from titrating zinc into concentrations of E,E-SOD1^{SH} that are representative of the initial injection of the dimer dissociation experiment (see Section 2.2.1). Previous studies found that

H46R has a weakened affinity for copper and zinc (112), thus it is not surprising that H46R is the only one of the fALS mutants studied here that shows limited heats for zinc binding to the first site (green dashed line in Figure 3.3A). V148I and A4V still bind the first zinc with a similar affinity to that of pWT, whereas V148G appears slightly weaker (Figure 3.3A,B).

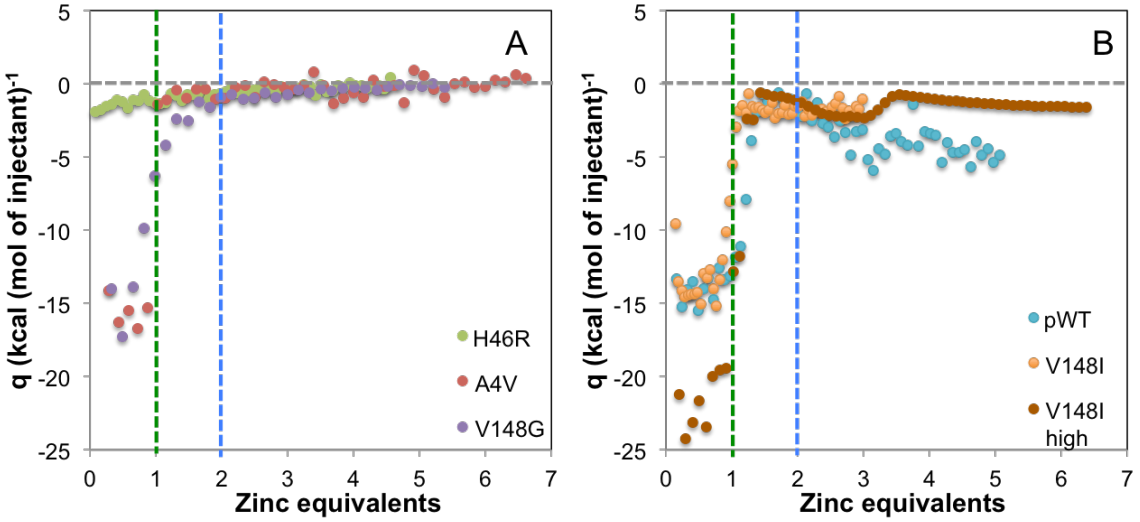

Figure 3.3. ITC upon addition of zinc to E,E-SOD1^{SH}. Zinc titration (0.393 mM) into ~0.008 mM SOD1 monomer produced exothermic peaks for all variants (except V148I, 86.8 mM Zn into 1.46 mM E,E-V148I^{SH} monomer, brown). The initial phase (Phase 1, up to ~ 1 equivalent of added zinc, green dashed line) corresponds to tight binding of zinc to the zinc site. In a second phase (Phase 2, around 2 equivalents of added zinc, blue dashed line), zinc may bind to the copper site. Associated heats of subunit association depend on the protein concentration (see main text). Horizontal gray dashed line is the reference for zero heats. (A) Zinc titration for A4V, H46R and V148G; all three variants did not have a second process occurring in Phase 2. (B) Zinc titration data for pWT and V148I with high (1.46 mM) and low (0.008 mM) concentrations, respectively. Both variants have clear apparent heats for Phase 2.

To validate that the heats observed for pWT for Phase 2 include not only the heat of binding of the second zinc but also the heat of dimerization, as proposed earlier (see results Section 2.3.1, Figure 2.3), a higher concentration of E,E-V148I^{SH} (200-fold higher than pWT and other variants, Figure 3.3B) was also analyzed. This higher protein concentration helps to isolate the heats of the second zinc binding

from those of the dimerization process observed in Phase 2. As stated in Section 2.3.1, Phase 1 involves the first zinc binding to the zinc site (green dashed line in Figure 3.3), and Phase 2 involves the second zinc binding the copper site (blue dashed line in Figure 3.3). The higher protein concentration promotes both the first zinc binding (process 1) and dimerization (process 4) in Phase 1.Then, in Phase 2, it promotes observation of the heats of Zn binding to the Cu site of E,Zn-V148I^{SH} dimer (process 5), rather than monomer; in contrast, Zn binding to the monomer (process 3) is predominantly observed at lower protein concentrations, e.g. for pWT (Section 2.3.1) and other mutants (Figure 3.3). Figure 2.3 summarizes the processes observed for both phases at high protein concentrations, such as 1.46 mM of E,Zn-V148I^{SH}, during Phase 1 processes 1 and 4 are occurring followed by process 5 in Phase 2.

In contrast for low protein concentrations, such as ~0.008 mM for all fALS mutants and pWT, Phase 1 reflects predominately process 1, and Phase 2 includes heats from both the processes of 2 (second zinc binding) and 3 (dimerization) (Figure 2.3, Figure 3.3). Notably, only the two variants with the strongest dimer interfaces, V148I and pWT, appear to exhibit the combination of heats of dimerization and zinc binding to the copper site in Phase 2 at low protein concentration (Figure 3.3B). For pWT, the protein concentration is lower than the $K_{d,d}$ for pWT E,Zn-SOD1^{SH}, thus the protein remains mostly monomeric throughout binding of the first Zn (Phase 1, process 1). However, the heats for Phase 2 appear to involve both the heats of metal binding and associated dimerization of Zn,Zn-pWT^{SH} (processes 2 and 3), due to the heats being larger in Phase 2 at lower protein

concentrations in pWT than for V148I at higher concentrations (Figure 3.3B). In contrast, for E,E-V148I^{SH} at 200-fold higher concentration, binding of the first zinc (Phase 1, process 1) includes dimerization of E,Zn-SOD1^{SH} (process 4), as indicated by larger observed heats due to both processes occurring, compared to pWT which has only process 1. Also, the heats for V148I Phase 2 are decreased because they correspond only to the binding of the second zinc (process 5) to the already largely formed dimer, whereas for pWT at lower protein concentration, Phase 2 reflects a combination of heats from binding of the second zinc and dimerization. Heats for Phase 2 are not apparent for V148G and A4V (Figure 3.3A), which suggests that the binding of the second zinc is either too weak or cannot stabilize the interface enough for the protein to dimerize at these concentrations, unlike pWT. Together, the data for the mutants support the interpretation of observed ITC heats upon zinc titration as proposed for pWT (section 2.3.1), and are also consistent with DSC results, described below.

3.3.4 A4V with bound zinc has thermal stability similar to that of Zn,Zn-pWT^{SH} dimer

Thermal unfolding of A4V at varying concentrations (0.40-1.76 mg/mL) was measured, and based on the dimer dissociation ITC results, the samples are predominately monomer (84.8-95.6%, respectively, Table 3.3). The observed thermogram for E,Zn-A4V^{SH} is a broad peak comparable to that of E,E-A4V^{SS} (56). The broadness is characteristic of non-2-state like behavior, where typically 2-state unfolding provides a sharp thermogram. Although the broadness of E,E-A4V^{SS} is explained by monomer intermediate becoming populated along the dimer unfolding

and fitting well to 3-state dimer unfolding (56), E,Zn-A4V^{SH} did not fit to this 3-state model due to the lack of dimerization (Figure 3.4A, Figure A1.4, Table A1.1). The lack of dimer is supported by the absence of the characteristic increase in observed temperature ($t_{m,app}$) with increasing protein concentration that arises from increased dimer formation. The DSC data for A4V were also fit to 2-state monomer and 2-state dimer models again with little success likely due to the broadness of the endotherm, and the presence of a large exotherm present at high temperatures (Figure A1.5-6, Table A1.4-5).

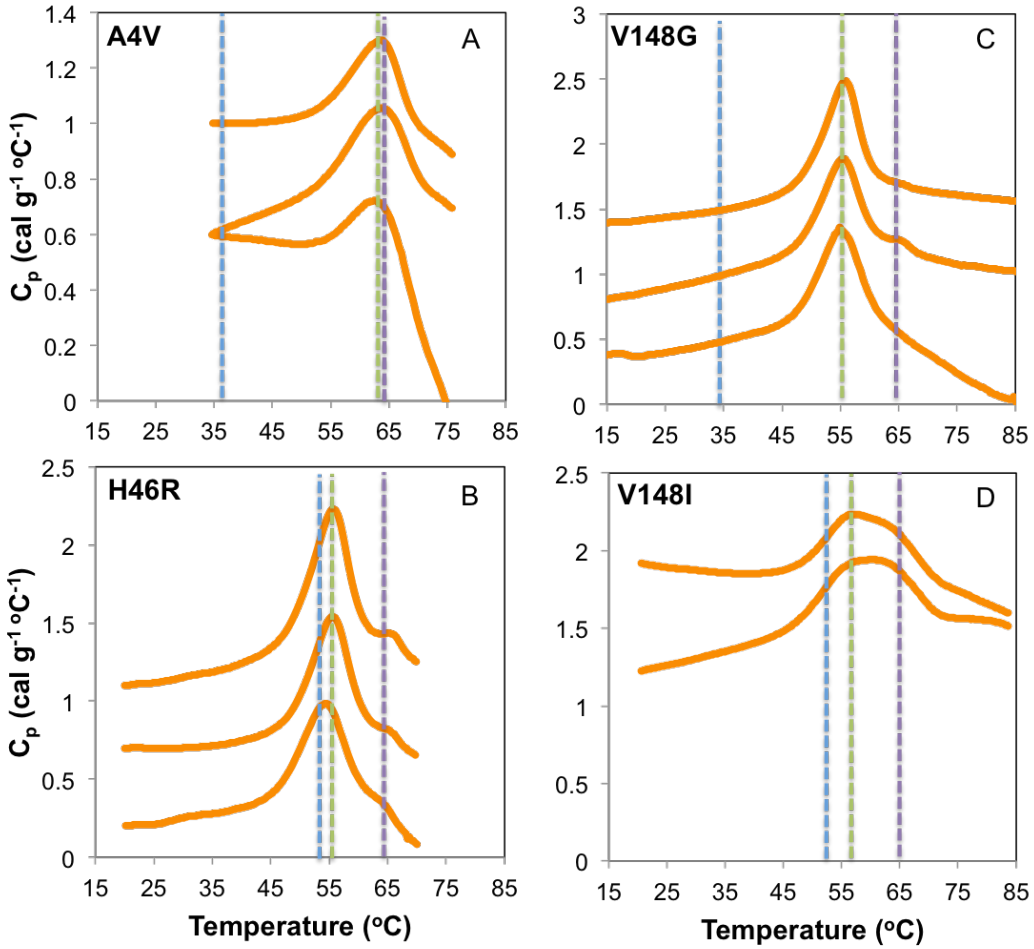

Figure 3.4. Thermogram for fALS SOD1 mutants at varying protein concentrations. Each scan is offset for clarity, with the lower scans representing the lower concentrations, to the highest scan belonging to the largest protein concentration. The blue, green, and purple dashed lines represent the t_m of different forms, E,E-SOD1^{SH} monomer, E,Zn-SOD1^{SH} monomer/dimer, and Zn,Zn-pWT^{SH} dimer, respectively. H46R concentrations were 0.42 mg/mL, 0.92 mg/mL, and 1.52 mg/mL. A4V concentrations were 0.31 mg/mL, 0.79 mg/mL, and 1.76 mg/mL. V148G concentrations were 0.35 mg/mL, 0.82 mg/mL, and 1.80 mg/mL. V148I concentrations included 0.59 mg/mL, 1.17 mg/mL, and 2.10 mg/mL.

Table 3.3. Fraction of monomer at 25°C in DSC protein concentrations and their $t_{m,app}$

SOD1 mutant	*Conc* (mg/mL)	$t_{m,app}$[1] (°C)	Monomer Fraction[2] (%)
pWT	**0.68**	**55.8, 59.1**[3]	**52.8**
	0.98	**56.9, 59.6**[3]	**46.7**
	1.54	**57.1, 60.5**[3]	**39.7**
	2.30	**57.7, 51.2**[3]	**34.0**
A4V	**0.40**	**62.9**	**95.6**
	0.79	**63.5**	**92.9**
	1.76	**63.7**	**84.8**
H46R	**0.42**	**54.2**	**87.3**
	0.92	**55.5**	**78.0**
	1.52	**55.6**	**70.3**
V148G	**0.35**	**55.1**	**99.7**
	0.82	**55.5**	**99.7**
	1.80	**55.8**	**99.7**
V148I	**0.59**	**56.0, 60.8**[3]	**50.6**
	1.16	**56.2, 61.4**[3]	**39.8**
	2.10	**56.0, 62.2**[3]	**31.6**
0.5 Zn pWT	**1.16**	**58.0**	**na**
	1.85	**57.5**	**na**
	2.96	**58.0**	**na**
2.0 Zn pWT	**0.72**	**61.6**	**na**
	1.30	**63.2**	**na**
	2.34	**64.8**	**na**
	4.14	**67.0**	**na**

na, not applicable.
[1]Values are based on visual observation of the maximum of the transition peak.
[2]Monomer fractions were calculated using eq. 2.2.
[3]The initial value is for the initial transition, and then for the second transition observed

The $t_{m,app}$, for E,Zn-A4V^{SH} of ~63°C (green dashed line in Figure 3.4A) is unexpectedly high for a monomer despite all other forms of this mutant are significantly thermally destabilized relative to pWT (40, 56). Based on the pronounced broadness of the endotherm corresponding to non-2-state like behaviour, and considering the increased thermal stability is similar to that of with Zn,Zn-pWT^{SH} (purple dashed line in Figure 3.4A), not E,Zn-pWT^{SH} (~57°C), it is likely that additional forms are becoming populated along the thermogram. Analogous to pWT (Section 2.3.3), the zinc from unfolding E,Zn-A4V^{SH} monomer

may be released and bind to a folded E,Zn-A4V^{SH} monomer, to form Zn,Zn-A4V^{SH} monomer. For pWT, when both metal binding sites are occupied, the protein forms a strong dimer as indicated by the following: the $t_{m,app}$ dependence on protein concentration of Zn,Zn-pWT^{SH} (Section 2.3.3), and the zinc titration isotherm (Figure 2.2), which showed heats during Phase 2 for zinc binding to the second site and dimerization at low protein concentrations (Section 2.2.1). However, for A4V, the $t_{m,app}$ remains constant with varying protein concentration and the ITC isotherm (Figure 3.3A, Section 3.3.3) did not show additional heats for Phase 2, supporting that Zn,Zn-A4V^{SH} is likely a monomer. In order to further validate the preceding conclusions, similar experiments to those performed for pWT (e.g. DSC with varying protein concentrations and zinc equivalents) should be performed for A4V.

Recent research using chemical exchange saturation transfer (CEST) experiments found E,Zn-A4V^{SH} disrupts the native interface, shifting the equilibrium of this mutant to favor monomer and not dimer (56). These results support our calorimetry findings of the weakened dimer interface for E,Zn-A4V^{SH} (Section 3.3.2). The prior studies also showed that E,Zn-A4V^{SH} binding to CCS is significantly weaker than CCS with pWT (69), and multiple studies found that A4V is able to bind copper and have similar functional enzymatic activity to WT (30, 119). However, *in vivo* A4V populations have a copper-deficiency, suggesting this mutant may be impaired in maturation due to impaired binding of CCS rather than the inability to bind copper as stated earlier (120). It was proposed that being unable to mature causes an accumulation of less stable forms that results in the protein folding chaperones becoming overloaded, and functionally depleted (121). Thus, A4V's inability to form

a strong dimer may prevent it from forming a heterodimer with CCS, and ultimately not fully maturing.

3.3.5 Zinc shuffling is not observed in H46R due to weakened metal affinity

H46R is a metal binding mutant with weakened affinity for zinc and copper (112). H46 is a copper liganding residue, and its mutation to arginine greatly weakens copper binding but also significantly weakens Zn binding to an extent (117). Although the DSC sample contained predominately monomer (70.3-87.2%, Table 3.3), there was a slight increase in $t_{m,app}$ with increasing protein concentration (green dashed line in Figure 3.4B), characteristic of dimer formation. However, attempting to fit to a 2-state dimer or monomer model, and 3-state dimer unfolding with monomer intermediate model did not give consistent values (Figure A1.4-6, Table A1.1, A1.4-5), likely again due to additional protein forms becoming populated along the thermogram, as well as the presence of an exotherm at high temperature. Due to H46R being a metal-binding mutant, the copper may compete for binding to the zinc site because it is incapable of binding metal to the copper site (122). Consequently Zn,Zn-H46R^{SH} (monomer or dimer) is likely not populated during DSC scans because zinc shuffling will not occur; thus the observed dimer unfolding is likely representative of E,Zn-H46R^{SH}. Notably, for H46R the weakened zinc binding (Section 3.3.3, Figure 2.3A) may cause the zinc to become unbound from a fraction of the E,Zn-H46R^{SH} protein population along the transition, which manifests as unfolding of E,E-H46R^{SH} monomer, which has a t_m of 52.6°C (blue dashed line in Figure 3.4B) (40). The similar thermal stability between E,E-H46R^{SH} (blue dashed

line in Figure 3.4B) monomer and E,Zn-H46R^{SH} dimer/monomer (green dashed line in Figure 3.4B), reinforces that the weakened zinc affinity results in little thermal stabilization. Due to H46R having weakened metal binding, zinc shuffling is not observed, rather the thermogram may be representative of metal free and zinc bound forms.

Other studies have also found that zinc binding did not thermally stabilize the E,E-H46R^{SH} significantly relative to disulfide bond formation (56). When analyzing the crystal structures of E,E-H46R^{SS} and E,Zn-H46R^{SS}, it was found that zinc coordination may be occurring using only 3 of the 4 typical residues involved, leading to less structural stability (123). This unusual fALS mutant behavior may also explain why the electrostatic and zinc binding loops are largely structurally disordered (118), further supporting that zinc binding to H46R, probably due to the weakened zinc affinity, does not thermally stabilize the mutant.

3.3.6 V148G serves as a monomer control for the zinc-bound form, whereas stabilizing mutant, V148I had a global endotherm similar to pWT

Due to E,Zn-V148G^{SH} having the weakest dimer interface (Table 3.1), DSC samples consisted of 99.7% monomer. Not surprisingly, there is no change in $t_{m,app}$ (green dashed line in Figure 3.4C) with increasing protein concentration, consistent with monomer unfolding. Zinc binding provides a large increase in thermal stability ($t_{m,app}$ of ~55°C) to the E,E-V148G^{SH} monomer ($t_{m,app}$ of ~34°C) (blue dashed line in Figure 3.4C) compared to the stabilizing effect of disulfide bond formation (E,E-V148G^{SS}, t_m is 48.6°C). If this state is truly E,Zn-V148G^{SH} monomer, it would be the

only mutant studied here where zinc binding is more stabilizing than oxidizing the disulfide bond. However, there was no clear evidence of multiple Zn-bound species in the thermogram, thus, it is not clear whether the peak observed at 55°C corresponds to V148G with one or two bound zincs. Studies using NMR CEST experiments on E,E-SOD1^{SH} variants, revealed an impaired ability of E,E-V148G^{SH} and E,E-A4V^{SH} to form a transient dimer which may contribute to decreased metal binding (see also Section 3.3.3) (124). Also, the CEST experiments may explain the definite lack of zinc binding to the copper site for H46R and potentially V148G (if strictly only populate E,Zn-V148G^{SH} during the endotherm) because E,E-V148G^{SH} and E,E-H46R^{SH} are unable to access an excited state where the native helix is present in the electrostatic loop (124). This trend is supported by E,E-A4V^{SH} as well: it can bind zinc to both sites, as suggested by DSC data in section 3.3.4, and is able to transiently form the native helix similarly to pWT through CEST (119). Taken together, the lack of excited conformers with the helix in the electrostatic loop and weak dimerization in the most immature form may propagate to disrupt metal binding in V148G and H46R and do not form species with 2 bound zincs in the DSC scans, whereas A4V and pWT do.

Comparing V148G to V148I, it is very interesting to see the dramatic difference that an amino acid substitution can make. The endotherm for V148I (31.6-50.6% monomer at 25°C, Table 3.1) is pWT-like, with peak broadening due to zinc shuffling and both sites binding zinc (Figure 3.4D). The initial portion of the transition is expected to be E,Zn-V148I^{SH} monomer (green dashed line in Figure

3.4A), due to the similarities in $t_{m,app}$ with E,Zn-pWT^{SH} monomer and the characteristic constant $t_{m,app}$ at varying protein concentrations. Similar to pWT, the later half of the transition likely reports on Zn,Zn-V148I^{SH} dimer. There is a slight shift in the estimated center of the endotherm for Zn,Zn-V148I^{SH} to higher $t_{m,app}$ with increased protein concentrations, and the $t_{m,app}$ occurs at a similar temperature to that observed for Zn,Zn-pWT^{SH} (purple dashed line in Figure 3.4A). Additional support for Zn,Zn-V148I^{SH} existing as a dimer is the small heats observed in the 2nd phase of the zinc ITC titration experiments at low protein concentration for both pWT and V148I, inferred to be dimerization and second zinc binding (Figure 3.3B). This WT-like behavior of V148I is also seen structurally for the homodimer for E,Zn-V148I^{SS} (114) and Cu,Zn-V148I^{SS} (68) through NMR experiments. In summary, the calorimetric experiments are consistent with other studies, and collectively show a wide range of effects of disease mutations on metal binding affinity and dimerization of the E,Zn-SOD1^{SH} form.

3.4 SUMMARY

The calorimetry data for fALS mutants showed the variable stabilizing effects mutants can have on the E,Zn-SOD1^{SH}. Our ITC data revealed that most fALS mutants, aside from V148I, have a significantly weakened dimer interface relative to pWT. Binding of the first zinc promotes dimerization, but not as tightly as disulfide formation, which is expected due to the zinc binding site being located more distal from the interface relative to the disulfide bond. The $\Delta C_{p,d}$ are small values, indicating minimal structural rearrangement upon dimer dissociation. However in

the E,E-SOD1^{SS} form, the values are larger due to the form having more of the structure conformation stemming from being a dimer, rather than a monomer. Interestingly, binding of the second zinc is associated with increased dimer affinity (Figure 2.2, section 2.1, Figure 3.3, and section 3.3). Due to the weakened interface for V148G, A4V and H46R, the thermal unfolding using DSC captured mostly a monomeric species. V148G and H46R are thought to be E,Zn-SOD1^{SH} form, whereas from zinc shuffling A4V formed Zn,Zn-SOD1^{SH}. V148I proved hard to fit due to similarities in the endotherm with pWT, where the zinc shuffling and stable dimer interface allowed for multiple forms to unfold. Moreover, the thermal stability E,Zn-SOD1^{SH} of pWT and mutants relative to each other did not vary significantly. Considering most of the DSC endotherms reported on monomer species, the E,Zn-SOD1^{SH} monomer is quite stable based on the relatively high $t_{m,app}$ values. This form, E,Zn-SOD1^{SH}, is biologically relevant as it binds to CCS to mature further, and mutations, such as A4V, may disrupt this vital interaction leading to potential protein misfolding and aggregation. More research would need to be done to validate these conclusions including varying zinc concentration with protein.

CHAPTER 4
Future works

The studies in this thesis elucidated how truly weak the interface is for most fALS mutants in the reduced, zinc-bound form, regardless of their thermal stability. This form of SOD1 is believed to be a crucial in protein maturation, however it has been relatively little characterized structurally and thermodynamically. This opens up many avenues for future research. Recently, NMR was used to investigate the structure and dynamics of the disulfide reduced zinc bound form for pWT (69), but little is yet known about the fALS mutants. Conducting experiments on fALS mutants could provide great insight into their folding. Here we used ITC to assess the strength of the SOD dimer interface and DSC to characterize the monomer stability.

Further key experiments could involve the CCS, and characterizing the strength of the interface between the CCS and fALS mutants SOD1s for various maturation forms, and comparing with previous studies (26). This may provide key data as to whether some fALS mutants are unable to bind to the CCS (16), and paired with NMR, may reveal the structural reasons behind it. Besides pWT characterization of the form, exploring possible excited conformers of fALS mutants through CEST may elucidate potential explanations for aberrant interactions. Previously, CEST showed that some fALS mutants were unable to access excited conformers that the WT was able to access, which may be essential for maturation (119). Another avenue to explore would be the interface in the Zn,Zn-SOD1^{SH} dimer for fALS mutants, which would help resolve heats for different transitions in the complicated one zinc equivalent per monomer endotherms (Section 3.3.4-6). This

experiment, paired with structurally studying the form of interest with NMR, would help explain effects of zinc binding aberrantly to the copper site on the structure. Further understanding the structural and thermodynamics components of this form will provide an insight to a potential interface disruption, which may be linked to protein misfolding that is characteristic of ALS.

References

1. Daggett, V., and Fersht, A. (2003) The present view of the mechanism of protein folding, *Nat Rev Mol Cell Biol 4*, 497-502.

2. Onuchic, J. N., and Wolynes, P. G. (2004) Theory of protein folding, *Curr Opin Struct Biol 14*, 70-75.

3. Jahn, T. R., and Radford, S. E. (2005) The Yin and Yang of protein folding, *FEBS J 272*, 5962-5970.

4. Englander, S. W., Mayne, L., and Krishna, M. M. (2007) Protein folding and misfolding: mechanism and principles, *Q Rev Biophys 40*, 287-326.

5. Hartl, F. U., and Hayer-Hartl, M. (2009) Converging concepts of protein folding in vitro and in vivo, *Nat Struct Mol Biol 16*, 574-581.

6. Toal, S., and Schweitzer-Stenner, R. (2014) Local Order in the Unfolded State: Conformational Biases and Nearest Neighbor Interactions, *Biomolecules 4*, 725-773.

7. Dobson, C. M. (2004) Principles of protein folding, misfolding and aggregation, *Semin Cell Dev Biol 15*, 3-16.

8. Wood, L. K., and Langford, S. J. (2014) Motor neuron disease: a chemical perspective, *J Med Chem 57*, 6316-6331.

9. Rosen, D. R., Siddique, T., Patterson, D., Figlewicz, D. A., Sapp, P., Hentati, A., Donaldson, D., Goto, J., O'Regan, J. P., Deng, H. X., and et al. (1993) Mutations in Cu/Zn superoxide dismutase gene are associated with familial amyotrophic lateral sclerosis, *Nature 362*, 59-62.

10. Valentine, J. S., Doucette, P. A., and Zittin Potter, S. (2005) Copper-zinc superoxide dismutase and amyotrophic lateral sclerosis, *Annu Rev Biochem 74*, 563-593.

11. Gulesserian, T., Seidl, R., Hardmeier, R., Cairns, N., and Lubec, G. (2001) Superoxide dismutase SOD1, encoded on chromosome 21, but not SOD2 is overexpressed in brains of patients with Down syndrome, *J Investig Med 49*, 41-46.

12. Jaarsma, D., Haasdijk, E. D., Grashorn, J. A., Hawkins, R., van Duijn, W., Verspaget, H. W., London, J., and Holstege, J. C. (2000) Human Cu/Zn superoxide dismutase (SOD1) overexpression in mice causes mitochondrial vacuolization, axonal degeneration, and premature motoneuron death and

accelerates motoneuron disease in mice expressing a familial amyotrophic lateral sclerosis mutant SOD1, *Neurobiol Dis 7*, 623-643.

13. Ling, S. C., Polymenidou, M., and Cleveland, D. W. (2013) Converging mechanisms in ALS and FTD: disrupted RNA and protein homeostasis, *Neuron 79*, 416-438.

14. Pasinelli, P., and Brown, R. H. (2006) Molecular biology of amyotrophic lateral sclerosis: insights from genetics, *Nat Rev Neurosci 7*, 710-723.

15. Fukai, T., and Ushio-Fukai, M. (2011) Superoxide dismutases: role in redox signaling, vascular function, and diseases, *Antioxid Redox Signal 15*, 1583-1606.

16. Furukawa, Y., Torres, A. S., and O'Halloran, T. V. (2004) Oxygen-induced maturation of SOD1: a key role for disulfide formation by the copper chaperone CCS, *EMBO J 23*, 2872-2881.

17. Tainer, J. A., Getzoff, E. D., Beem, K. M., Richardson, J. S., and Richardson, D. C. (1982) Determination and analysis of the 2 A-structure of copper, zinc superoxide dismutase, *J Mol Biol 160*, 181-217.

18. Banci, L., Benedetto, M., Bertini, I., Del Conte, R., Piccioli, M., and Viezzoli, M. S. (1998) Solution structure of reduced monomeric Q133M2 copper, zinc superoxide dismutase (SOD). Why is SOD a dimeric enzyme?, *Biochemistry 37*, 11780-11791.

19. Broom, H. R., Rumfeldt, J. A., and Meiering, E. M. (2014) Many roads lead to Rome? Multiple modes of Cu,Zn superoxide dismutase destabilization, misfolding and aggregation in amyotrophic lateral sclerosis, *Essays Biochem 56*, 149-165.

20. Rakhit, R., and Chakrabartty, A. (2006) Structure, folding, and misfolding of Cu,Zn superoxide dismutase in amyotrophic lateral sclerosis, *Biochim Biophys Acta 1762*, 1025-1037.

21. Banci, L., Bertini, I., Boca, M., Girotto, S., Martinelli, M., Valentine, J. S., and Vieru, M. (2008) SOD1 and amyotrophic lateral sclerosis: mutations and oligomerization, *PLoS One 3*, e1677.

22. Reaume, A. G., Elliott, J. L., Hoffman, E. K., Kowall, N. W., Ferrante, R. J., Siwek, D. F., Wilcox, H. M., Flood, D. G., Beal, M. F., Brown, R. H., Jr., Scott, R. W., and Snider, W. D. (1996) Motor neurons in Cu/Zn superoxide dismutase-deficient mice develop normally but exhibit enhanced cell death after axonal injury, *Nat Genet 13*, 43-47.

23. Gurney, M. E., Pu, H., Chiu, A. Y., Dal Canto, M. C., Polchow, C. Y., Alexander, D. D., Caliendo, J., Hentati, A., Kwon, Y. W., Deng, H. X., and et al. (1994) Motor neuron degeneration in mice that express a human Cu,Zn superoxide dismutase mutation, *Science 264*, 1772-1775.

24. Tu, P. H., Raju, P., Robinson, K. A., Gurney, M. E., Trojanowski, J. Q., and Lee, V. M. (1996) Transgenic mice carrying a human mutant superoxide dismutase transgene develop neuronal cytoskeletal pathology resembling human amyotrophic lateral sclerosis lesions, *Proc Natl Acad Sci U S A 93*, 3155-3160.

25. Joyce, P. I., Fratta, P., Fisher, E. M., and Acevedo-Arozena, A. (2011) SOD1 and TDP-43 animal models of amyotrophic lateral sclerosis: recent advances in understanding disease toward the development of clinical treatments, *Mamm Genome 22*, 420-448.

26. Banci, L., Bertini, I., Cantini, F., Kozyreva, T., Massagni, C., Palumaa, P., Rubino, J. T., and Zovo, K. (2012) Human superoxide dismutase 1 (hSOD1) maturation through interaction with human copper chaperone for SOD1 (hCCS), *Proc Natl Acad Sci U S A 109*, 13555-13560.

27. Lindberg, M. J., Normark, J., Holmgren, A., and Oliveberg, M. (2004) Folding of human superoxide dismutase: disulfide reduction prevents dimerization and produces marginally stable monomers, *Proc Natl Acad Sci U S A 101*, 15893-15898.

28. Stathopulos, P. B., Rumfeldt, J. A., Karbassi, F., Siddall, C. A., Lepock, J. R., and Meiering, E. M. (2006) Calorimetric analysis of thermodynamic stability and aggregation for apo and holo amyotrophic lateral sclerosis-associated Gly-93 mutants of superoxide dismutase, *J Biol Chem 281*, 6184-6193.

29. Endo, T., Fujii, T., Sato, K., Taniguchi, N., and Fujii, J. (2000) A pivotal role of Zn-binding residues in the function of the copper chaperone for SOD1, *Biochem Biophys Res Commun 276*, 999-1004.

30. Goto, J. J., Zhu, H., Sanchez, R. J., Nersissian, A., Gralla, E. B., Valentine, J. S., and Cabelli, D. E. (2000) Loss of in vitro metal ion binding specificity in mutant copper-zinc superoxide dismutases associated with familial amyotrophic lateral sclerosis, *J Biol Chem 275*, 1007-1014.

31. Culotta, V. C., Klomp, L. W., Strain, J., Casareno, R. L., Krems, B., and Gitlin, J. D. (1997) The copper chaperone for superoxide dismutase, *J Biol Chem 272*, 23469-23472.

32. Proescher, J. B., Son, M., Elliott, J. L., and Culotta, V. C. (2008) Biological effects of CCS in the absence of SOD1 enzyme activation: implications for disease in a mouse model for ALS, *Hum Mol Genet 17*, 1728-1737.

33. Crow, J. P., Sampson, J. B., Zhuang, Y., Thompson, J. A., and Beckman, J. S. (1997) Decreased zinc affinity of amyotrophic lateral sclerosis-associated superoxide dismutase mutants leads to enhanced catalysis of tyrosine nitration by peroxynitrite, *J Neurochem 69*, 1936-1944.

34. Wang, Q., Johnson, J. L., Agar, N. Y., and Agar, J. N. (2008) Protein aggregation and protein instability govern familial amyotrophic lateral sclerosis patient survival, *PLoS Biol 6*, e170.

35. Rumfeldt, J. A., Galvagnion, C., Vassall, K. A., and Meiering, E. M. (2008) Conformational stability and folding mechanisms of dimeric proteins, *Prog Biophys Mol Biol 98*, 61-84.

36. Khare, S. D., Caplow, M., and Dokholyan, N. V. (2004) The rate and equilibrium constants for a multistep reaction sequence for the aggregation of superoxide dismutase in amyotrophic lateral sclerosis, *Proc Natl Acad Sci U S A 101*, 15094-15099.

37. Vassall, K. A., Stathopulos, P. B., Rumfeldt, J. A., Lepock, J. R., and Meiering, E. M. (2006) Equilibrium thermodynamic analysis of amyotrophic lateral sclerosis-associated mutant apo Cu,Zn superoxide dismutases, *Biochemistry 45*, 7366-7379.

38. Jackson, S. E. (1998) How do small single-domain proteins fold?, *Fold Des 3*, R81-91.

39. Svensson, A. K., Bilsel, O., Kayatekin, C., Adefusika, J. A., Zitzewitz, J. A., and Matthews, C. R. (2010) Metal-free ALS variants of dimeric human Cu,Zn-superoxide dismutase have enhanced populations of monomeric species, *PLoS One 5*, e10064.

40. Vassall, K. A., Stubbs, H. R., Primmer, H. A., Tong, M. S., Sullivan, S. M., Sobering, R., Srinivasan, S., Briere, L. A., Dunn, S. D., Colon, W., and Meiering, E. M. (2011) Decreased stability and increased formation of soluble aggregates by immature superoxide dismutase do not account for disease severity in ALS, *Proc Natl Acad Sci U S A 108*, 2210-2215.

41. Rumfeldt, J. A., Stathopulos, P. B., Chakrabarrty, A., Lepock, J. R., and Meiering, E. M. (2006) Mechanism and thermodynamics of guanidinium chloride-induced denaturation of ALS-associated mutant Cu,Zn superoxide dismutases, *J Mol Biol 355*, 106-123.

42. Lindberg, M. J., Bystrom, R., Boknas, N., Andersen, P. M., and Oliveberg, M. (2005) Systematically perturbed folding patterns of amyotrophic lateral sclerosis (ALS)-associated SOD1 mutants, *Proc Natl Acad Sci U S A 102*, 9754-9759.

43. Sekhar, A., Rumfeldt, J. A., Broom, H. R., Doyle, C. M., Bouvignies, G., Meiering, E. M., and Kay, L. E. (2015) Thermal fluctuations of immature SOD1 lead to separate folding and misfolding pathways, *Elife 4*, e07296.

44. Furukawa, Y., and O'Halloran, T. V. (2005) Amyotrophic lateral sclerosis mutations have the greatest destabilizing effect on the apo- and reduced form of SOD1, leading to unfolding and oxidative aggregation, *J Biol Chem 280*, 17266-17274.

45. Rumfeldt, J. A., Lepock, J. R., and Meiering, E. M. (2009) Unfolding and folding kinetics of amyotrophic lateral sclerosis-associated mutant Cu,Zn superoxide dismutases, *J Mol Biol 385*, 278-298.

46. Kayatekin, C., Zitzewitz, J. A., and Matthews, C. R. (2010) Disulfide-reduced ALS variants of Cu, Zn superoxide dismutase exhibit increased populations of unfolded species, *J Mol Biol 398*, 320-331.

47. Potter, S. Z., Zhu, H., Shaw, B. F., Rodriguez, J. A., Doucette, P. A., Sohn, S. H., Durazo, A., Faull, K. F., Gralla, E. B., Nersissian, A. M., and Valentine, J. S. (2007) Binding of a single zinc ion to one subunit of copper-zinc superoxide dismutase apoprotein substantially influences the structure and stability of the entire homodimeric protein, *J Am Chem Soc 129*, 4575-4583.

48. Hwang, Y. M., Stathopulos, P. B., Dimmick, K., Yang, H., Badiei, H. R., Tong, M. S., Rumfeldt, J. A., Chen, P., Karanassios, V., and Meiering, E. M. (2010) Nonamyloid aggregates arising from mature copper/zinc superoxide dismutases resemble those observed in amyotrophic lateral sclerosis, *J Biol Chem 285*, 41701-41711.

49. Mulligan, V. K., Kerman, A., Laister, R. C., Sharda, P. R., Arslan, P. E., and Chakrabartty, A. (2012) Early steps in oxidation-induced SOD1 misfolding: implications for non-amyloid protein aggregation in familial ALS, *J Mol Biol 421*, 631-652.

50. Rodriguez, J. A., Shaw, B. F., Durazo, A., Sohn, S. H., Doucette, P. A., Nersissian, A. M., Faull, K. F., Eggers, D. K., Tiwari, A., Hayward, L. J., and Valentine, J. S. (2005) Destabilization of apoprotein is insufficient to explain Cu,Zn-superoxide dismutase-linked ALS pathogenesis, *Proc Natl Acad Sci U S A 102*, 10516-10521.

51. Bai, Y., Englander, J. J., Mayne, L., Milne, J. S., and Englander, S. W. (1995) Thermodynamic parameters from hydrogen exchange measurements, *Methods Enzymol 259*, 344-356.

52. Broom, H. R., Rumfeldt, J. A., Vassall, K. A., and Meiering, E. M. (2015) Destabilization of the dimer interface is a common consequence of diverse ALS-associated mutations in metal free SOD1, *Protein Sci 24*, 2081-2089.

53. Velazquez-Campoy, A., Leavitt, S. A., and Freire, E. (2015) Characterization of protein-protein interactions by isothermal titration calorimetry, *Methods Mol Biol 1278*, 183-204.

54. Freire, E., Mayorga, O., and Straume, M. (1990) Isothermal Titration Calorimetry, *Analytical Chemistry 62*, 950A-959A.

55. McMahon, H. T. Isothermal Titration Calorimetry (ITC), MRC Laboratory of Molecular Biology, Cambridge, UK.

56. Broom, H. R., Vassall, K. A., Rumfeldt, J. A., Doyle, C. M., Tong, M. S., Bonner, J. M., and Meiering, E. M. (2016) Combined Isothermal Titration and Differential Scanning Calorimetry Define Three-State Thermodynamics of fALS-Associated Mutant Apo SOD1 Dimers and an Increased Population of Folded Monomer, *Biochemistry 55*, 519-533.

57. Makhatadze, G. I., and Privalov, P. L. (1995) Energetics of protein structure, *Adv Protein Chem 47*, 307-425.

58. Khechinashvili, N. N., Janin, J., and Rodier, F. (1995) Thermodynamics of the temperature-induced unfolding of globular proteins, *Protein Sci 4*, 1315-1324.

59. Sanchez-Ruiz, J. M. (2011) Probing free-energy surfaces with differential scanning calorimetry, *Annu Rev Phys Chem 62*, 231-255.

60. Sturtevant, J. M. (1987) Biochemical Applications of Differential Scanning Calorimetry, *Annu. Rev. Phys. Chem*, 463-488

.

61. Burgos, I., Dassie, S. A., and Fidelio, G. D. (2008) Thermodynamic model for the analysis of calorimetric data of oligomeric proteins, *J Phys Chem B 112*, 14325-14333.

62. Cooper, A. (2005) Heat capacity effects in protein folding and ligand binding: a re-evaluation of the role of water in biomolecular thermodynamics, *Biophys Chem 115*, 89-97.

63. Burgos, I., Dassie, S. A., Villarreal, M. A., and Fidelio, G. D. (2012) Thermodynamic and structural analysis of homodimeric proteins: model of beta-lactoglobulin, *Biochim Biophys Acta 1824*, 383-391.

64. Doyle, C. M., Rumfeldt, J. A., Broom, H. R., Broom, A., Stathopulos, P. B., Vassall, K. A., Almey, J. J., and Meiering, E. M. (2013) Energetics of oligomeric protein folding and association, *Arch Biochem Biophys 531*, 44-64.

65. Broom, H. R. (2015) Decreased stability and increased formation of soluble aggregates by immature SOD1 do not account for disease severity in ALS.

66. Bruylants, G., Wouters, J., and Michaux, C. (2005) DIfferential Scanning Calorimetry in Life Sciences: Thermodynamics, Stability, Molecular Recognition and Application in Drug Design, *Current Medicinal Chemistry 1*, 2011-2020.

67. Nordlund, A., Leinartaite, L., Saraboji, K., Aisenbrey, C., Grobner, G., Zetterstrom, P., Danielsson, J., Logan, D. T., and Oliveberg, M. (2009) Functional features cause misfolding of the ALS-provoking enzyme SOD1, *Proc Natl Acad Sci U S A 106*, 9667-9672.

68. Doyle, C. M., Rumfeldt, J. A., Broom, H. R., Sekhar, A., Kay, L. E., and Meiering, E. M. (2016) Concurrent Increases and Decreases in Local Stability and Conformational Heterogeneity in Cu, Zn Superoxide Dismutase Variants Revealed by Temperature-Dependence of Amide Chemical Shifts, *Biochemistry 55*, 1346-1361.

69. Culik, R. M., Sekhar, A., Nagesh, J., Deol, H., Rumfeldt, J. A. O., Meiering, E. M., and Kay, L. E. (2018) Effects of maturation on the conformational free-energy landscape of SOD1, *Proc Natl Acad Sci U S A 115*, E2546-E2555.

70. McCord, J. M., and Fridovich, I. (1969) Superoxide dismutase. An enzymic function for erythrocuprein (hemocuprein), *J Biol Chem 244*, 6049-6055.

71. Robberecht, W., and Philips, T. (2013) The changing scene of amyotrophic lateral sclerosis, *Nat Rev Neurosci 14*, 248-264.

72. Chiti, F., and Dobson, C. M. (2006) Protein misfolding, functional amyloid, and human disease, *Annu Rev Biochem 75*, 333-366.

73. Khare, S. D., Caplow, M., and Dokholyan, N. V. (2006) FALS mutations in Cu, Zn superoxide dismutase destabilize the dimer and increase dimer dissociation propensity: a large-scale thermodynamic analysis, *Amyloid 13*, 226-235.

74. Hough, M. A., Grossmann, J. G., Antonyuk, S. V., Strange, R. W., Doucette, P. A., Rodriguez, J. A., Whitson, L. J., Hart, P. J., Hayward, L. J., Valentine, J. S., and Hasnain, S. S. (2004) Dimer destabilization in superoxide dismutase may result in disease-causing properties: structures of motor neuron disease mutants, *Proc Natl Acad Sci U S A 101*, 5976-5981.

75. Doucette, P. A., Whitson, L. J., Cao, X., Schirf, V., Demeler, B., Valentine, J. S., Hansen, J. C., and Hart, P. J. (2004) Dissociation of human copper-zinc superoxide dismutase dimers using chaotrope and reductant. Insights into the molecular basis for dimer stability, *J Biol Chem 279*, 54558-54566.

76. Culotta, V. C., Yang, M., and O'Halloran, T. V. (2006) Activation of superoxide dismutases: putting the metal to the pedal, *Biochim Biophys Acta 1763*, 747-758.

77. Furukawa, Y., and O'Halloran, T. V. (2006) Posttranslational modifications in Cu,Zn-superoxide dismutase and mutations associated with amyotrophic lateral sclerosis, *Antioxid Redox Signal 8*, 847-867.

78. Furukawa, Y., Kaneko, K., Yamanaka, K., O'Halloran, T. V., and Nukina, N. (2008) Complete loss of post-translational modifications triggers fibrillar aggregation of SOD1 in the familial form of amyotrophic lateral sclerosis, *J Biol Chem 283*, 24167-24176.

79. Brown, N. M., Torres, A. S., Doan, P. E., and O'Halloran, T. V. (2004) Oxygen and the copper chaperone CCS regulate posttranslational activation of Cu,Zn superoxide dismutase, *Proc Natl Acad Sci U S A 101*, 5518-5523.

80. Galiazzo, F., Ciriolo, M. R., Carri, M. T., Civitareale, P., Marcocci, L., Marmocchi, F., and Rotilio, G. (1991) Activation and induction by copper of Cu/Zn superoxide dismutase in Saccharomyces cerevisiae. Presence of an inactive proenzyme in anaerobic yeast, *Eur J Biochem 196*, 545-549.

81. Bourassa, M. W., Brown, H. H., Borchelt, D. R., Vogt, S., and Miller, L. M. (2014) Metal-deficient aggregates and diminished copper found in cells expressing SOD1 mutations that cause ALS, *Front Aging Neurosci 6*, 110.

82. Rodriguez, J. A., Valentine, J. S., Eggers, D. K., Roe, J. A., Tiwari, A., Brown, R. H., Jr., and Hayward, L. J. (2002) Familial amyotrophic lateral sclerosis-associated mutations decrease the thermal stability of distinctly metallated

species of human copper/zinc superoxide dismutase, *J Biol Chem 277*, 15932-15937.

83. Wright, G. S., Antonyuk, S. V., and Hasnain, S. S. (2016) A faulty interaction between SOD1 and hCCS in neurodegenerative disease, *Sci Rep 6*, 27691.

84. Arnesano, F., Banci, L., Bertini, I., Martinelli, M., Furukawa, Y., and O'Halloran, T. V. (2004) The unusually stable quaternary structure of human Cu,Zn-superoxide dismutase 1 is controlled by both metal occupancy and disulfide status, *J Biol Chem 279*, 47998-48003.

85. Hornberg, A., Logan, D. T., Marklund, S. L., and Oliveberg, M. (2007) The coupling between disulphide status, metallation and dimer interface strength in Cu/Zn superoxide dismutase, *J Mol Biol 365*, 333-342.

86. Banci, L., Bertini, I., Cantini, F., D'Onofrio, M., and Viezzoli, M. S. (2002) Structure and dynamics of copper-free SOD: The protein before binding copper, *Protein Sci 11*, 2479-2492.

87. Banci, L., Bertini, I., Cramaro, F., Del Conte, R., and Viezzoli, M. S. (2003) Solution structure of Apo Cu,Zn superoxide dismutase: role of metal ions in protein folding, *Biochemistry 42*, 9543-9553.

88. Jonsson, P. A., Graffmo, K. S., Andersen, P. M., Brannstrom, T., Lindberg, M., Oliveberg, M., and Marklund, S. L. (2006) Disulphide-reduced superoxide dismutase-1 in CNS of transgenic amyotrophic lateral sclerosis models, *Brain 129*, 451-464.

89. Karch, C. M., Prudencio, M., Winkler, D. D., Hart, P. J., and Borchelt, D. R. (2009) Role of mutant SOD1 disulfide oxidation and aggregation in the pathogenesis of familial ALS, *Proc Natl Acad Sci U S A 106*, 7774-7779.

90. Schmidt, P. J., Kunst, C., and Culotta, V. C. (2000) Copper activation of superoxide dismutase 1 (SOD1) in vivo. Role for protein-protein interactions with the copper chaperone for SOD1, *J Biol Chem 275*, 33771-33776.

91. Steinkuhler, C., Sapora, O., Carri, M. T., Nagel, W., Marcocci, L., Ciriolo, M. R., Weser, U., and Rotilio, G. (1991) Increase of Cu,Zn-superoxide dismutase activity during differentiation of human K562 cells involves activation by copper of a constantly expressed copper-deficient protein, *J Biol Chem 266*, 24580-24587.

92. Petrovic, N., Comi, A., and Ettinger, M. J. (1996) Identification of an apo-superoxide dismutase (Cu,Zn) pool in human lymphoblasts, *J Biol Chem 271*, 28331-28334.

93. Lepock, J. R., Frey, H. E., and Hallewell, R. A. (1990) Contribution of conformational stability and reversibility of unfolding to the increased thermostability of human and bovine superoxide dismutase mutated at free cysteines, *J Biol Chem 265*, 21612-21618.

94. Lyons, T. J., Liu, H., Goto, J. J., Nersissian, A., Roe, J. A., Graden, J. A., Cafe, C., Ellerby, L. M., Bredesen, D. E., Gralla, E. B., and Valentine, J. S. (1996) Mutations in copper-zinc superoxide dismutase that cause amyotrophic lateral sclerosis alter the zinc binding site and the redox behavior of the protein, *Proc Natl Acad Sci U S A 93*, 12240-12244.

95. Mulligan, V. K., Kerman, A., Ho, S., and Chakrabartty, A. (2008) Denaturational stress induces formation of zinc-deficient monomers of Cu,Zn superoxide dismutase: implications for pathogenesis in amyotrophic lateral sclerosis, *J Mol Biol 383*, 424-436.

96. Doyle, C. M. (2014) A Refined Method for Quantitation of Divalent Metal Ions in Metalloproteins and Local Stability and Conformational Hterogeneity of Amytrophic Lateral Sclerosis-Associated Cu,Zn Superoxide Dismutase.

97. Velazquez-Campoy, A., Ohtaka, H., Nezami, A., Muzammil, S., and Freire, E. (2004) Isothermal titration calorimetry, *Curr Protoc Cell Biol Chapter 17*, Unit 17 18.

98. Burrows, S. D., Doyle, M. L., Murphy, K. P., Franklin, S. G., White, J. R., Brooks, I., McNulty, D. E., Scott, M. O., Knutson, J. R., Porter, D., and et al. (1994) Determination of the monomer-dimer equilibrium of interleukin-8 reveals it is a monomer at physiological concentrations, *Biochemistry 33*, 12741-12745.

99. Marky, L. A., and Breslauer, K. J. (1987) Calculating thermodynamic data for transitions of any molecularity from equilibrium melting curves, *Biopolymers 26*, 1601-1620.

100. Kayatekin, C., Zitzewitz, J. A., and Matthews, C. R. (2008) Zinc binding modulates the entire folding free energy surface of human Cu,Zn superoxide dismutase, *J Mol Biol 384*, 540-555.

101. Duff, M. R., Jr., Grubbs, J., and Howell, E. E. (2011) Isothermal titration calorimetry for measuring macromolecule-ligand affinity, *J Vis Exp 55*, 2796.

102. Furukawa, Y., Anzai, I., Akiyama, S., Imai, M., Cruz, F. J., Saio, T., Nagasawa, K., Nomura, T., and Ishimori, K. (2016) Conformational Disorder of the Most Immature Cu, Zn-Superoxide Dismutase Leading to Amyotrophic Lateral Sclerosis, *J Biol Chem 291*, 4144-4155.

103. Luchinat, E., Barbieri, L., and Banci, L. (2017) A molecular chaperone activity of CCS restores the maturation of SOD1 fALS mutants, *Sci Rep 7*, 17433.

104. Stathopulos, P. B., Rumfeldt, J. A., Scholz, G. A., Irani, R. A., Frey, H. E., Hallewell, R. A., Lepock, J. R., and Meiering, E. M. (2003) Cu/Zn superoxide dismutase mutants associated with amyotrophic lateral sclerosis show enhanced formation of aggregates in vitro, *Proc Natl Acad Sci U S A 100*, 7021-7026.

105. Shrake, A., and Ross, P. D. (1992) Origins and consequences of ligand-induced multiphasic thermal protein denaturation, *Biopolymers 32*, 925-940.

106. Roe, J. A., Butler, A., Scholler, D. M., Valentine, J. S., Marky, L., and Breslauer, K. J. (1988) Differential scanning calorimetry of Cu,Zn-superoxide dismutase, the apoprotein, and its zinc-substituted derivatives, *Biochemistry 27*, 950-958.

107. Di Noto, L., Whitson, L. J., Cao, X., Hart, P. J., and Levine, R. L. (2005) Proteasomal degradation of mutant superoxide dismutases linked to amyotrophic lateral sclerosis, *J Biol Chem 280*, 39907-39913.

108. Tiwari, A., and Hayward, L. J. (2003) Familial amyotrophic lateral sclerosis mutants of copper/zinc superoxide dismutase are susceptible to disulfide reduction, *J Biol Chem 278*, 5984-5992.

109. Bouldin, S. D., Darch, M. A., Hart, P. J., and Outten, C. E. (2012) Redox properties of the disulfide bond of human Cu,Zn superoxide dismutase and the effects of human glutaredoxin 1, *Biochem J 446*, 59-67.

110. Assfalg, M., Banci, L., Bertini, I., Turano, P., and Vasos, P. R. (2003) Superoxide dismutase folding/unfolding pathway: role of the metal ions in modulating structural and dynamical features, *J Mol Biol 330*, 145-158.

111. Das, A., and Plotkin, S. S. (2013) Mechanical probes of SOD1 predict systematic trends in metal and dimer affinity of ALS-associated mutants, *J Mol Biol 425*, 850-874.

112. Luchinat, E., Barbieri, L., Rubino, J. T., Kozyreva, T., Cantini, F., and Banci, L. (2014) In-cell NMR reveals potential precursor of toxic species from SOD1 fALS mutants, *Nat Commun 5*, 5502.

113. Borchelt, D. R., Lee, M. K., Slunt, H. S., Guarnieri, M., Xu, Z. S., Wong, P. C., Brown, R. H., Jr., Price, D. L., Sisodia, S. S., and Cleveland, D. W. (1994) Superoxide dismutase 1 with mutations linked to familial amyotrophic

lateral sclerosis possesses significant activity, *Proc Natl Acad Sci U S A 91*, 8292-8296.

114. Prudencio, M., Hart, P. J., Borchelt, D. R., and Andersen, P. M. (2009) Variation in aggregation propensities among ALS-associated variants of SOD1: correlation to human disease, *Hum Mol Genet 18*, 3217-3226.

115. Kerman, A., Liu, H. N., Croul, S., Bilbao, J., Rogaeva, E., Zinman, L., Robertson, J., and Chakrabartty, A. (2010) Amyotrophic lateral sclerosis is a non-amyloid disease in which extensive misfolding of SOD1 is unique to the familial form, *Acta Neuropathol 119*, 335-344.

116. Forsberg, K., Jonsson, P. A., Andersen, P. M., Bergemalm, D., Graffmo, K. S., Hultdin, M., Jacobsson, J., Rosquist, R., Marklund, S. L., and Brannstrom, T. (2010) Novel antibodies reveal inclusions containing non-native SOD1 in sporadic ALS patients, *PLoS One 5*, e11552.

117. Valentine, J. S., Doucette, P. A., and Potter, S. Z. (2005) Copper-zinc superoxide dismutase and amyotrophic lateral sclerosis, In *Annual Review of Biochemistry*, pp 563-593, Annual Reviews, Palo Alto.

118. Antonyuk, S., Elam, J. S., Hough, M. A., Strange, R. W., Doucette, P. A., Rodriguez, J. A., Hayward, L. J., Valentine, J. S., Hart, P. J., and Hasnain, S. S. (2005) Structural consequences of the familial amyotrophic lateral sclerosis SOD1 mutant His46Arg, *Protein Sci 14*, 1201-1213.

119. Sekhar, A., Rumfeldt, J. A., Broom, H. R., Doyle, C. M., Sobering, R. E., Meiering, E. M., and Kay, L. E. (2016) Probing the free energy landscapes of ALS disease mutants of SOD1 by NMR spectroscopy, *Proc Natl Acad Sci U S A*.

120. Shriver, J. W. (2009) Protein structure, stability, and interactions. Preface, *Methods Mol Biol 490*, V.

121. Tamura, A., Kojima, S., Miura, K., and Sturtevant, J. M. (1995) A thermodynamic study of mutant forms of Streptomyces subtilisin inhibitor. II. Replacements at the interface of dimer formation, Val13, *J Mol Biol 249*, 636-645.

122. Shriver, J. W., and Edmondson, S. P. (2009) Defining the stability of multimeric proteins, *Methods Mol Biol 490*, 57-82.

123. Sabel, C. E., Shepherd, J. L., and Siemann, S. (2009) A direct spectrophotometric method for the simultaneous determination of zinc and cobalt in metalloproteins using 4-(2-pyridylazo)resorcinol, *Anal Biochem 391*, 74-76.

124. Sabel, C. E., Neureuther, J. M., and Siemann, S. (2010) A spectrophotometric method for the determination of zinc, copper, and cobalt ions in metalloproteins using Zincon, *Anal Biochem 397*, 218-226.

125. Jezorek, J. R., and Freiser, H. (1979) 4-(Pyridylazo)Resorcinol-Based Continuous Detection System for Trace Levels of Metal-Ions, *Analytical Chemistry 51*, 373-376.

126. Hunt, J. B., Neece, S. H., Schachman, H. K., and Ginsburg, A. (1984) Mercurial-promoted Zn2+ release from Escherichia coli aspartate transcarbamoylase, *J Biol Chem 259*, 14793-14803.

Appendix

A1.0 Derivation of two state versus three state unfolding model

A1.1 Thermodynamic analysis models for homodimeric protein folding

Various methods for analyzing protein stability using different thermodynamic parameters have been formulated (64, 120). For thermal unfolding analysis, two models have been developed for quantitatively characterizing multimers, concentrating on homodimers in this case, and both models have been previously applied to SOD1.(56) The first unfolding model is the simplest, a reversible 2-state transition, which involves the simultaneous dissociation and unfolding of a homodimer (N_2), to produce unfolded monomers (U):

$$N_2 \xleftrightarrow{K(T)} 2U \tag{A1.1}$$

where *K(T)* is the equilibrium constant for unfolding at any temperature *T*. The concentrations of the native dimer (N_2) and unfolded monomers (*2U*) are defined as:

$$[N_2] = P_{dimer}(1-\alpha) \tag{A1.2}$$

$$[U] = 2P_{dimer}(\alpha) \tag{A1.3}$$

where P_{dimer} is the total protein concentration in moles of dimer per liter and α is degree of unfolding (i.e. fraction). The equilibrium constant, *K(T)* at temperature *T* is expressed as:

$$K(T) = \frac{[U]^2}{[N_2]} = \frac{4P_{dimer}\alpha^2}{(1-\alpha)} \tag{A1.4}$$

Equation A1.4 can be rearranged to obtain an expression for α:

$$\alpha = \frac{-K(T) + \sqrt{K(T)(K(T)+16P_{dimer})}}{8P_{dimer}} \tag{A1.5}$$

The change in heat capacity of unfolding ($\Delta C_{p,unf}$) is defined by the difference between the heat capacities of the native ($C_{p(N_2)}$) and unfolded ($C_{p(U)}$) protein:

$$\Delta C_{p,unf}(t) = C_{p(U)} - C_{p(N_2)} \quad \text{(A1.5)}$$

$$C_{p(N_2)} = A + Bt \quad \text{(A1.6)}$$

$$C_{p(U)} = E + Ft \quad \text{(A1.7)}$$

where A and E are the intercepts; B and F are the slopes of the folded and unfolded baseline, respectively; and t is the temperature in °C. Substituting equation A1.6 and A1.7 into A1.5 gives:

$$\Delta C_{p,unf}(t) = (E - A) + (F - B)t \quad \text{(A1.8)}$$

By definition:

$$\Delta h_{cal}(t) = \int_{t_{ref}}^{t} \Delta C_{p,unf}\, dt \quad \text{(A1.9)}$$

Substituting equation A1.8 into equation A1.9 and integrating, gives the specific calorimetric enthalpy of the unfolding transition in calories per gram of protein, in terms of temperature is:

$$\Delta h_{cal}(t) = \Delta h_{cal}(t_{ref}) + (E - A)(t - t_{ref}) + \frac{1}{2}(F - B)(t^2 - t_{ref}^2) \quad \text{(A1.10)}$$

where t_{ref} is the reference temperature, usually set to t_m, the midpoint in the reaction where half of the total protein is unfolded, and $\Delta h_{cal}(t_{ref})$ is the Δh_{cal} at t_{ref}.

The $\Delta C_{p,unf}$ becomes constant with temperature if folding (pre-transition) and unfolding (post-transition) baselines have the same slope. In this case, Equation A1.10 simplifies to:

$$\Delta h_{cal}(t) = \Delta h_{cal}(t_{ref}) + (E - A)(t - t_{ref}) \quad \text{(A1.11)}$$

which is a reasonable assumption over a limited temperature range.(57, 60, 121, 122) For two-state fitting, $\Delta h_{cal}(t)$ is extrapolated to 0°C to give:

$$\Delta h^{\circ} = \Delta h(t_{ref}) - (E - A)(t_{ref}) - \frac{1}{2}(F - B)(t_{ref}^2) \quad \text{(A1.12)}$$

where Δh^o is the standard enthalpy of reaction for unfolding. By rearranging the equation, Δh_{cal} can be calculated at any temperature, t, using:

$$\Delta h_{cal}(t) = \Delta h^{\circ} + (E - A)t + \frac{1}{2}(F - B)t^2 \quad \text{(A1.13)}$$

Using the van't Hoff equation, the temperature dependence of K is given by:

$$\frac{d \ln K(T)}{dT} = \frac{\Delta H_{vH}(T)}{RT^2} \quad \text{(A1.14)}$$

$$\beta = \frac{\Delta H_{vH}(T)}{\Delta h_{cal}(T)} \quad \text{(A1.15)}$$

where T is the temperature in Kelvin, R is the universal gas constant, ΔH_{vH} is the van't Hoff enthalpy for the change in enthalpy for unfolding and Δh_{cal} is specific change in enthalpy. Substituting A1.15 into A1.14 to give:

$$\frac{d \ln K(T)}{dT} = \frac{\beta \Delta h_{cal}(T)}{RT^2} \quad \text{(A1.16)}$$

The van't Hoff enthalpy (ΔH_{vH}) depends on the shape of transition, whereas the calorimetric enthalpy (ΔH_{cal}) reflects the area under the endothermic peak. By setting β to be a fitting parameter, the van't Hoff and calorimetric enthalpy are allowed to vary with respect to each other. However if there is cooperative unfolding, β will converge to the molecular weight of the cooperative unfolding unit (dimer):

$$\beta = \frac{\Delta H_{vH}}{\Delta H_{cal}} \bullet M_w \quad \text{(A1.17)}$$

If there is two-state transition, then the van't Hoff to calorimetric enthalpy ratio is equal to 1.

The temperature-dependence of K can be determined by substituting equation (A1.18) into (A1.21), and then integrating:

$$\int_{T_{ref}}^{T} d\ln K(T) = \ln\left(\frac{K(T)}{K(T_{ref})}\right) = \frac{\beta}{R}\int_{T_{ref}}^{T}\frac{\Delta h_{cal}(T)}{T^2}dT \tag{A1.18}$$

Integrating and rearranging gives:

$$\frac{R}{\beta}\ln\left(\frac{K(T)}{K(T_{ref})}\right) = x\left(\frac{1}{T}-\frac{1}{T_{ref}}\right) + y\ln\left(\frac{T}{T_{ref}}\right) + z(T-T_{ref}) \tag{A1.19}$$

$$\begin{aligned} x &\equiv -\Delta h^\circ + 273.15(E-A) - \frac{1}{2}(273.15)^2(F-B) \\ y &\equiv (E-A) - (273.15)(F-B) \\ z &\equiv \frac{1}{2}(F-B) \end{aligned} \tag{A1.20}$$

Isolating for *K(T)* gives:

$$K(T) = K(T_{ref})\times\exp\left(\left(x\left(\frac{1}{T}-\frac{1}{T_{ref}}\right) + y\ln\left(\frac{T}{T_{ref}}\right) + z(T-T_{ref})\right)\times\frac{\beta}{R}\right) \tag{A1.21}$$

The total measured heat capacity ($C_{p,total}$) is the sum of the baseline heat capacity ($C_{p,baseline}$) plus the excess heat capacity ($C_{p,excess}$) from the absorption of heat during the unfolding transition:

$$C_{p,total} = C_{p,baseline} + C_{p,excess} \tag{A1.22}$$

$$C_{p,baseline} = (1-\alpha(t))C_{p,N_2} + \alpha(t)C_{p,U} \tag{A1.23}$$

$$C_{p,excess} = \left(\frac{\partial\alpha}{\partial T}\right)\Delta h_{cal}(T) \tag{A1.24}$$

In order to determine the partial derivative $\left(\frac{\partial\alpha}{\partial T}\right)$, analytically evaluating equation (A1.17):

$$\frac{d\ln K(T)}{dT} = \frac{\beta\Delta h_{cal}(T)}{RT^2} = \frac{2}{\alpha}\frac{d\alpha}{dT} + \frac{1}{1-\alpha}\frac{d\alpha}{dT} \tag{A1.25}$$

which is rearranges to:

$$\frac{d\alpha}{dT} = \frac{\beta\Delta h_{cal}(T)}{RT^2}\frac{\alpha(1-\alpha)}{2-\alpha} \tag{A1.26}$$

The $\Delta h_{cal}(T)$ is the same value as $\Delta h_{cal}(t)$ regardless of the units of temperature, thus substituting equation (A1.24) into (A1.36) gives:

$$C_{p,excess} = \frac{\beta \Delta h_{cal}^2(t)}{RT^2} \frac{\alpha(1-\alpha)}{2-\alpha} \tag{A1.27}$$

Substituting equation (A1.6) and (A1.7) into (A1.23) gives:

$$C_{p,baseline} = (A+Bt)(1-\alpha)+(E+Ft)\alpha \tag{A1.28}$$

Then substituting equation (A1.27) and (A1.28) into (A1.22) gives equation (A1.1), used to fit DSC scan to 2-state unfolding transition.

A1.2 Three-state transition of dimer unfolding with monomer intermediate model

The thermal unfolding of homodimeric proteins may follow a 3-state transition, which entails a homodimer (N_2) dissociating to a folded monomeric intermediate (M) and then to a completely unfolded monomer (U). This model may be described by:

$$N_2 \xleftarrow{K_1(T)} 2M \xleftarrow{K_2(T)} 2U \tag{A1.29}$$

$$[N_2] = P_{dimer}(1-\alpha_1) \tag{A1.30}$$

$$[M] = 2P_{dimer}\alpha_1(1-\alpha_2) \tag{A1.31}$$

$$[U] = 2P_{dimer}\alpha_1\alpha_2 \tag{A1.32}$$

where $K_1(T)$ and $K_2(T)$ are the equilibrium constants, α_1 and α_2 are the extent of unfolding reaction at any temperature for the dimer dissociation and monomer unfolding transitions, respectively.

$$K_1(T) = \frac{[M]^2}{[N_2]} = 4P_{dimer}\frac{\alpha_1^2(1-\alpha_2)^2}{1-\alpha_1} \tag{A1.33}$$

$$K_2(T) = \frac{[U]^2}{[M]^2} = \frac{\alpha_2^2}{(1-\alpha_2)^2} \tag{A1.34}$$

The degree of the unfolding reaction at any temperature can be determined by rearranging equation (A1.38) and (A1.39):

$$\alpha_1 = \frac{2}{1+\sqrt{1+\frac{16P_{dimer}}{K_1(T)\left(1+\sqrt{K_2(T)}\right)^2}}} \quad \text{(A1.35)}$$

$$\alpha_2 = \frac{\sqrt{K_2(T)}}{1+\sqrt{K_2(T)}} \quad \text{(A1.36)}$$

The specific heat capacity of the folded monomer intermediate ($C_{p,M}$) is assumed to vary linearly with temperature:

$$C_{p,M} = C + Dt \quad \text{(A1.37)}$$

where C is the intercept (at 0°C) and D is the slope of the folded baseline.

The change in heat capacity of the first transition $\left(\Delta C_{p,N_2\leftrightarrow 2M}\right)$ and second transition $\left(\Delta C_{p,M\leftrightarrow U}\right)$ is determined at any temperature by:

$$\Delta C_{p,N_2\leftrightarrow 2M}(t) = (C-A)+(D-B)t \quad \text{(A1.38)}$$

$$\Delta C_{p,M\leftrightarrow U}(t) = (E-C)+(F-D)t \quad \text{(A1.39)}$$

Using the same derivation approach as for equations (A1.15)-(A1.26), gives K_1 and K_2 as a function of temperature:

$$K_1(T) = K(T_{ref1})\times\exp\left(\left(x_1\left(\frac{1}{T}-\frac{1}{T_{ref1}}\right)+y_1\ln\left(\frac{T}{T_{ref1}}\right)+z_1(T-T_{ref1}\right)\times\frac{\beta}{R}\right) \quad \text{(A1.40)}$$

$$K_2(T) = K(T_{ref2})\times\exp\left(\left(x_2\left(\frac{1}{T}-\frac{1}{T_{ref2}}\right)+y_2\ln\left(\frac{T}{T_{ref2}}\right)+z_2(T-T_{ref2}\right)\times\frac{\beta}{R}\right) \quad \text{(A1.41)}$$

where:

$$\begin{aligned} x_1 &\equiv -\Delta h_1^{\circ} + 274.15(C-A) - \frac{1}{2}(273.15)^2(D-B) \\ y_1 &\equiv (C-A) - (273.15)(D-B) \\ z_1 &\equiv \frac{1}{2}(D-B) \end{aligned} \quad \text{(A1.42)}$$

$$x_2 \equiv -\Delta h_2^{\circ} + 274.15(E-C) - \frac{1}{2}(273.15)^2(F-D)$$
$$y_2 \equiv (E-C) - (273.15)(F-D) \quad \text{(A1.43)}$$
$$z_2 \equiv \frac{1}{2}(F-D)$$

where $K(T_{ref1})$ and $K(T_{ref2})$ are equilibrium constants at the reference temperatures for the first transition (dimer dissociation) and the second transition (monomer unfolding), respectively.

Using the procedure for deriving equation (A1.43), the same is applied using equations (A1.38) and (A1.39):

$$\frac{d\alpha_1}{dT} = \left(\frac{\beta_1 \Delta h_{cal,N_2 \leftrightarrow 2M}(T)}{RT^2} + \frac{\alpha_2 \beta_2 \Delta h_{cal,M \leftrightarrow U}(T)}{RT^2} \right) \frac{\alpha_1(1-\alpha_1)}{2-\alpha_1} \quad \text{(A1.44)}$$

$$\frac{d\alpha_2}{dT} = \frac{\beta \Delta h_{cal,M \leftrightarrow U}(T)}{2RT^2} \times \alpha_2(1-\alpha_2) \quad \text{(A1.45)}$$

The $C_{p,excess}$ and $C_{p,baseline}$ are given by:

$$C_{p,excess} = \frac{d\alpha_1}{dT} \Delta h_{cal1}(t) + \left(\frac{d\alpha_1}{dT} \alpha_2 + \frac{d\alpha_2}{dT} \alpha_1 \right) \Delta h_{cal2}(t) \quad \text{(A1.46)}$$

$$C_{p,baseline} = f_{N_2} C_{p,N_2} + f_M C_{p,M} + f_U C_{p,U} \quad \text{(A1.47)}$$

where f_{N_2}, f_M, and f_U are the fractions of homodimeric protein, folded monomer intermediate and unfolded monomer, respectively, calculated using:

$$f_{N_2} = (1-\alpha_1) \quad \text{(A1.48)}$$
$$f_M = \alpha_1(1-\alpha_2) \quad \text{(A1.49)}$$
$$f_U = \alpha_1 \alpha_2 \quad \text{(A1.50)}$$
$$f_{N_2} + f_M + f_U = 1 \quad \text{(A1.51)}$$

Substituting equations (A1.11), (A1.12), (A1.42), (A1.53), (A1.54) and (A1.55) into (A1.52) gives:

$$C_{p,baseline} = (1-\alpha_1)(A+Bt) + (\alpha_1)(1-\alpha_2)(C+Dt) + (\alpha_1\alpha_2)(E+Ft) \quad \text{(A1.52)}$$

Substituting equations (A1.49) and (A1.50) into (A1.51) gives:

$$C_{p,excess} = \left(\frac{\beta_1 \Delta h_{cal,N_2 \leftrightarrow 2M}(T)}{RT^2} + \frac{\alpha_2 \beta_2 \Delta h_{cal,M \leftrightarrow U}(T)}{RT^2} \right) \Delta h_{cal,N_2 \leftrightarrow 2M}(t) \frac{\alpha_1(1-\alpha_1)}{2-\alpha_1} + \left(\left(\frac{\beta_1 \Delta h_{cal,N_2 \leftrightarrow 2M}(T)}{RT^2} + \frac{\alpha_2 \beta_2 \Delta h_{cal,M \leftrightarrow U}(T)}{RT^2} \right) \frac{\alpha_1 \alpha_2 (1-\alpha_1)}{2-\alpha_1} + \frac{\beta \Delta h_{cal,M \leftrightarrow U}(T)}{2RT^2} \times \alpha_1 \alpha_2 (1-\alpha_2) \right) \Delta h_{cal,M \leftrightarrow U}(t) \quad \text{(A1.53)}$$

Substituting equation (A1.57) and (A1.58) into (A1.27) gives equation (A1.2) which is used to fit DSC scan to the 3-state unfolding model.

Table A1.1 3-dimer unfolding with monomer intermediate model fit values for different zinc equivalents and pWT.

SOD1 mutant	$\Delta H_{N_2 \leftrightarrow 2M}$[1] (kcal (mol dimer)$^{-1}$)	$\Delta G_{N_2 \leftrightarrow 2M}$[1] (kcal (mol dimer)$^{-1}$)	$t_{m,\, M \leftrightarrow U}$[2] (°C)	$\Delta H_{tavg,\, M \leftrightarrow U}$[2] (kcal (mol monomer)$^{-1}$)	$\Delta G_{25\,°C,\, M \leftrightarrow U}$ (kcal (mol monomer)$^{-1}$)	$\Delta G_{tavg,\, M \leftrightarrow U}$[3] (kcal (mol monomer)$^{-1}$)
1 Zn pWT	4.01	5.86	57.0	40.4	0.27	-0.02
0.5 Zn pWT	4.01	5.86	34.1	51.8??	-0.31	-1.89
2.0 Zn pWT	4.01	5.86	61.4	37.7	0.62	0.54
A4V	6.00	4.06	59.4	32.4	-0.48	0.24
H46R	3.40	4.76	53.1	68.8	2.31	-0.79
V148G	1.90	3.60	54.0	62.8	0.80	-0.55
V148I	4.12	6.01	49.8	34.5	-0.88	-0.59

[1]Values were fixed from ITC dimer dissociation.
[2]Values from individual data set being fit to a 3-state dimer unfolding model.
[3]ΔG_{tavg} calculated at 57.1°C.

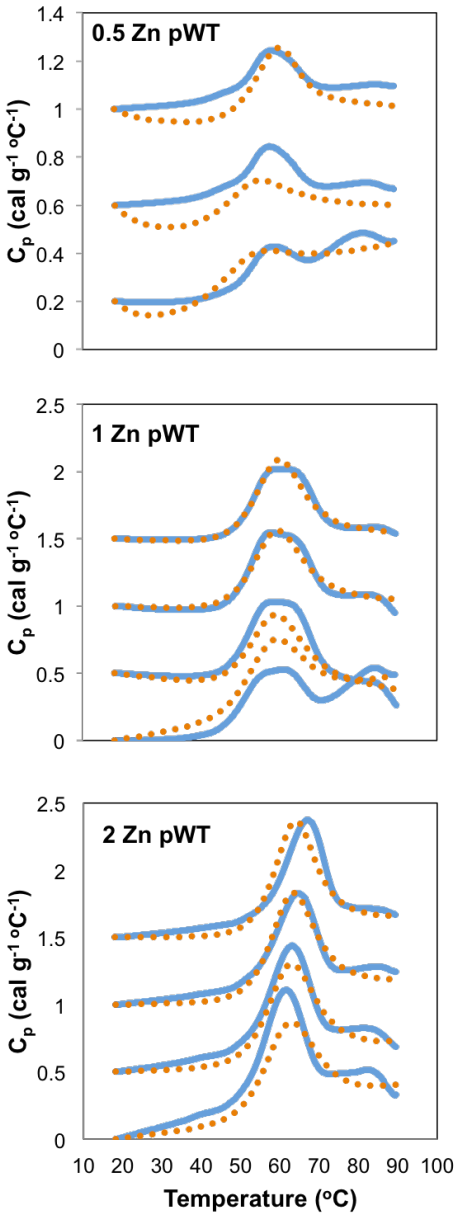

Figure A1.1 3-state dimer unfolding with monomer intermediate model fits for fALS mutants. The blue lines are the raw endotherms, with the fits represented by the orange dashed lines. DSC scans were offset for clarity, with the lowest concentration being the lower of the three scans and the highest concentration being at the top of each plot. Half a Zn equivalents concentrations were 1.16 mg/mL, 1.85 mg/mL, and 2.96 mg/mL. 1 Zn equivalence concentrations were 0.68 mg/mL, 0.98 mg/mL, 1.54 mg/mL and 2.30 mg/mL. 2 Zn equivalents concentrations included 0.72 mg/mL, 1.30 mg/mL, 2.34 mg/mL and 4.14 mg/mL.

Table A1.2 2-state dimer fit values for varying zinc equivalents and disulfide reduced pWT SOD1.

SOD1 mutant	*Conc* (mg/mL)	t_m[1] (°C)	ΔH_{vH}[1] (kcal (mol dimer)$^{-1}$)	$\Delta H_{vH}/\Delta H_{cal}$	ΔG_{tavg}[2] (kcal (mol dimer)$^{-1}$)	$\Delta G_{25\,°C}$ (kcal (mol dimer)$^{-1}$)	n[3]
0.5 Zn pWT	1.16	52.3	5714957	1.04	5.27	4.40	2.25
	1.85	55.5	71331	0.74	5.45	7.11	2.56
	2.96	56.2	77004	0.97	5.40	5.01	2.69
2.0 Zn pWT	0.72	63.1	104916	0.27	8.16	6.68	2.17
	1.30	62.6	106502	0.34	7.68	6.64	2.19
	2.34	64.6	107484	0.36	7.74	5.85	2.20
	4.14	66.4	114059	0.40	7.56	5.74	2.27

[1]Values from individual data set being fit to a 2-state dimer unfolding model Eq. A1.1 in Origin 7.0.
[2]ΔG_{tavg} calculated at 57.1°C.
[3]Molecularity was calculated using $n = \frac{-\Delta H_{vH}}{slope * R} + 1$.

Table A1.3 2-state monomer fit values for half and double zinc equivalent of pWT[SH]

SOD1 mutant	*Conc* (mg/mL)	t_m[1] (°C)	ΔH_{vH}[1] (kcal (mol dimer)$^{-1}$)	$\Delta H_{vH}/\Delta H_{cal}$
0.5 Zn pWT	**1.157**	**55.03**	**58.16**	**2.28**
	1.853	**58.11**	**64.04**	**2.15**
	2.959	**57.85**	**62.56**	**1.87**
2.0 Zn pWT	**0.717**	**65.03**	**53.51**	**0.24**
	1.303	**65.06**	**61.11**	**0.33**
	2.344	**68.18?**	**52.99**	**0.28**
	4.143	**66.52?**	**72.98**	**0.54**

[1]Values from individual data set being fit to a 2-state monomer unfolding model Eq. A1.1 in Origin 7.0.

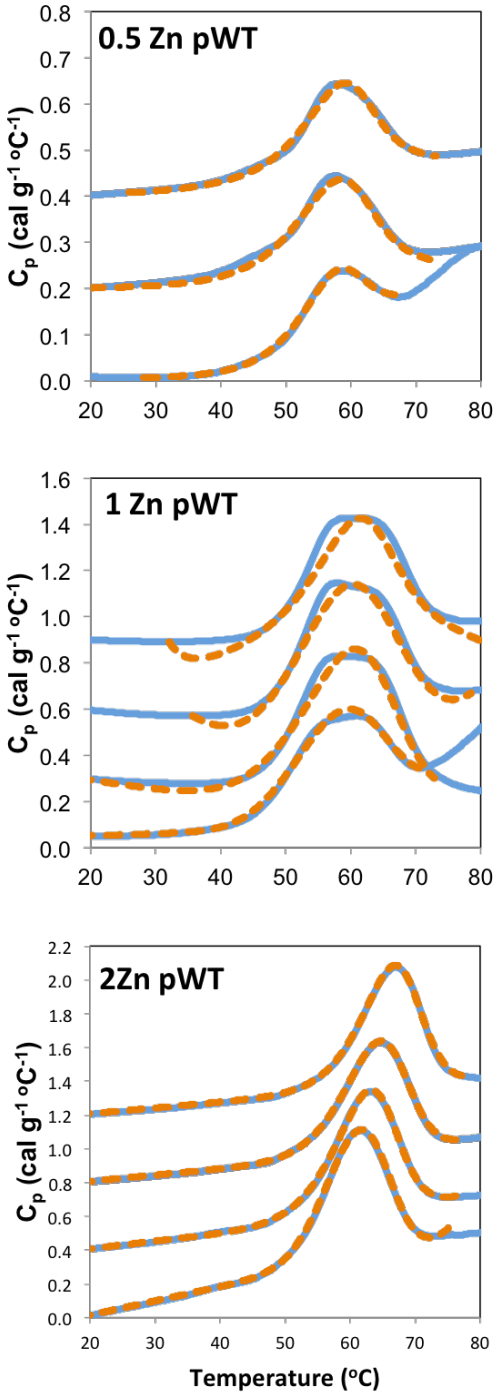

Figure A1.2. 2-state monomer unfolding model fits for fALS mutants. The blue lines are the raw endotherms, with the fits represented by the orange dashed lines. DSC scans were offset for clarity, with the lowest concentration being the lower of the three scans and the highest concentration being at the top of each plot. Half a Zn equivalents concentrations were 1.16 mg/mL, 1.85 mg/mL, and 2.96 mg/mL. 1 Zn equivalence concentrations were 0.68 mg/mL, 0.98 mg/mL, 1.54 mg/mL and 2.30 mg/mL. 2 Zn equivalents concentrations included 0.72 mg/mL, 1.30 mg/mL, 2.34 mg/mL and 4.14 mg/mL.

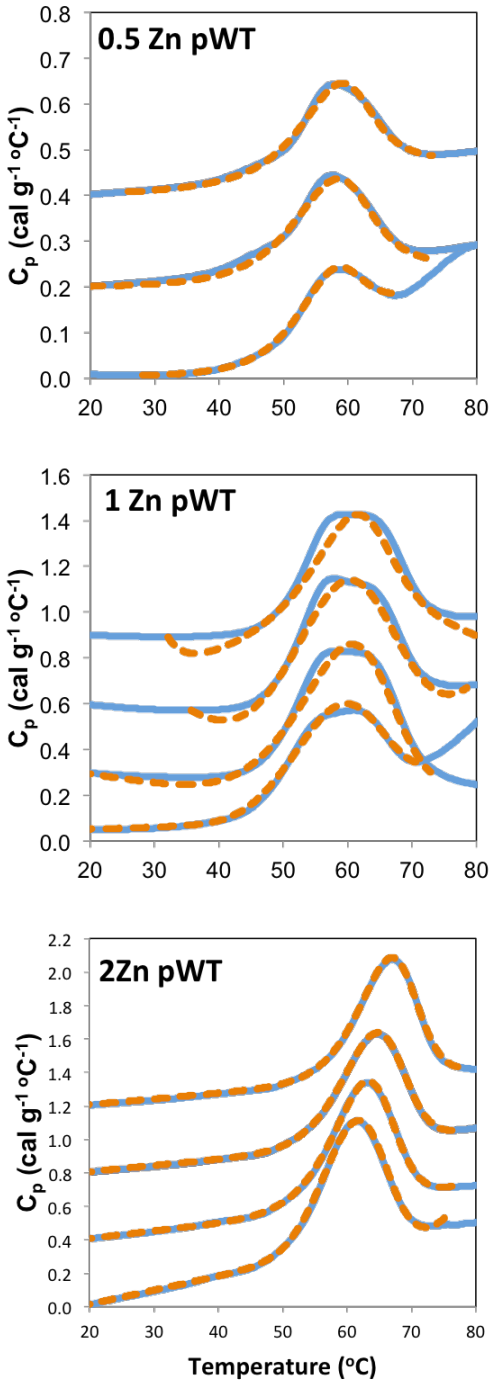

Figure A1.3 2-state dimer unfolding model fits for fALS mutants. The blue lines are the raw endotherms, with the fits represented by the orange dashed lines. DSC scans were offset for clarity, with the lowest concentration being the lower of the three scans and the highest concentration being at the top of each plot. Half a Zn equivalents concentrations were 1.16 mg/mL, 1.85 mg/mL, and 2.96 mg/mL. 1 Zn equivalence concentrations were 0.68 mg/mL, 0.98 mg/mL, 1.54 mg/mL and 2.30 mg/mL. 2 Zn equivalents concentrations included 0.72 mg/mL, 1.30 mg/mL, 2.34 mg/mL and 4.14 mg/mL.

Table 1.4 2-state monomer fit values for varying concentrations for fALS mutants.

SOD1 mutant	*Conc* (mg/mL)	t_m[1] (°C)	ΔH_{vH}[1] (kcal (mol dimer)$^{-1}$)	ΔH_{vH} /ΔH_{cal}
A4V	0.397	67.04	47.18	0.78
A4V	0.793	67.28	47.29	0.66
A4V	1.76	67.63	45.98	0.57
H46R	0.424	56.92	66.29	0.54
H46R	0.916	56.67	86.35	0.77
H46R	1.523	56.60	80.37	0.61
V148G	0.35	56.92	85.83	0.80
V148G	0.825	56.67	91.11	0.93
V148G	1.8	56.60	96.75	0.95

[1]Values from individual data set being fit to a 2-monomer unfolding dissociation model in Origin 7.0.

Table 1.5 2-state dimer fit values for varying protein conc of E,Zn-SOD1^{SH} fALS mutants.

SOD1 mutant	*Conc* (mg/mL)	t_m[1] (°C)	ΔH_{vH}[1] (kcal (mol dimer)$^{-1}$)	ΔH_{vH} /ΔH_{cal}	ΔG_{tavg}[2] (kcal (mol dimer)$^{-1}$)	n[3]
A4V	0.397	64.2	87.31	0.55	8.41	0.94
A4V	0.793	64.3	101.86	0.86	8.06	1.07
A4V	1.76	64.0	103.63	0.85	7.74	0.93
H46R	0.42	54.3	141.04	0.74	5.66	1.41
H46R	0.92	55.0	152.65	0.80	5.37	1.44
H46R	1.52	55.0	148.70	0.68	5.08	1.43
V148G	0.35	54.9	160.13	0.85	5.92	0.61
V148G	0.82	54.5	147.46	0.86	5.27	0.64
V148G	1.8	54.8	152.67	0.82	4.83	0.63

[1]Values from individual data set being fit to a 2-state dimer unfolding model Eq. A1.1 in Origin 7.0.
[2]ΔG_{tavg} calculated at 57.1°C.
[3]Molecularity was calculated using $n = \frac{-\Delta H_{vH}}{slope * R} + 1$.

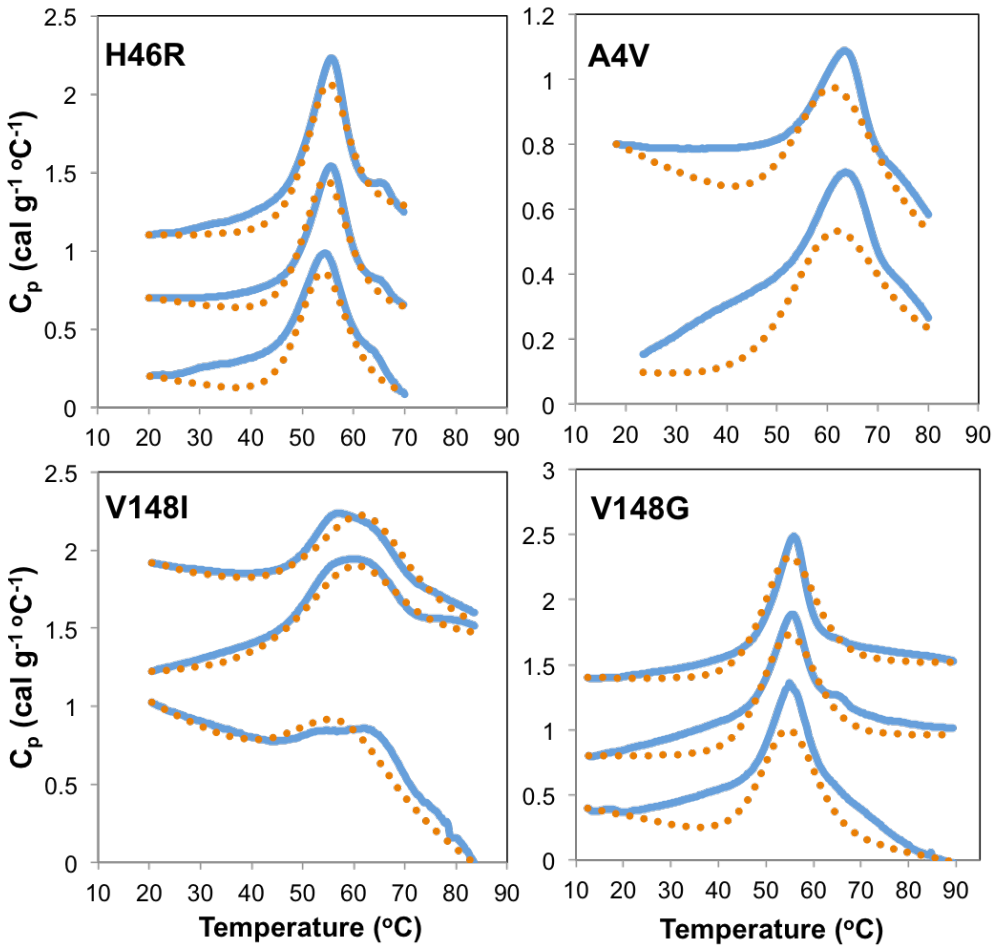

Figure A1.4. 3-state dimer unfolding with monomer intermediate model fits for fALS mutants. The blue lines are the raw endotherms, with the fits represented by the orange dashed lines. DSC scans were offset for clarity, with the lowest concentration being the lower of the three scans and the highest concentration being at the top of each plot. H46R concentrations were 0.42 mg/mL, 0.92 mg/mL, and 1.52 mg/mL. A4V concentrations were 0.31 mg/mL, 0.79 mg/mL, and 1.76 mg/mL. V148I concentrations included 0.59 mg/mL, 1.17 mg/mL, and 2.10 mg/mL. V148G concentrations were 0.35 mg/mL, 0.82 mg/mL, and 1.80 mg/mL.

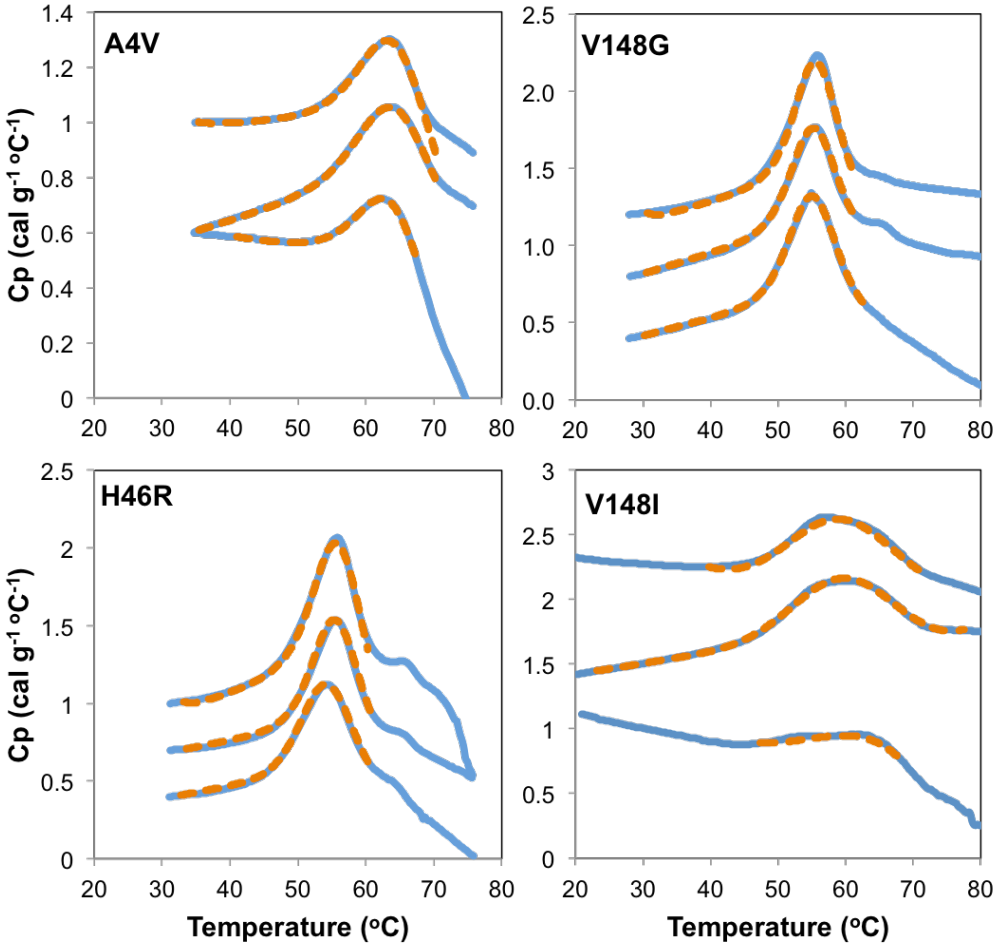

Figure A1.5. 2-state monomer unfolding model fits for fALS mutants. The blue lines are the raw endotherms, with the fits represented by the orange dashed lines. DSC scans were offset for clarity, with the lowest concentration being the lower of the three scans and the highest concentration being at the top of each plot. H46R concentrations were 0.42 mg/mL, 0.92 mg/mL, and 1.52 mg/mL. A4V concentrations were 0.31 mg/mL, 0.79 mg/mL, and 1.76 mg/mL. V148I concentrations included 0.59 mg/mL, 1.17 mg/mL, and 2.10 mg/mL. V148G concentrations were 0.35 mg/mL, 0.82 mg/mL, and 1.80 mg/mL.

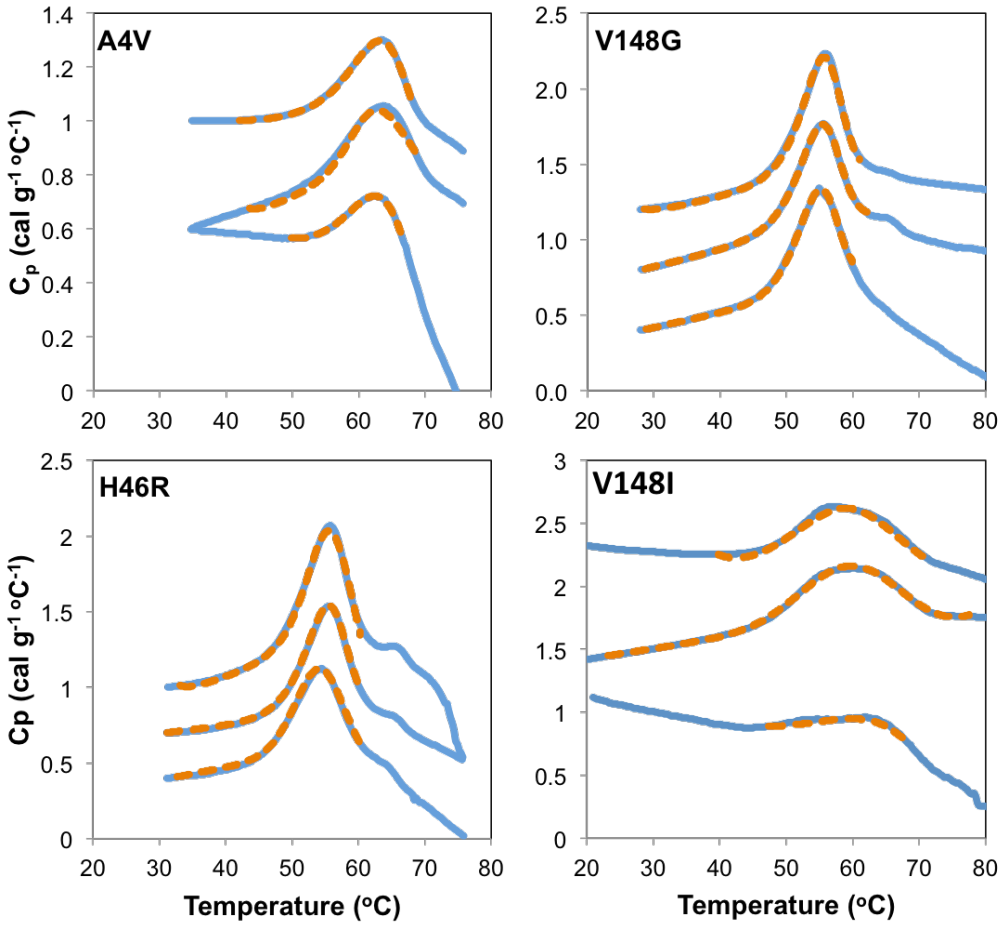

Figure A1.6 2-state dimer unfolding model fits for fALS mutants. The blue lines are the raw endotherms, with the fits represented by the orange dashed lines. DSC scans were offset for clarity, with the lowest concentration being the lower of the three scans and the highest concentration being at the top of each plot. H46R concentrations were 0.42 mg/mL, 0.92 mg/mL, and 1.52 mg/mL. A4V concentrations were 0.31 mg/mL, 0.79 mg/mL, and 1.76 mg/mL. V148I concentrations included 0.59 mg/mL, 1.17 mg/mL, and 2.10 mg/mL. V148G concentrations were 0.35 mg/mL, 0.82 mg/mL, and 1.80 mg/mL.

A2.0 Par assay used to quanitate zinc and metal contamination

4-(2-pyridylazo)resorcinol (PAR) is a chelator used to quantify copper and zinc ions spectroscopically. It was initially developed by Crow *et al.,* in 1997 and Mulligan *et al.,* in 2009 (33, 95) and it involved denaturing a known amount of protein completely, allowing for the release of zinc ions, and adding PAR to form a Zn^{2+}:PAR complex, but further modified by Colleen Doyle and Heather Primmer

(96). However, with reduced apo SOD1, the protein is quite susceptible to binding metals with a high affinity (~6.8 x 10^{-18} M^{-1} and ~4.2 x 10^{-14} M^{-1}, for Cu^{2+} and Zn^{2+}, respectively) (33), and for the 1 zinc bound form, prior metal contamination needs to be limited. All reduced apo samples were denatured completely to allow for the release of possible contaminating ions, which would bind to PAR and form a complex. Qualitatively metal contamination was easily detectable since the characteristic peak for PAR in water is at 415 nM and once bound with certain metals, the amplitude at 415 nM decreases and a shoulder is formed for the metal:PAR complex at 500 nM (123-125). When there is copper contamination, PAR is able to bind it with a 1:1 binding stoichiometry and an affinity of 7.7 x 10^{-11} M^{-1} (33). However, PAR binds to zinc with a weaker affinity of 2.6 x 10^{-15} M^{-1} and binds with 2:1 stoichiometry for zinc (33). If there is no observed peak at 500 nM then it was assumed the protein sample was truly apo.

The PAR assay was also used to quantitate whether our zinc bounds samples were truly 1:1, by denaturing the samples using 8 M guanidine hydrochloride (GdnHCl) and adding an excess of PAR. The spectra obtained from the samples were quantitated in two manners: one using the Beer-Lambert's law, as described below:

$$A = \varepsilon lc \qquad \text{(Eq. 479.1)}$$

the second was using SpectraLab program to perform spectral decomposition on sample spectra, using PAR, Zn:PAR, Cu:PAR as controls. The program would output weighted coefficients for each control, which cumulatively added to the sample spectra (126).

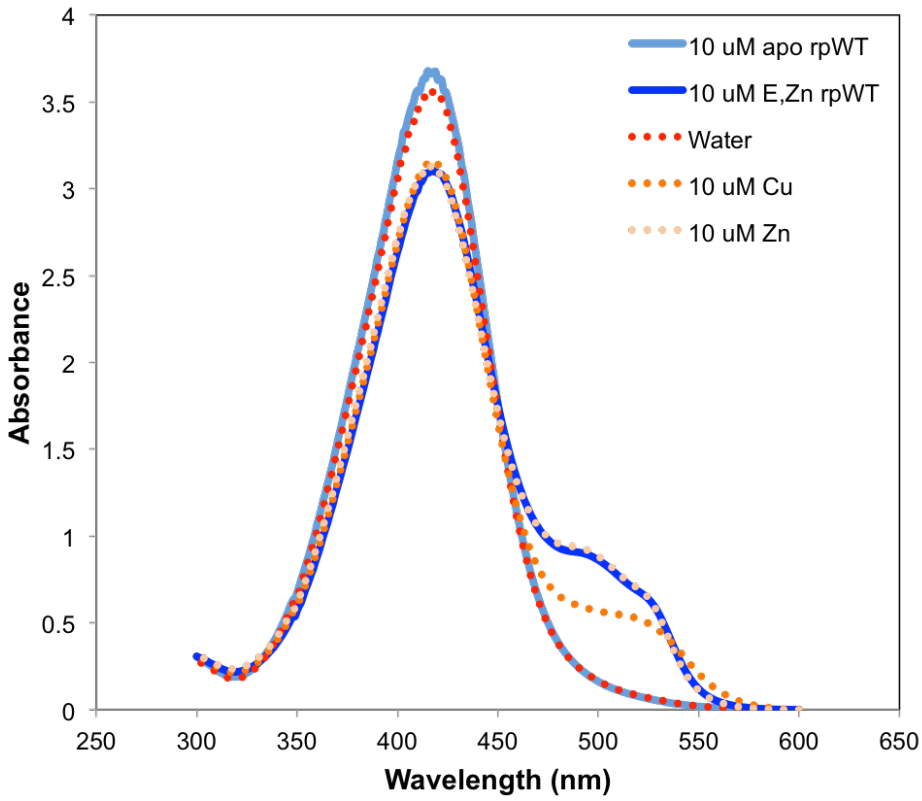

Figure A2.1. Representative absorption spectra for PAR binding to Cu, Zn, and Zn from 2 samples.

A3.0 Iodoacetamide labeling SDS-PAGE

To ensure samples remained reduced during ITC and DSC experiments, the free thiols were labeled with iodoacetamide that prevented them from oxidizing while running an SDS-PAGE gel. The samples were run against controls that would produce both oxidized and reduced bands, with the reduced band showing up higher than the oxidized.